Design Analysis and Performance Evaluation of Electroosmotic Micromixers

Thesis submitted by
Amrendra Kumar

Doctor of Philosophy (Engineering)

Department of Mechanical Engineering
Faculty Council of Engineering and Technology
Jadavpur University
Kolkata, India

2025

JADAVPUR UNIVERSITY
FACULTY OF ENGINEERING AND TECHNOLOGY

INDEX NO. 272/18/E

1. Title of the thesis:	**Design Analysis and Performance Evaluation of Electroosmotic Micromixers**
2. Name, Designation & Institution of the Supervisor/s:	**1. Dr. Nirmal Kumar Manna** Professor Department of Mechanical Engineering Jadavpur University Kolkata –700032, India
3. List of Publications:	**Journal Publications:~** **1. Kumar, A.**, Manna, N.K., Sarkar, S. and Biswas, N., 2025. Enhanced mixing efficiency via strategic parameter selection in diamond-shaped electroosmotic micromixers. Physics of Fluids, 37(9). doi: 10.1063/5.0283417. **2. Kumar, A.**, Manna, N. K., Sarkar, S. and Biswas, N., 2024. Enhancing mixing efficiency of a circular electroosmotic micromixer with cross-reciprocal electrodes. Physics of Fluids, 36(8). doi: 10.1063/5.0225659 **3. Kumar, A.**, Manna, N.K., Sarkar, S. and Biswas, N., 2023. Analysis of a square split-and-recombined electroosmotic micromixer with non-aligned inlet-outlet channels. Nanoscale and Microscale Thermophysical Engineering, 27(1), pp.55-73. doi: 10.1080/15567265.2023.2173108 **Book Chapter:** 1. **Kumar, A.**, Manna, N.K. and Sarkar, S., 2022. Effect of electrode length and ac frequency on mixing in a diamond-shaped split-and-recombine electroosmotic micromixer. In Recent Advancements in Mechanical Engineering: Select Proceedings of ICRAME 2021 (pp. 83-92). Singapore: Springer Nature Singapore. doi: 10.1007/978-981-19-3266-3_7

	International Conference Publications:~ **1. Kumar, A.**, Sarkar, S. and Manna, N.K., 2020. Passive mixing of microchannel mixers with staggered and opposed obstacles: a comparative study, Proceedings of International Conference on Energy and Sustainable Development 2020, Jadavpur University Press: ISBN 978-93-83660-56-8, pp. 305-308. **2. Kumar, A.**, Manna, N.K. and Sarkar, S., 2024. Numerical assessment of electroosmotic micromixer with time-varying electric potential, Proceedings of the 2nd International Conference on Mechanical Engineering 2024, Jadavpur University Press: ISBN: 978-81-954806-6-1, pp. 789-792.
4. List of Patents	NIL
5. List of Presentation in National / International Conference:	**Paper presentation:~** 1. **Kumar, A.**, Manna, N.K. and Sarkar, S., 2022. Effect of electrode length and ac frequency on mixing in a diamond-shaped split-and-recombine electroosmotic micromixer. In Recent Advancements in Mechanical Engineering: Select Proceedings of ICRAME 2021 (pp. 83-92). Singapore: Springer Nature Singapore, doi: 10.1007/978-981-19-3266-3_7. 2. **Kumar, A.**, Sarkar, S. and Manna, N.K., 2020. Passive mixing of microchannel mixers with staggered and opposed obstacles: a comparative study, Proceedings of International Conference on Energy and Sustainable Development 2020, Jadavpur University Press: ISBN 978-93-83660-56-8, pp. 305-308. 3. **Kumar, A.**, Manna, N.K. and Sarkar, S., 2024. Numerical assessment of electroosmotic micromixer with time-varying electric potential, Proceedings of the 2nd International Conference on Mechanical Engineering 2024, Jadavpur University Press: ISBN: 978-81-954806-6-1 , pp. 789-792.

JADAVPUR UNIVERSITY

FACULTY OF ENGINEERING AND TECHNOLOGY

"Statement of Originality"

I, Amrendra Kumar registered on **22.05.2018** do hereby declare that this thesis entitled "**Design Analysis and Performance Evaluation of Electroosmotic Micromixers**" contains literature survey and original research work done by the undersigned candidate as part of Doctoral studies.

All information in this thesis have been obtained and presented in accordance with existing academic rules and ethical conduct. I declare that, as required by these rules and conduct, I have fully cited and referred all materials and results that are not original to this work.

I also declare that I have checked this thesis as per the "Policy on Anti Plagiarism, Jadavpur University, 2019", and the level of similarity as checked by iThenticate software is 3 %.

Signature of Candidate:

Date : 18/11/2025

Certified by Supervisor:

18/11/2025

(Signature with date, seal)

PROFESSOR
Mechanical Engineering Deptt
Jadavpur University
Kolkata - 700 032

JADAVPUR UNIVERSITY
FACULTY OF ENGINEERING AND TECHNOLOGY

CERTIFICATE FROM THE SUPERVISORS

This is to certify that the thesis entitled "**Design Analysis and Performance Evaluation of Electroosmotic Micromixers**" submitted by Shri AMRENDRA KUMAR who got his name registered on 22th May, 2018 for the award of Ph. D. (Engineering) degree of Jadavpur University, is absolutely based upon his own work under the supervisions of Dr. NIRMAL KUMAR MANNA that neither his thesis nor any part of the thesis has been submitted for any degree/diploma or any other academic award anywhere before.

18/11/2025

Signature of the Supervisor
and date with Office Seal

PROFESSOR
Mechanical Engineering Deptt.
Jadavpur University
Kolkata - 700 032

In loving memory of my father.

ACKNOWLEDGEMENTS

It gives me immense pleasure to express my deepest gratitude to my respected supervisor, **Prof. Nirmal Kumar Manna**, for his invaluable guidance throughout my research journey. His expertise, vision, and mentorship have been instrumental in helping me comprehend the complexities of the subject and in sustaining my motivation throughout this academic pursuit. His encouragement and patience guided me through each stage of the research process—from problem identification and investigation to the articulation of findings in an accessible and coherent manner. I remain profoundly indebted to him for introducing me to the fields of **Computational Fluid Dynamics (CFD)** and **Microfluidics**, and for his unwavering support during my doctoral tenure.

I am particularly thankful to **Prof. Sandip Sarkar** and **Dr. Nirmalendu Biswas**, who were directly involved in this work and provided significant guidance. **Prof. Sarkar** helped me deepen my understanding of the critical aspects of microfluidics and made valuable contributions during the manuscript preparation and publication phases. His mentorship extended beyond academics, offering guidance and inspiration in other aspects of life as well. **Dr. Nirmalendu Biswas** deserves special acknowledgment for his constant encouragement during the challenging COVID-19 period and for his valuable assistance in learning micro-processing techniques for document preparation, as well as for his meticulous micro-refinement of the work—like an artist perfecting every detail. I also wish to acknowledge **Prof. Achintya Mukhopadhyay** for his constructive suggestions and continuous support, which have greatly enriched the quality of this research.

I extend my sincere appreciation to the esteemed faculty members of the **Project Neptune Laboratory—Prof. Sankar Dhar, Prof. Dipankar Sanyal, Prof. Swarnendu Sen, Prof. Sanjib Acharyya, Prof. Rana Saha, Prof. Saikat Mookherjee,** and **Prof. Koushik Ghosh**—for their encouragement and the stimulating discussions that significantly enhanced my research experience. I also express my gratitude to the **Head of the Department**, all members of the **Mechanical Engineering Department**, and the **Jadavpur University administration** for providing the necessary facilities and support to carry out this work.

I am also deeply thankful to my seniors **Dr. Pranibesh Mandal, Dr. Shouvik Chaudhuri,** and **Dr. Nitesh Mondal** for their constant motivation and support during both the joyful and challenging phases of life, which made my time easier both on and off the campus. I consider myself extremely fortunate to have received guidance and assistance from senior research fellows **Dr. Aranyak Chakravarty, Dr. Priyankan Datta, Dr. Ritabrata Saha,** and **Dr. Sourav Sarkar**, who are now serving in reputed institutions. Their cooperation and valuable insights were indispensable to the successful completion of this research. My heartfelt thanks also go to my colleague and friend **Dr. Md Naim Hossain** for his thoughtful suggestions and constructive discussions. I am equally grateful to **Sabyasachi, Soumendra, Sudipta, Manish, Hassan,** and other current scholars of the **Project Neptune Laboratory** for fostering a collaborative, motivating, and pleasant research environment.

On a deeply personal note, I owe my profound gratitude to my mother for her unwavering faith in me, to my wife, **Rakhi**, whose constant support has been my anchor, and to my little daughter, **Ishani**, whose laughter and boundless energy illuminate even the most demanding days. Their unconditional love, patience, and encouragement have been the silent strength behind every step of this challenging yet immensely rewarding academic journey.

Additionally, I would like to express my sincere appreciation to my extended family, especially my younger brother and my in-laws, for graciously sharing many of my responsibilities during this period. This achievement belongs, in no small measure, to everyone who stood firmly by my side—just as much as it belongs to me.

Date: 18/11/2025

(Amrendra Kumar)

ABSTRACT

Efficient mixing in microfluidic systems remains a formidable challenge due to the inherently laminar flow characteristics at the microscale, where Reynolds numbers are typically below one. The absence of turbulence in microchannels confines mixing primarily due to molecular diffusion—an inherently slow process that limits the performance of microfluidic devices in various applications including chemical synthesis, biological assays, and medical diagnostics. This thesis presents a comprehensive investigation into the design, analysis, and performance optimization of electroosmotic micromixers with novel geometric configurations to enhance mixing efficiency at the microscale.

The research explores four innovative microchamber geometries: circular, diamond, diamond split-and-recombined (DSAR), and square split-and-recombined (SSAR) designs. For each configuration, a systematic numerical analysis examines the effects of critical design parameters and operational conditions on mixing performance. The key parameters investigated include chamber dimensions, inlet velocity, AC voltage amplitude, frequency, electrode length, and phase difference between electrode potentials. The numerical approach employs finite element modeling with appropriate mesh refinement and validation against experimental data from the literature to ensure the accuracy and reliability of the results.

The circular chamber micromixer investigation reveals that smaller chamber diameters (20 μm) produce superior mixing through enhanced electroosmotic vortex interactions, achieving an efficiency of approximately 98% under optimal conditions (energy requirement: 500mV). Diamond chambers, designed with flat walls to facilitate electrode fabrication, demonstrate improved mixing performance through effective stretching and folding of fluid interfaces, reaching efficiencies of up to 99% with optimal parameters (energy requirement: 500mV).

A significant advancement is introduced through the novel diamond split-and-recombined (DSAR) configuration, which incorporates internal obstacles to synergistically combine passive and active mixing mechanisms. This design creates complex flow patterns through forced separation and recombination of fluid streams, achieving mixing efficiencies exceeding 99% with optimal obstacle dimensions (15 μm) and electrode configurations (energy requirement: 300mV). Further innovation is demonstrated with the square split-and-recombined (SSAR) design featuring non-

aligned inlet-outlet channels, which substantially enhances mixing through induced recirculation patterns while simplifying fabrication. By optimizing electrode polarity arrangements and operational parameters, the SSAR configuration achieves mixing efficiencies of up to 99.36% at significantly reduced operational voltages (energy requirement: 250mV).

Comparative analysis shows that split-and-recombined micromixers (DSAR and SSAR) outperform conventional circular and diamond designs, with the SSAR achieving the best balance between mixing performance and fabrication simplicity. The voltage required for peak efficiency decreased from 500 mV in baseline designs to 300 mV in the DSAR and 250 mV in the SSAR, reflecting 40% and an additional 16.7% reduction in energy demand, respectively. Optimal inlet velocity remained within 100–150 μm/s for all designs, while the SSAR exhibited the widest frequency stability range and greatest operational flexibility, confirming the superior electrokinetic efficiency of split-and-recombine geometries.

This research contributes significantly to the field of microfluidics by demonstrating how strategic integration of electroosmotic actuation with optimized chamber geometries can dramatically enhance mixing performance at the microscale. The insights gained from this work have important implications for the development of more efficient lab-on-a-chip devices, particularly for applications requiring rapid and homogeneous mixing of reagents, biological samples, or nanoparticles under controlled microfluidic conditions.

TABLE OF CONTENTS

Abstract i

Table of Contents iii

List of Figures ix

List of Tables xv

Nomenclature xvi

Chapter – 1 Introduction, Scope of Work, and Outline of Thesis.....1

1.1 Background and Importance of Micromixers.....1

1.2 Motivation and Needs for Micromixers.....2

1.3 Electroosmotic Flow in Micromixers.....3

1.4 Advantages of Electroosmotic Micromixer.....4

1.5 Objectives and Scope of the Study.....4

1.6 Structure of the Thesis.....6

Chapter – 2 Literature Review and Research Gaps.....9

2.1 Overview of Micromixing Techniques.....9

2.2 Classification of Micromixers.....9

2.3 Passive Mixing Methods.....10

2.3.1 *Mixing by Chaotic Advection*.....10

2.3.2 *Multilamination and Split-Recombine Designs*.....11

2.3.3 *Surface Modification Approaches*.....12

2.4 Active Mixing Methods.....12

2.4.1 *Pressure-Driven Micromixers*.....12

2.4.2 *Acoustic-Driven Micromixers*.....13

2.4.3 *Magnetic-Field Driven Micromixers*.....14

2.4.4 *Thermal-Field Driven Micromixers*.....14

2.5 Electroosmotic Micromixer Designs.....15

2.5.1 *Planar Electrode Configurations*.....15

2.5.2 *Electrode Geometry Innovations*.....16

2.5.3 *Temporal Activation Strategies*.....17

2.6 Channel Geometry Innovations 17
2.6.1 *Constriction and Expansion Designs* 17
2.6.2 *Zigzag and Serpentine Configurations* 18
2.6.3 *Chamber-Based Designs* 18
2.6.4 *Other Recent Geometric Innovations* 19
2.7 Surface Modification Approaches 20
2.7.1 *Heterogeneous Surface Charges* 20
2.7.2 *Conductive Surface Elements* 21
2.8 Combined Approaches 22
2.9 Challenges and Gaps in Current Research 22
2.9.1 *Integration and Fabrication Challenges* 22
2.9.2 *Performance Limitations* 23
2.9.3 *Theoretical and Computational Challenges* 23
2.9.4 *Application-Specific Requirements* 24
2.9.5 *Research Opportunities* 24
2.10 Closure 26

Chapter – 3 Mathematical Formulation and Numerical Procedure 27
3.1 Electroosmotic Flow Principles 27
3.2 Factors Affecting Electroosmotic Flow 28
3.2.1 *Zeta Potential Variations* 28
3.2.2 *Electric Field Characteristics* 28
3.2.3 *Fluid Properties* 29
3.3 Governing Equations 30
3.3.1 *Fluid Dynamic Equations* 30
3.3.2 *Electric Field Equations* 30
3.3.3 *Ion Transport Equations* 31
3.3.4 *Species Transport Equations* 31
3.3.5 *Electroosmotic Force and Velocity* 32
3.4 Boundary Conditions 32

3.4.1 *Hydrodynamic Boundary Conditions* 32

3.4.2 *Electric Field Boundary Conditions* 33

3.4.3 *Concentration Field Boundary Conditions* 33

3.5 Performance Metrics 34

3.6 Numerical Methods and Solution Procedure 35

3.6.1 *Finite Element Method* 35

3.6.2 *Simulation Workflow* 36

3.6.3 *Computational Approach* 36

3.6.4 *Parametric Study Approach* 37

3.7 Mesh Generation and Independence Study 38

3.7.1 *Mesh Generation Strategy* 38

3.7.2 *Mesh Independence Study and Mesh Structure* 39

3.8 Validation of Numerical Models 42

3.8.1 *Validation of Electroosmotic Flow Model* 42

3.8.2 *Validation against Experimental Data* 42

3.9 Closure 44

Chapter – 4 Mixing Enhancement in an AC Electroosmotic Micromixer with a Circular Mixing Microchamber 45

4.1 Introduction 45

4.2 Relevant background works 45

4.3 Research Gaps and Opportunities 47

4.4 Objectives of the Study 47

4.5 Design and Concept of Circular Mixing Microchamber 48

4.5.1 *Geometric Configuration* 48

4.5.2 *Rationale for Circular Chamber Design* 49

4.5.3 *Electrokinetic Actuation Mechanism* 49

4.5.4 *Theoretical Considerations* 50

4.5.5 *Design Parameters and Variables* 50
4.6 Results and Discussion 52
4.6.1 *Effect of Mixing Chamber Diameter on Micromixing Performance* 52
4.6.2 *Influence of Inlet Velocity* 56
4.6.3 *Impact of AC Voltage Amplitude* 58
4.6.4 *Effect of AC Frequency* 61
4.6.5 *Optimal Conditions for Micromixer Performance* 64
4.6.6 *Potential Challenges and Limitations* 65
4.7 Conclusion 65

Chapter – 5 Mixing Enhancement in an AC Electroosmotic Micromixer with a Diamond Mixing Microchamber 69
5.1 Introduction 69
5.2 Relevant background works 69
5.3 Research Gaps and Opportunities 70
5.4 Objectives of the Study 70
5.5 Design and Concept of Diamond Mixing Microchamber 71
5.5.1 *Geometric Configuration* 71
5.5.2 *Rationale for Diamond Chamber Design* 72
5.5.3 *Electrokinetic Actuation Mechanism* 72
5.5.4 *Theoretical Considerations* 72
5.5.5 *Design Parameters and Variables* 73
5.6 Results and Discussion 73
5.6.1 *Effect of Mixing Chamber Side Length on Micromixing Performance* 73
5.6.2 *Influence of Inlet Velocity* 77
5.6.3 *Impact of AC Voltage Amplitude* 80
5.6.4 *Effect of AC Frequency* 81
5.6.5 *Optimal Conditions for Micromixer Performance* 85

5.6.6 *Potential Challenges and Limitations* 85

5.7 Conclusion 86

Chapter – 6 Enhanced Micromixing in a Diamond Split and Recombined (DSAR) Electroosmotic Micromixer 89

6.1 Introduction 89

6.2 Relevant background works 89

6.3 Research Gaps and Opportunities 90

6.4 Objectives of the Study 91

6.5 Design and Concept of Diamond Split and Recombined (DSAR) Micromixer 91

6.5.1 *Geometric Configuration* 91

6.5.2 *Rationale for DSAR Design* 92

6.5.3 *Electrokinetic Actuation Mechanism* 93

6.5.4 *Design Parameters and Variables* 93

6.6 Results and Discussion 93

6.6.1 *Effect of Obstacle Size on Micromixing Performance* 93

6.6.2 *Effect of Electrode Length on Mixing Performance* 97

6.6.3 *Identification of Suitable Inlet Velocity* 100

6.6.4 *Impact of AC Voltage Amplitude* 104

6.6.5 *Effect of AC Frequency* 106

6.6.6 *Optimal Conditions for DSAR Micromixer Performance* 110

6.6.7 *Potential Challenges and Limitations* 111

6.7 Conclusion 112

Chapter – 7 Analysis of a Square Split-and-Recombined (SSAR) Electroosmotic Micromixer with Non-aligned Inlet-Outlet Channels 115

7.1 Introduction 115

7.2 Relevant background works 116

7.3 Research Gaps and Opportunities 117
7.4 Objectives of the Study 117
7.5 Design Concept of SSAR with Offset Inlet-Outlet Channels 117
7.6 Results and Discussion 120
7.6.1 *Effect of Obstacle Size on Micromixing Performance* 120
7.6.2 *Effect of Electrode Length on Mixing Performance* 124
7.6.3 *Identification of Suitable Inlet Velocity* 127
7.6.4 *Impact of AC Voltage Amplitude* 130
7.6.5 *Effect of AC Frequency* 133
7.6.6 *Optimal Conditions for SSAR Micromixer Performance* 136
7.6.7 *Potential Challenges and Limitations* 137
7.7 Conclusion 138

Chapter – 8 Outcome Summary, Contribution and Future Scope 141
8.1 Overall Outcomes of the Present Investigations 141
8.2 Contributions and Future Scope of the Present Work 144

References 147

LIST OF FIGURES

Figure 3.1 Circular electroosmotic micromixer with cross-reciprocal electrodes: (a) Schematic diagram, (b) Grid structure of the computational domain with mesh G5 for mesh study with u = 300 μm/s, ϕ_0 = 100 mV, f = 8 Hz. 40

Figure 3.2 Square Split And Recombined (SSAR) electroosmotic micromixer with cross-reciprocal electrodes: (a) Schematic diagram, (b) Grid structure of the computational domain with mesh MG4 for mesh study with u = 200 μm/s, ϕ_0 = 100 mV, f = 8 Hz. 41

Figure 3.3 Numerical verification against the published results: (a) experimental concentration results of Biddiss et al. (2004) for applied electric field 70 and 280 V/cm; (b) experimental and numerical concentration results of Wu and Li (2008) for applied electric field 50 V/cm at 500 μm offset distance; (c) numerical concentration results of Shamloo et al. (2016) at the outlet of the micromixer. 43

Figure 4.1 Schematic diagram of the AC electroosmotic micromixer with circular mixing microchamber, depicting the main microchannel, inlets, outlet, circular mixing chamber, and electrode positions. 49

Figure 4.2 Spatial distribution of species concentration and fluid streamlines in circular mixing microchambers of varying diameters. (a) D = 20 μm, (b) D = 25 μm, (c) D = 30 μm, (d) D = 35 μm, and (e) D = 40 μm. Simulation parameters: inlet velocity (u_0) = 100 μm/s, AC voltage amplitude (ϕ_0) = 100 mV, frequency (f) = 8 Hz, at a time (t) = 0.575 s. 53

Figure 4.3 Temporal evolution of mixing efficiency for circular mixing microchambers with diameters ranging from 20 to 40 μm. (a) Absolute mixing efficiency vs. time. (b) Relative mixing efficiency with respect to steady state vs. time. Simulation parameters: inlet velocity (u_0) = 100 μm/s, AC voltage amplitude (ϕ_0) = 100 mV, frequency (f) = 8 Hz.....55

Figure 4.4 Effect of inlet velocity on mixing efficiency [D = 20 μm, ϕ_o = 100 mV, f = 8 Hz]: (a) Mixing efficiency versus time for various inlet velocities, and (b) Relative mixing efficiency change with respect to steady state for different inlet velocities. ...56

Figure 4. 5 Concentration and streamline profiles for various inlet velocities at t = 0.55 s [D = 20 μm, ϕ_o = 100 mV, f = 8 Hz]: (a) u_o = 50 μm/s, (b) u_o = 100 μm/s, (c) u_o = 150 μm/s, (d) u_o = 200 μm/s, (e) u_o = 250 μm/s, and (f) u_o = 500 μm/s. 57

Figure 4.6 Mixing efficiency as a function of voltage amplitude for various inlet velocities at t = 1.0 s. 59

Figure 4.7 Temporal evolution of mixing efficiency for voltage amplitudes ranging from 100 mV to 500 mV at inlet velocities of (a) 100 μm/s, (b) 150 μm/s, and (c) 200 μm/s.....60

Figure 4.8 Mixing efficiency as a function of AC frequency for inlet velocities of 100, 150, and 200 μm/s at t = 1 s. 61

Figure 4.9 Temporal evolution of mixing efficiency for frequencies f = 2–18 Hz and inlet velocities of 100, 150, and 200 μm/s. 62

Figure 5.1 Schematic diagram of the AC electroosmotic micromixer with diamond mixing microchamber, depicting the main microchannel, inlets, outlet, diamond mixing chamber, and electrode positions.....71

Figure 5.2 Spatial distribution of species concentration and fluid streamlines in circular mixing microchambers of varying diameters. (a) L_s = 20 μm, (b) L_s = 25 μm, (c) L_s = 30 μm, (d) L_s = 35 μm, and (e) L_s = 40 μm. Simulation parameters: inlet velocity (u_o) = 100 μm/s, AC voltage amplitude (ϕ_o) = 100 mV, frequency (f) = 8 Hz, at a time (t) = 0.8625 s. 74

Figure 5.3 Temporal evolution of mixing efficiency for diamond mixing microchambers with side lengths ranging from 20 to 40 μm. (a) Absolute mixing efficiency vs. time. (b) Relative mixing efficiency with respect to steady state vs. time. Simulation parameters: inlet velocity (u_o) = 100 μm/s, AC voltage amplitude (ϕ_o) = 100 mV, frequency (f) = 8 Hz.....76

Figure 5.4 Effect of inlet velocity on mixing efficiency [L_s = 20 μm, ϕ_o = 100 mV, f = 8 Hz]: (a) Mixing efficiency versus time for various inlet velocities, and (b) Relative mixing efficiency change with respect to steady state for different inlet velocities. ... 77

Figure 5. 5 Concentration and streamline profiles for various inlet velocities at t = 0.92917 s [L_s = 20 μm, ϕ_o = 100 mV, f = 8 Hz]: (a) u_o = 50 μm/s, (b) u_o = 100 μm/s, (c) u_o = 150 μm/s, (d) u_o = 200 μm/s, (e) u_o = 250 μm/s, and (f) u_o = 500 μm/s..... 79

Figure 5.6 Mixing efficiency as a function of voltage amplitude for various inlet velocities at t = 1.0 s. 79

Figure 5.7 Temporal evolution of mixing efficiency for voltage amplitudes ranging from 100 mV to 500 mV at inlet velocities of (a) 100 μm/s, (b) 150 μm/s, and (c) 200 μm/s..... 80

Figure 5.8 Mixing efficiency as a function of AC frequency for inlet velocities of 100, 150, and 200 μm/s at t = 1 s. 82

Figure 5.9 Temporal evolution of mixing efficiency for frequencies f = 2–18 Hz and inlet velocities of 100, 150, and 200 μm/s. 83

Figure 6.1 Schematic diagram of the AC electroosmotic micromixer with Diamond split and recombined (DSAR) mixing microchamber, depicting the main microchannel, inlets, outlet, diamond mixing chamber, and electrode positions. 92

Figure 6.2 Spatial distribution of species concentration and fluid streamlines in Diamond split and recombined (DSAR) mixing microchamber of varying obstacle sizes. (a) L_o = 0 μm, (b) L_o = 5 μm, (c) L_o = 10 μm, (d) L_o = 15 μm, (e) L_o = 20 μm, (f) L_o = 25 μm, Simulation parameters: inlet velocity (u_o) = 100 μm/s, AC voltage amplitude (ϕ_o) = 100 mV, frequency (f) = 8 Hz electrode length (L_e) = 2 μm, at a time (t) = 0.775. 94

Figure 6.3 Temporal evolution of absolute mixing efficiency for Diamond Split and Recombined (DSAR) mixing microchamber with obstacles size ranging from 0 to 25

μm. Simulation parameters: inlet velocity (u_o) = 100 μm/s, AC voltage amplitude (ϕ_o) = 100 mV, frequency (f) = 8 Hz, electrode length (L_o = 2 μm). 96

Figure 6.4 Combined spatial distribution of species concentration and fluid streamlines in Diamond split and recombined (DSAR) mixing microchamber of varying obstacle sizes and electrode length. Simulation parameters: inlet velocity (u_o) = 100 μm/s, AC voltage amplitude (ϕ_o) = 100 mV, frequency (f) = 8 Hz, at a time (t) = 0.725 s. 98

Figure 6.5 Absolute mixing efficiency versus electrode length (L_e) for diamond mixing microchamber with obstacle sizes ranging from 5 to 20 μm. Simulation parameters: inlet velocity (u_o) = 100 μm/s, AC voltage amplitude (ϕ_o) = 100 mV, frequency (f) = 8 Hz. 99

Figure 6.6 Concentration and streamline profiles for various inlet velocities at t = 0.975 s [L_o = 15 μm, ϕ_o = 100 mV, f = 8 Hz]: (a) u_o = 50 μm/s, (b) u_o = 100 μm/s, (c) u_o = 150 μm/s, (d) u_o = 200 μm/s, (e) u_o = 250 μm/s, and (f) u_o = 500 μm/s. 101

Figure 6.7 Effect of inlet velocity on mixing efficiency [L_o = 15 μm, L_e = 10 μm, ϕ_o = 100 mV, f = 8 Hz]: (a) Mixing efficiency versus time for various inlet velocities, and (b) Relative mixing efficiency change with respect to steady state for different inlet velocities. 102

Figure 6.8 Mixing efficiency as a function of voltage amplitude for various inlet velocities at t = 1.0 s. 104

Figure 6.9 Temporal evolution of mixing efficiency for voltage amplitudes ranging from 50 mV to 300 mV at inlet velocities of (a) 100 μm/s, (b) 150 μm/s, and (c) 200 μm/s. 105

Figure 6.10 Mixing efficiency as a function of AC frequency for inlet velocities of 100, 150, and 200 μm/s at t = 1 s. 107

Figure 6.11 Temporal evolution of mixing efficiency for frequencies f = 2–18 Hz and inlet velocities of 100, 150, and 200 μm/s. 108

Figure 7.1 Schematic diagram of the AC electroosmotic micromixer with Square split and recombined (SSAR) mixing microchamber, depicting the offset connecting microchannel, inlets, outlet, square mixing chamber, and electrode positions. 118

Figure 7.2 Spatial distribution of species concentration and fluid streamlines in Square split and recombined (SSAR) electroosmotic micromixer of varying obstacle sizes. (a) L_o = 0 μm, (b) L_o = 5 μm, (c) L_o = 10 μm, (d) L_o = 15 μm, (e) L_o = 20 μm, (f) L_o = 25 μm, Simulation parameters: inlet velocity (u_0) = 100 μm/s, AC voltage amplitude (ϕ_0) = 100 mV, frequency (f) = 8 Hz electrode length (L_e) = 2 μm, at a time (t) = 0.9625 s. 121

Figure 7.3 Temporal evolution of absolute mixing efficiency for Square split and recombined (SSAR) electroosmotic micromixer with obstacle sizes ranging from 0 to 25 μm. Simulation parameters: inlet velocity (u_0) = 100 μm/s, AC voltage amplitude (ϕ_0) = 100 mV, frequency (f) = 8 Hz, electrode length (L_o = 2 μm). 122

Figure 7.4 Combined spatial distribution of species concentration and fluid streamlines in square split and recombined (SSAR) mixing microchamber of varying obstacle sizes and electrode length. Simulation parameters: inlet velocity (u_0) = 100 μm/s, AC voltage amplitude (ϕ_0) = 100 mV, frequency (f) = 8 Hz, at a time (t) = 0.98333 s. 124

Figure 7.5 Absolute mixing efficiency versus electrode length (L_e) for square mixing microchamber with obstacle sizes ranging from 5 to 20 μm. Simulation parameters: inlet velocity (u_0) = 100 μm/s, AC voltage amplitude (ϕ_0) = 100 mV, frequency (f) = 8 Hz. 126

Figure 7.6 Concentration and streamline profiles for various inlet velocities at t = 0.83333 s [L_o = 20 μm, ϕ_0 = 100 mV, f = 8 Hz]: (a) u_0 = 50 μm/s, (b) u_0 = 100 μm/s, (c) u_0 = 150 μm/s, (d) u_0 = 200 μm/s, (e) u_0 = 250 μm/s, and (f) u_0 = 500 μm/s..... 128

Figure 7.7 Effect of inlet velocity on mixing efficiency [L_o = 20 μm, L_e = 9 μm, ϕ_0 = 100 mV, f = 8 Hz]: (a) Mixing efficiency versus time for various inlet velocities, and (b) Relative mixing efficiency change with respect to steady state for different inlet velocities. 129

Figure 7.8 Mixing efficiency as a function of voltage amplitude for various inlet velocities at t = 1.0 s. 131

Figure 7.9 Temporal evolution of mixing efficiency for voltage amplitudes ranging from 50 mV to 250 mV at inlet velocities of (a) 100 μm/s, (b) 150 μm/s, and (c) 200 μm/s..... 132

Figure 7.10 Mixing efficiency as a function of AC frequency for inlet velocities of 100, 150, and 200 μm/s at t = 1 s. 134

Figure 7.11 Temporal evolution of mixing efficiency for frequencies f = 2–18 Hz and inlet velocities of 100, 150, and 200 μm/s. 135

LIST OF TABLES

Table 3.1 Mixing efficiency versus grid numbers at the micromixer outlet. 40

Table 3.2 Mixing efficiency versus grid numbers at the micromixer outlet. 41

Table 4.1 Constant properties and initial parameters employed in numerical modeling. 51

Table 4.2 Optimal parameters and maximum mixing efficiencies. 64

Table 5.1 Optimal parameters and maximum mixing efficiencies. 84

Table 6.1 Optimal parameters and maximum mixing efficiencies for the DSAR micromixer. 110

Table 7.1 Optimal parameters and maximum mixing efficiencies for the SSAR micromixer. 136

Table 8.1 Comprehensive Micromixer Design Evolution and Performance Comparison. 141

Table 8.2 Performance enhancement progression across design generations. 142

Table 8.3 Optimal design selection for application-specific requirements 143

Nomenclature

Roman Symbols

Symbol	Description
A	Area, m^2
AC	Alternating Current
c	Concentration, mol/m^3 or mM
c_0	Initial/Bulk concentration, mol/m^3 or mM
c_1, c_2	Inlet concentrations, mol/m^3 or mM
D	Diameter of circular mixing chamber, μm; also Diffusion coefficient, m^2/s
D_1	Diffusion coefficient of species, m^2/s
DC	Direct Current
$DSAR$	Diamond Split and Recombined
e	Elementary charge, C
E	Electric field vector, V/m
EDL	Electric Double Layer
EOF	Electroosmotic Flow
f	Frequency, Hz
F	Faraday's constant, 96,485 C/mol
$\bar{F}_e$	Electrokinetic body force, N/m^3
J	Current density vector, A/m^2
k	Boltzmann constant, J/K
L	Length of the micromixer, μm
L_0	Obstacle length, μm
L_e	Electrode length, μm
L_s	Side length of diamond or square chamber, μm
LOC	Lab-on-a-Chip
$MEMS$	Micro-Electro-Mechanical Systems
n	Unit normal vector
p	Pressure, Pa
P	Power consumption, W
Pe	Péclet number
R	Universal gas constant, 8.314,J/(mol·K)
Re	Reynolds number

Symbol	Description
t	Time, s
T	Absolute temperature, K
u	Velocity vector, m/s or mm/s
u_o	Inlet velocity, μm/s
u_{eo}	Electroosmotic slip velocity, m/s

Greek Symbols

Symbol	Description
ε	Dielectric constant/Relative permittivity of the medium
ε_0	Permittivity of vacuum, 8.854×10^{-12} F/m
ε_r	Relative permittivity of fluid
η	Mixing efficiency, %
η_0	Mixing efficiency at steady state (t = 0 s) %
κ^{-1}	Debye length, m
μ	Dynamic viscosity, Pa·s
ρ	Fluid density, kg/m^3
ρ_e	Net charge density, C/m^3
σ	Electrolyte conductivity, S/m
σ^2	Variance of the concentration distribution
σ^2_{max}	Maximum possible variance
φ	Electric potential, V
φ_0	Amplitude of applied electric potential, mV
Φ	Phase angle radiansradiansradians
ζ	Zeta potential, mV
∇	Gradient operator
∇_s	Tangential gradient along the surface

Abbreviations

Abbreviation	**Description**
AC-EO	Alternating Current Electroosmosis
AC-EOF	Alternating Current Electroosmotic Flow
CFD	Computational Fluid Dynamics
DNA	Deoxyribonucleic Acid
DCEO	Direct Current Electroosmosis
EM	Electroosmotic Micromixer
FEM	Finite Element Method
ICEO	Induced Charge Electroosmosis
LBB	Ladyzhenskaya-Babuska-Brezzi (stability condition)
μLOC	Micro-Lab-On-a-Chip
μ-TAS	Micro-Total-Analysis System
PAA	Polyacrylamide
PDMS	Polydimethylsiloxane
PIV	Particle Image Velocimetry
PNPNS	Poisson–Nernst–Planck–Navier–Stokes
REM	Rhombic Electroosmotic Micromixer
RMF	Rotating Magnetic Field
SAR	Split and Recombine
SSAR	Square Split and Recombined
Wi	Weissenberg number

Chapter – 1

Introduction, Scope of Work, and Outline of Thesis

1.1 Background and Importance of Micromixers

The field of microfluidics emerged in the 1990s, coinciding with advancements in micro-electro-mechanical systems (MEMS) technology and lab-on-a-chip (LOC) platforms. These innovations facilitated the development of novel fluid-handling devices operating at previously unexplored dimensions. Initially, applications were predominantly concentrated in chemistry, biology, and biomedicine, where researchers recognized the potential benefits of miniaturization. The unprecedented operational scale of these early MEMS devices necessitated a dedicated field of study focused on understanding fluid behavior at the microscale, thus giving rise to microfluidics as a distinct discipline.

Microfluidics specifically examines the behavior and manipulation of fluids—both liquids and gases—when confined to channels with dimensions typically ranging from 10 to 500 micrometers. Since its inception, the field has expanded its presence across numerous domains, including drug design in life sciences, regulation and monitoring of chemical reactions, and development of diagnostic equipment in biomedicine. This versatility stems from the considerable advantages offered by microscale operations compared to traditional macroscale approaches: cost-effectiveness, portability, reduced sample consumption, faster analysis times, and the ability to investigate various physical, chemical, and biological phenomena under precisely controlled conditions.

Despite the diversity of microfluidic applications, a common thread connecting most processes is the fundamental requirement for effective mixing. Liquid samples and reagents, frequently require homogenization before utilization in subsequent procedural stages within microdevices. This mixing necessity spans numerous applications, from homogenizing solutions in chemical reactions to combining solutions nanoparticles for targeted drug delivery, mixing liquid samples

containing enzymes and proteins in biological processes, and facilitating the production of nanoparticles.

1.2 Motivation and Needs for Micromixers

The process of mixing, while seemingly straightforward at the macroscale where mechanical agitation readily achieves homogeneity, becomes considerably more challenging at the microscale. This difficulty arises from several inherent characteristics of microscale fluid dynamics:

1. **Laminar Flow Regime**: Microfluidic devices typically operate at low Reynolds numbers, resulting in laminar flow where fluid layers tend to flow parallel to one another with minimal lateral mixing.
2. **Boundary Layer Effects**: The proportionally thicker boundary layers at the microscale significantly influence flow behavior.
3. **Surface-to-Volume Ratio**: The dramatically increased surface-to-volume ratio at the microscale enhances surface-related phenomena that affect fluid movement and mixing.
4. **Diffusion Limitations**: At the microscale, mixing primarily relies on molecular diffusion, which is characterized by diffusivity values of most liquids in the range of 10^{-9} to 10^{-11} m^2/s—exceedingly low magnitudes that lead to extended mixing durations.

Given these challenges, the pursuit of efficient microscale mixing is motivated by the desire to leverage the numerous advantages offered by microfluidic systems compared to their macroscale counterparts. For instance, microfluidic systems enable the manipulation of samples in minute quantities, which is particularly valuable for costly, hazardous, or scarce materials such as DNA. Additionally, microdevices facilitate high-quality separation and detection processes, resulting in reduced analysis times while maintaining advantageous characteristics such as compact size, portability, and ease of disposal.

A micromixer refers to a microchannel system designed to introduce multiple fluids into a primary channel to facilitate their mixing. The dimensions of conventional microchannels typically range from 10 to 500 micrometers in width and depth, while the length of the micromixer may extend to several millimeters or more.

The predominant influence of molecular diffusion in microscale mixing often necessitates relatively lengthy channels to achieve desired mixing outcomes.

The ability to seamlessly integrate micromixers into various other processes within a single integrated system further enhances their appeal. The multitude of benefits associated with advancing microfluidic devices makes the optimization of micromixers a highly compelling area of study with significant practical implications.

1.3 Electroosmotic Flow in Micromixers

Electroosmosis represents a fundamental electrokinetic phenomenon wherein liquid motion is induced by an applied electric field across a surface with electric charge characteristics. This effect manifests when the surface of a microchannel—typically constructed from materials such as silicon, glass, or polymer—develops an electric double layer (EDL) upon contact with an ionizable liquid under the influence of an applied electric field.

The EDL consists primarily of two distinct regions:

1. A layer of immobile counter-ions redistributed on the boundary surface of the microchannel in contact with the liquid (Stern layer)
2. A diffuse layer of mobile counter-ions in the liquid vicinity of the solid surface (Gouy–Chapman layer)

When an external electric field is applied in the vicinity of the microchannel (either along the channel or at a certain angle), the mobile ions in the diffuse layer (Gouy–Chapman layer) experience electrostatic and viscous drag forces. This force subsequently drags the surrounding liquid along with the ions, generating fluid flow without mechanical moving parts.

Electroosmotic flow is governed by the Helmholtz-Smoluchowski equation, when EDL thickness ≤ 100 times the characteristic dimension of the microchannel. It relates the electroosmotic velocity to the applied electric field, the zeta potential at the wall, and the properties of the fluid as $u = -\varepsilon\zeta E / \mu$, where u is the electroosmotic velocity, ε is the permittivity of the fluid, ζ is the zeta potential at the wall, E is the applied electric field, and μ is the dynamic viscosity of the fluid.

The zeta potential, representing the electric potential at the shear plane of the EDL, is a critical parameter determining the magnitude and direction of electroosmotic flow. This potential can be manipulated through surface modifications

or the application of external potentials to control fluid flow patterns within microchannels.

1.4 Advantages of Electroosmotic Micromixer

Electroosmotic micromixers possess several distinctive characteristics that make them particularly advantageous for microscale mixing applications:

1. **Simpler Geometry**: Electroosmotic micromixers can employ relatively simpler and shorter microchannel designs to achieve comparable mixing efficiency as passive micromixers, which often require complex geometrical features.
2. **Precision and Operational Control**: The direction and magnitude of electroosmotic forces can be precisely controlled by adjusting the magnitude and direction of the applied electric field and selecting appropriate electrolyte compositions. This allows for dynamic control over the mixing process.
3. **Absence of Moving Mechanical Components**: Unlike some other active mixing approaches, electroosmotic micromixers generally lack moving mechanical parts such as microstirrers, reducing complexity and enhancing reliability.
4. **Compatibility with Microscale Systems**: Electroosmotic flow can be readily integrated with other microfluidic operations, such as pumping and separation, facilitating comprehensive system functionality.
5. **Energy Efficiency**: Electroosmotic micromixers typically require relatively low power to operate, making them suitable for portable and point-of-care applications.

These advantages position electroosmotic micromixers as a promising approach for addressing the challenges of efficient microscale mixing, particularly in applications where precise control over the mixing process is desirable.

1.5 Objectives and Scope of the Study

The primary aim of this research is to design, analyze, and evaluate the performance of electroosmotic micromixers with varied geometries and electric potential configurations. Through systematic numerical investigations, this study seeks to address several research gaps in the field of microfluidic mixing, which will be comprehensively reviewed in **Chapter 2**. The specific objectives of this study are:

1. **Design and analyze novel electroosmotic micromixer geometries** that enhance mixing efficiency through strategic electrode placements and chamber configurations. This includes the development and investigation of circular, diamond, diamond split-and-recombined (DSAR), and square split-and-recombined (SSAR) mixing chamber designs.
2. **Optimize operational parameters** to maximize mixing performance while minimizing energy consumption. This involves systematic parametric studies to determine optimal:
    - Inlet velocity ranges
    - Electric potential amplitudes
    - AC frequency characteristics
    - Electrode configurations and dimensions
    - Mixing chamber geometries and specific dimensions
3. **Characterize mixing mechanisms** in different chamber geometries to elucidate the fundamental physics governing electroosmotic mixing processes, including vortex formation, chaotic advection, and interface stretching phenomena.
4. **Evaluate performance metrics** across various design configurations and operational conditions to establish comprehensive performance criteria and design guidelines for practical applications.

The scope of this research encompasses:

- Design variations including microchamber geometries, obstacle sizing, electrode configurations, and inlet and outlet channel arrangements
- Parametric studies of electric field characteristics (AC frequency ranges, amplitude variations, phase shifts)
- Mixing performance evaluations using both qualitative visualization and quantitative metrics
- Practical implementation considerations including fabrication feasibility and integration potential

This study employs computational fluid dynamics (CFD) simulations using COMSOL Multiphysics to predict and analyze the mixing behavior of different electroosmotic micromixer designs. The numerical approach allows for the systematic investigation of multiple design parameters and operational conditions without the time and resource constraints of physical prototype fabrication and testing. This computational approach provides valuable insights that can guide subsequent experimental work, potentially reducing development costs and accelerating the path to practical implementation.

It is important to note that while experimental validation is beyond the scope of the current study, the numerical models are developed with careful consideration of real-world physical constraints and validated against established theoretical principles. The findings from this research establish a foundation for future experimental investigations and practical applications of electroosmotic micromixers in various fields including biomedical diagnostics, chemical synthesis, and lab-on-chip technologies.

1.6 Structure of the Thesis

This thesis is organized into eight chapters that systematically present the research methodology, findings, and implications. This chapter **(Chapter 1)** presents the background and significance of micromixers, introduces electroosmotic flow principles, and outlines the research objectives and scope. **Chapter 2** thoroughly addresses the literature review and research gaps, providing a comprehensive overview of micromixing techniques, electroosmotic flow fundamentals, and advances in electroosmotic micromixer designs, and identifies specific research gaps in the current literature that this study aims to address. **Chapter 3** deals with mathematical formulation and numerical procedure. It establishes the mathematical models governing electroosmotic flows and mixing processes, and details the numerical approaches employed for simulation and analysis, including mesh generation strategies and validation procedures. The subsequent four chapters are dedicated to individual four problems:

Chapter 4 introduces the Circular Mixing Microchamber as the initial problem of this research work. It examines the proposed circular electroosmotic micromixer design, discusses the rationale behind geometric configurations and

electrode arrangements, and presents a systematic analysis of operational parameters influencing mixing performance.

Chapter 5 investigates the Diamond Mixing Microchamber. It examines the performance of a diamond-shaped mixing chamber, comparing its characteristics with the circular design and investigating the effects of geometric and operational parameters on mixing efficiency.

Chapter 6 deals with the Diamond Split and Recombined Electroosmotic Micromixer (**DSAR**). It presents an advanced design that incorporates obstacles within the diamond mixing chamber to create a split and recombined flow pattern, analyzing the synergistic effects of electrokinetic actuation and flow manipulation.

Chapter 7 considers Square Split-and-Recombined Electroosmotic Micromixer **(SSAR)**. Introduces a novel square-shaped mixing chamber design with offset inlet-outlet microchannels, investigating its performance characteristics and comparing it with previously studied geometries.

Chapter 8 is the conclusive chapter. It synthesizes key findings combining all four problems, highlights the contributions to the field of electroosmotic micromixers, and suggests avenues for future research and practical applications.

Each chapter is designed to build upon the preceding content, forming a cohesive narrative that progresses from fundamental principles to practical implementation considerations. The thesis aims to provide both theoretical insights and practical design guidelines for the development of efficient electroosmotic micromixers for a wide range of microfluidic applications.

Chapter – 2

Literature Review and Research Gaps

2.1 Overview of Micromixing Techniques

Efficient mixing at the microscale presents unique challenges primarily due to the laminar flow regime that dominates microfluidic systems. In this regime, characterized by Reynolds numbers typically below 100, turbulent mixing is absent, and molecular diffusion becomes the primary mechanism for mixing. However, the inherently slow nature of diffusion necessitates alternative approaches to enhance mixing efficiency in microfluidic devices. This section provides a comprehensive overview of the diverse techniques employed to overcome these challenges.

2.2 Classification of Micromixers

Micromixers are broadly classified into two categories based on their operational principles: passive and active micromixers. This fundamental classification was established in seminal works by Nguyen and Wu (2004) and further refined by Hessel et al. (2005) and Bayareh et al. (2020).

Passive Micromixers rely solely on channel geometry modifications and flow energy to enhance mixing without external energy inputs. The effectiveness of these mixers derives from their ability to increase interfacial area between mixing fluids and create recirculation zones through surface modifications. Mixing in passive devices occurs primarily through:

1. **Molecular Diffusion**: The natural process where molecules move from regions of higher concentration to regions of lower concentration.
2. **Chaotic Advection**: A process where fluid elements are stretched and folded through geometric manipulations, significantly enhancing the interfacial area between fluids and consequently accelerating diffusion.

Passive mixers are particularly advantageous when working with fluids having relatively high diffusion coefficients (10^{-9} to 10^{-10} m^2/s) as noted by Vatankhah and Shamloo (2018) and Mondal et al. (2019).

Active Micromixers employ external energy sources in conjunction with fluid pumping energy to enhance mixing. These devices prove especially valuable when diffusion coefficients of working fluids are extremely low (10^{-10} to 10^{-11} m^2/s). External energy sources employed in active micromixers include:

1. **Magnetohydrodynamic forces**
2. **Acoustic excitation**
3. **Thermal activation**
4. **Electrokinetic mechanisms**

The architectural designs of active micromixers are typically simpler and shorter than their passive counterparts, facilitating easier cleaning processes. However, they require the strategic integration of energy sources within the vicinity of the microchannel.

2.3 Passive Mixing Methods

Passive mixing techniques leverage channel geometry and flow characteristics to enhance mixing without external energy input. Several key approaches have been developed and refined:

2.3.1 Mixing by Chaotic Advection

Chaotic advection represents a complex yet effective approach for mixing intensification in laminar flow regimes. The concept was pioneered by Aref (1984), who conducted a two-dimensional numerical analysis demonstrating enhanced mixing through chaotic advection in an idealized stirred tank. Subsequent numerical studies by Aref and Balachandar (1986) established that chaotic advection could be developed even at low Reynolds numbers, with their findings experimentally verified by Chaiken et al. (1986).

The patterns observed in these studies revealed concentric structures termed “whorl” and “tendril” patterns, indicative of chaotic advection. Building upon these foundational insights, numerous researchers have proposed microscale mixer designs to leverage chaotic advection for enhanced mixing efficiency, including works by Liu et al. (2000), Song et al. (2003), and more recently, Vatankhah and Shamloo (2018) and Tripathi et al. (2021).

The essence of chaotic advection can be understood as the stretching of fluid layers in directions deviating from the original flow direction, as articulated by Aref

(2002) and further elaborated by Hardt and Schonfeld (2007). However, the inherently laminar nature of microscale flows presents challenges in altering flow path directions to induce chaotic advection.

To overcome this limitation, researchers have explored diverse microchannel designs that force the original flow field to change course, thereby generating chaotic advection effects. These designs include:

1. **Serpentine Channels**: Wang et al. (2021) demonstrated enhanced mixing in serpentine configurations through induced secondary flows.
2. **Zigzag Structures**: Tsai and Lin (2019) investigated how abrupt direction changes in zigzag microchannels promote chaotic advection.
3. **Spiral Channels**: Tripathi et al. (2021) examined how curved geometries in spiral configurations generate Dean vortices that enhance mixing.
4. **Tesla Structures**: Hong et al. (2004) explored specialized Tesla-inspired geometries that create flow separation and recirculation zones.
5. **Integrated Obstacles**: Chen and Zhao (2017) studied how strategically placed obstacles disrupt laminar flow patterns to enhance mixing.
6. **Twisted Channels**: Yousefi et al. (2024) investigated three-dimensional flow effects in twisted channel configurations.

While these passive mixers demonstrate considerable effectiveness, they commonly exhibit limitations including reduced efficiency at very low Reynolds numbers (below one), significant pressure drops, cleaning challenges after use, and fabrication complexities.

2.3.2 Multilamination and Split-Recombine Designs

Another passive approach involves the repeated splitting and recombination of fluid streams to reduce diffusion distances. This technique has been extensively investigated by researchers including Kim et al. (2005) and Hossain et al. (2017), who demonstrated that such designs can achieve mixing efficiencies exceeding 96% even at low Reynolds numbers.

The split-recombine principle operates by dividing the flow into multiple streams, redirecting them through different paths, and then recombining them. This process increases the interfacial area between different fluid streams and reduces the characteristic diffusion length, significantly enhancing mixing efficiency.

2.3.3 Surface Modification Approaches

Surface modifications represent another passive strategy to enhance mixing. Grooved surfaces, as studied by Rasouli et al. (2015), can induce helical flows that promote mixing by creating transverse velocity components. Their investigations showed that T-shaped micromixers with strategically placed grooves could increase mixing efficiency by up to 43.8% compared to basic designs.

Similarly, Heo and Suh (2005) demonstrated that channels with periodically attached blocks underneath can significantly enhance stirring at specific parametric values, with optimal performance achieved when the block height is approximately 0.8 times the channel width and positioned at a stagger angle of 45 degrees.

2.4 Active Mixing Methods

Active mixing methods employ external energy sources to disrupt laminar flow patterns and enhance mixing. Various approaches have been developed, each with distinct mechanisms and applications:

2.4.1 Pressure-Driven Micromixers

Pressure-perturbed mixing represents one of the earliest active approaches documented in the literature. Deshmukh et al. (2000) pioneered this approach with a simple Y-junction design incorporating a planar positive displacement micropump to generate pulsatile flow. By alternately pushing and stopping fluids in the inlets, they created interface lengthening between the two liquids, which could be controlled through the duty-cycle and frequency of the pulses.

Building upon this foundation, Glasgow and Aubry (2003) conducted a systematic study of pressure-perturbation methods in T-shaped microchannels. Their investigations encompassed nine different cases across three methodologies, revealing that pulsatile flow at two inlets with a 180° phase difference yielded optimal mixing performance.

Further advancements were achieved by Niu and Lee (2003), who introduced multiple side channels for generating periodic perturbations. Their design induced stretching and folding of fluid layers in the main channel through velocity pulsing from the side microchannels, significantly enhancing mixing.

More recently, Zhang et al. (2019) expanded the application to include both Newtonian and viscoelastic fluids in a microchannel with a T-junction inlet and sudden expansion mixing section. They found that for viscoelastic fluids at Reynolds

number 0.002 and Weissenberg number 1, mixing efficiency reached up to 82%, exceeding that of Newtonian fluids under identical conditions.

2.4.2 Acoustic-Driven Micromixers

Acoustic streaming has been effectively utilized to enhance mixing in various microscale devices. Liu et al. (2002) demonstrated that air bubbles in liquid can serve as actuators under ultrasonic sound wave stimulation, with the bubble-liquid interface functioning as a vibrating membrane. This vibration induces frictional forces that generate convective flow around the bubble, promoting mixing. Their studies identified optimal excitation frequencies around 5 kHz, with higher frequencies potentially proving harmful to biological samples.

Building on similar principles, Ahmed et al. (2009) employed a bubble trapped in a horseshoe-shaped obstacle positioned at the center of two different concentration fluid streams. By exciting the bubble with acoustic waves, they achieved remarkable mixing with an estimated mixing time of approximately 7 milliseconds.

Wang et al. (2008) further explored acoustic excitation by investigating frequency effects in a Y-channel design with a dedicated mixing chamber. Their findings indicated that while very low (0.5 kHz) and very high (10 kHz) frequencies produced minimal mixing enhancement, the 1.0-5.0 kHz range generated both single and multiple bubbles within the mixing chamber, significantly disrupting local flow and enhancing mixing.

A different approach was taken by Luong et al. (2010), who developed surface-acoustic-wave-driven micromixers using electrodes to generate acoustic waves transverse to the flow direction. Their comparison of parallel and focusing interdigitated electrode configurations revealed superior performance for the focusing design at equivalent applied voltages, with mixing efficiency proportional to the square of the applied voltage magnitude.

While acoustic approaches offer effective mixing without direct fluid contact, they face limitations related to heating issues at higher operational frequencies, restricting their applicability for heat-sensitive biological fluids.

2.4.3 Magnetic-Field Driven Micromixers

Magnetic actuation provides another effective approach for generating chaotic flow patterns to enhance mixing. Fu et al. (2010) conducted both experimental and numerical investigations of the interaction between DI water-based ferrofluid and DI water in a Y-shaped microchannel under magnetic fields generated by DC electromagnets. Upon application of the magnetic field, they observed uniform expansion of the nanofluid toward the DI water, forming numerous small finger-like structures at the fluid interface. These structures continuously evolved over time, increasing the interfacial length between the fluids and achieving 95% mixing efficiency within just 2 seconds.

Nouri et al. (2017) employed permanent magnets with a Y-shaped microchannel to characterize the mixing of Fe_3O_4 nanofluid with DI water. Their results demonstrated a significant enhancement of mixing efficiency and reduction in mixing length with the application of magnetic fields. They also found that increasing nanoparticle mass fraction improved mixing performance up to the magnetization saturation level of the ferrofluid, achieving maximum efficiency of 90% with a 2000G magnet.

A different approach was explored by Veldurthi et al. (2015), who investigated a design incorporating a cylindrical mixing chamber and a microrotor actuated by magnetic fields. At a rotational speed of 1500 rpm, they reported approximately 90% mixing efficiency and demonstrated practical application through single-step loading of rifampicin (an anti-tuberculosis drug) on TiO_2 nanoparticles.

Jeon et al. (2017) focused on magnetohydrodynamics-driven mixing of phosphate-buffered solution and reagents, examining the effects of electrode shape, size, and configuration arrangements. Their findings highlighted the significant influence of electrode configurations on mixing efficiency due to their varied effects on flow field patterns.

2.4.4 Thermal-Field Driven Micromixers

Thermally actuated disturbances have been effectively employed as external energy sources for enhancing microscale mixing. Darhuber et al. (2003) pioneered the use of temperature gradients to induce wavy helical patterns, significantly increasing the interfacial length between mixing fluids and reducing mixing time by a factor of three. Their portable microdevice achieved effective mixing using minimal power

from small battery-operated voltages (2-3V) while consuming very small sample volumes.

Huang et al. (2012) utilized non-uniform AC electric fields to induce electrothermal forces on the flow field, generating vortices that enhanced mixing efficiency. Their comparative analysis with obstacle-based passive mixers of equivalent dimensions revealed that their electrothermal micromixer achieved similar mixing quality with a pressure drop 3000 times lower, with maximum mixing quality reaching 99.18% while maintaining minimal temperature increases.

Zhang et al. (2016) numerically analyzed mixing enhancement through asymmetric planar AC electrodes with an underlying thin film resistive heater. Their results showed that the temperature gradient from external heating created chaotic flow patterns with continuous stretching-folding characteristics that significantly improved mixing efficiency.

Kunti et al. (2017) examined a hybrid semi-active semi-passive micromixer featuring a wavy bottom surface to increase contact length between fluid streams, combined with AC-actuated asymmetric electrodes at the bottom and symmetric electrode pairs at the top surface. Their findings indicated that mixing efficiency and flow rate depended on AC voltage amplitude, frequency, microchannel depth, and the configuration of active microelectrode pairs.

2.5 Electroosmotic Micromixer Designs

Electroosmotic micromixers have undergone significant evolution, with researchers exploring diverse designs to enhance mixing efficiency while minimizing energy consumption and simplifying fabrication. This section examines key advancements in electroosmotic micromixer designs, focusing on electrode configurations, channel geometries, and operational strategies.

2.5.1 Planar Electrode Configurations

Chen and Zhang (2003) pioneered the use of microelectrodes on channel walls by introducing four microelectrodes on the outer walls of a central loop to induce electroosmotic flow. Their analysis of particle traces revealed folding and stretching of material lines within the micromixer, contributing to chaotic-like mixing characterized by a positive Lyapunov exponent. This groundbreaking work

demonstrated the potential of strategically placed electrodes to enhance mixing efficiency.

Building upon this foundation, Chen et al. (2013) investigated an AC electro-osmotic (AC-EO) micromixer utilizing face-to-face, asymmetric pairs of planar electrodes. Their design featured a larger rectangular top electrode and a smaller bottom electrode with two protrusions, generating unique three-dimensional flow patterns that achieved mixing enhancement factors ranging from 290 to 360. They further demonstrated practical applications by successfully hybridizing single-stranded DNA and mixing Escherichia coli with RNA stains.

Huang et al. (2007) developed a novel patterned AC electroosmotic flow design using various electrode configurations to generate in-plane microvortices. Their device operated with AC signals below 20 V and 10 kHz, achieving significantly faster mixing times compared to direct diffusion—2 minutes for stationary fluids and 0.86 seconds for flowing fluids with viscosity ratios of 450. This approach offered enhanced mixing efficiency with shorter mixing lengths, particularly for flows with low Peclet numbers ($Pe < 3 \times 10^3$).

2.5.2 Electrode Geometry Innovations

The geometry of electrodes significantly influences flow patterns and mixing efficiency. Kim et al. (2009) investigated devices utilizing AC electroosmotic flow with arrays of planar asymmetric microelectrodes in diagonal or herringbone shapes for simultaneous mixing and pumping. Their results demonstrated superior pumping performance and enhanced mixing capabilities with the herringbone electrode configuration compared to reference designs.

More recently, Wu and Chen (2019) explored fractal electrode designs, examining the effects of fractal electrodes, length ratios of electrode pairs, and electrode positioning on mixing efficiency. By utilizing a Cantor fractal design with strategically arranged electrode pairs, their micromixer achieved mixing efficiency of up to 95.2% in one second at 5V and 8Hz, significantly outperforming traditional electrodeless designs.

An innovative approach was proposed by Xiong et al. (2021), who introduced a rhombic electroosmotic micromixer (REM) utilizing convergence-divergence structures to enhance mixing. Their design leveraged potential differences between microelectrodes to create uneven flow patterns that disturbed fluid streams and

increased mixing efficiency, achieving over 99% mixing efficiency with optimized parameters including asymmetric potential differences, 10 V AC voltage, and two sets of rhombic units.

2.5.3 Temporal Activation Strategies

The temporal characteristics of electrode activation provide additional control over mixing processes. Cheng et al. (2018) applied three types of periodic potentials on electrodes fixed to the wall of a T-shaped micromixer, analyzing mixing efficiency at different frequencies. Their findings revealed that mixing efficiency fluctuated with time at lower frequencies, with fluctuations diminishing as frequency increased. They identified an optimal frequency of 200 Hz for the applied voltage functions.

Cho et al. (2012) introduced a novel method using aperiodic time-varying electrokinetic perturbing flows in a crisscross micromixer. By employing an aperiodic oscillating source derived from the Sprott system to modulate the perturbing electric potential, they induced irregularly alternating flow recirculation structures that enhanced mixing through repeated stretching and folding of species streams. Their approach achieved average mixing efficiency exceeding 90% with optimized parameters.

2.6 Channel Geometry Innovations

While electrode configurations play a crucial role in electroosmotic mixing, channel geometry also significantly influences mixing performance. Researchers have explored various channel designs to enhance electroosmotic mixing effects:

2.6.1 Constriction and Expansion Designs

Lim and Lam (2012) investigated a micromixer based on periodic electroosmotic flow through constrictions, combining numerical and experimental approaches to verify their model's accuracy in predicting operating parameters like AC amplitude and frequency. Their work highlighted the importance of considering the electromigration effects of charged fluorescent dye for accurate simulations and determination of optimal operating conditions.

Afzal and Kim (2015) studied a micromixer featuring a convergent-divergent channel with sinusoidal walls, effectively coupling space-periodic characteristics with pulsatile flow. By analyzing mixing behavior using parameters like Reynolds and Strouhal numbers, they investigated the impact of sinusoidal pulsing on mixing

efficiency, achieving a high mixing index of 0.92 within just two periods of the sinusoidal walls.

More recently, Gong and Cheng (2023) presented a micromixer integrating inertial and electroosmotic flow with a contraction-expansion structure activated by AC electric fields. Their design generated multiple vortices that enhanced lateral flow, achieving optimal mixing quality (0.997) at an inflow velocity of 0.2 mm/s, voltage of 0.1 V, and channel length of 70 μm, with a pressure drop of only 1.58 Pa.

2.6.2 Zigzag and Serpentine Configurations

Chen and Yang (2007) investigated electroosmotic flow mixing in zigzag microchannels with sharp and flat corners. Their research revealed that flat-corner geometry enhanced mixing performance and prevented the accumulation of residual liquid or bubbles. The velocity gradient created a "racetrack effect" that increased diffusion rates, with numerical results indicating a mixing index of approximately 88.83%.

Building on these findings, Chen et al. (2022) combined a passive micromixer with a cosine channel wall with an active electroosmotic micromixer incorporating electrode pairs. Their design achieved fluid mixing through vortices induced by electroosmosis, with mixing efficiency reaching up to 96%. They found that more mixing units and a high amplitude-to-wavelength ratio resulted in effective mixing, with a phase shift of $3\pi/4$ coupled with four microelectrodes generating a high volume of electroosmotic vortices.

2.6.3 Chamber-Based Designs

Keshavarzian et al. (2018) enhanced mixing through electroosmotic phenomena using a microelectrode system with electrodes aligned in a mixing chamber integrated within a T-shaped micromixer. They investigated various design patterns based on different arrangements of microelectrodes on the inner and outer loops of an annular mixing chamber, identifying an optimal cross-like pattern that maximized mixing efficiency.

Jalili et al. (2020) conducted numerical investigations of an electroosmotic micromixer with a rhombus-like mixing chamber, optimizing parameters including inlet velocity, phase lag, frequency, and voltage amplitude. Their findings suggested

that once optimized parameter values were established, the obstacle shape inside the mixing chamber did not significantly affect mixing quality.

Seo et al. (2012) investigated a novel electrokinetic micromixer with a ring-type channel for rapid mixing. Their design combined two fluids in a ring-shaped mixing chamber from separate inputs, with four microelectrodes on the outside wall actuated by sinusoidal electric potentials. When evaluating concentration values based on frequency and zeta potential, they found optimal mixing with a frequency of 4 Hz and zeta potential of -0.1 V, with mixing performance improving as the applied voltage increased.

2.6.4 Other Recent Geometric Innovations

Zhang et al. (2023) proposed an active electroosmotic micromixer with twin diamond-shaped chambers and sawtooth structures to improve mixing efficiency by providing more space and increasing local velocity. Through optimization of parameters including fluid inlet velocity, AC voltage amplitude, frequency, and geometric dimensions, their micromixer achieved 99.9% mixing efficiency under specific conditions (velocity of 0.1 mm/s, voltage of 0.3 V, frequency of 3 Hz).

Khoshnod et al. (2024) carried out a comprehensive numerical investigation on a diamond-shaped electro-osmotic micromixer featuring four microelectrodes embedded within the inner diamond obstacle, creating an efficient split-and-recombine configuration. To further enhance mixing performance, rigid baffles were introduced near the inlet, and the geometric parameters were optimized using the Taguchi approach coupled with Response Surface Methodology (RSM). This optimization yielded an improvement of approximately 10.6% in the mixing index. Additionally, the study examined the effects of inlet velocity, AC frequency, applied voltage, and phase lag, reporting a maximum mixing efficiency of nearly 99.4% under optimal operating conditions.

Shahsavandi et al. (2025) numerically investigated a three-inlet electro-osmotic micromixer featuring dual circular obstacles with electrodes mounted on their surfaces. The geometric and positional parameters of the obstacles were optimized using the Taguchi method and Response Surface Methodology, achieving 2.5% and 5% improvements in the average mixing index and efficiency, respectively. Applying a $\pi/2$ phase lag and 0.5 V potential yielded an 88.4% mixing index, demonstrating efficient electrokinetic control and reduced pressure drop.

Saravanakumar et al. (2024) introduced a novel direct current electroosmosis (DCEO) micromixer with hexagonal cross-section channels—an uncommon practice in standard microfabrication. Their design leveraged DC actuation for active mixing without moving parts or driving circuitry, generating robust and stable helical vortices that achieved approximately 98.5% mixing efficiency within one second and 99.8% within two seconds in a channel only 1000 μm long.

Bahrami et al. (2023) developed an innovative electroosmotic micromixer incorporating fin-shaped electrodes within the mixing chamber. Their investigation examined the impact of electrode angle, electrode height, inflow velocity, alternating current, and frequency on mixing index and pressure drop. They found that optimal efficiency was attained with an electrode height of 5 μm and electrode angle of 60°, while the coefficient of performance exceeded that of reference mixers when the electrode height was 2.5 μm and electrode angle was 90°.

Poorreza (2025) performed a detailed numerical analysis of an electro-osmotic micromixer incorporating triangular-shaped electrodes subjected to a sinusoidal potential of 0.1 V at 8 Hz. The alternating electric field induced periodic vortices and electroosmotic recirculation, effectively enhancing fluid deformation and mixing. The optimized configuration achieved a mixing efficiency of approximately 96%, underscoring the critical influence of electrode geometry on electrokinetic mixing performance.

2.7 Surface Modification Approaches

Surface modification represents another strategy for enhancing electroosmotic mixing by creating spatially varying zeta potentials or introducing conductive elements that interact with applied electric fields.

2.7.1 Heterogeneous Surface Charges

Wang et al. (2007) investigated mixing enhancement through spatial zeta potential variations with opposite signs to the homogeneous surface, creating circulation zones within the bulk flow. Their study analyzed the effects of heterogeneous patch numbers, applied external voltage strength, and zeta potential on mixing efficiency. They found that adding four blocks with height half of the channel

width boosted mixing efficiency from approximately 50% to about 90% for a given channel length.

Wu and Liu (2005) introduced a micromixer that manipulates local flow fields through modulation of local ζ-potential, achieving over 90% mixing efficiency in a 5 mm long microchannel. Their work represented the first demonstration of temporal/spatial ζ-potential modulation for microfluidic mixer applications, offering a novel approach to enhancing microscale mixing.

Nayak (2014) examined electroosmotic flow in micro and nanochannels, finding that heterogeneous surface potential patches along channel walls induced strong recirculation vortices that increased mixing performance. These vortices generated robust pressure gradients that enhanced mixing efficiency, with streamlines near the patches following convoluted paths that contributed to effective mixing.

2.7.2 Conductive Surface Elements

Wu and Li (2008) investigated the mixing effect of induced-charge electrokinetic flow in a microchannel with embedded conducting hurdles. Their numerical modeling and experimental validation demonstrated that flow circulations caused by induced non-uniform zeta potential distribution along conducting obstacle surfaces significantly enhanced mixing between different solutions. Among the three hurdle shapes studied, rectangular hurdles produced the strongest mixing effect, with additional conducting hurdles in series further improving performance.

Shamloo et al. (2017) focused on a T-shaped micromixer with conducting hurdles, investigating parameters including inlet angle, hurdle arrangements, and geometry for improved mixing. Their results indicated that two conducting hurdles provided optimal mixing, with specific angles (45° for two hurdles, 90° for three hurdles, and 22.5° for four-hurdle setups) yielding maximum mixing indices. They concluded that a triangular chamber with circular conducting hurdles represented the optimal geometry for enhancing mixing efficiency.

Nazari et al. (2020) studied an induced-charge electrokinetic micromixer utilizing electrically conductive plates to induce vortices and improve the mixing index. By investigating various parameters including mounting, length, orientation, position, arrangement, and number of conductive plates, they demonstrated that increasing the plate angle from 0° to 40° improved mixing performance from 67.2% to 94.3%.

2.8 Combined Approaches

Deng et al. (2018) employed topology optimization to design electrode patterns for efficient micromixing over short channel lengths. Their approach coupled Navier-Stokes equations with charge transportation to optimize electrode patterns and achieve optimal electroosmotic micromixer performance for laminar microflow, demonstrating the capability to achieve complete mixing with customized electrode designs.

Farahinia et al. (2021) designed a micromixer utilizing a combination of electroosmotic and pressure-driven flows in a heterogeneous microchannel. Their three-segment design incorporated heterogeneous patches of non-uniform electric charge in the middle section to induce mixing. They discovered that the asymmetric degree of the charge pattern significantly influenced mixing efficiency—more so than absolute wall charge values—and that even with conventional zeta-potential surfaces, proper mixing could be achieved through strategic arrangement of charge patterns.

2.9 Challenges and Gaps in Current Research

Despite significant advances in electroosmotic micromixer designs, several challenges and research gaps remain that warrant further investigation. Addressing these issues is essential for realizing the full potential of electroosmotic mixing in practical applications.

2.9.1 Integration and Fabrication Challenges

The fabrication of electroosmotic micromixers presents several technical challenges:

1. **Electrode Integration**: Incorporating electrodes within microchannels while maintaining electrical isolation and proper connection to external power sources remains challenging. As noted by Wu et al. (2022), who demonstrated AC electroosmotic flow in a lab-on-a-foil electric device, the integration of electrodes in flexible or unconventional substrates requires specialized fabrication approaches.
2. **Surface Charge Control**: Precise control and patterning of surface charges for heterogeneous zeta potential designs present fabrication difficulties. Current methods often lack the spatial resolution and long-term stability required for consistent performance.

3. **Scalability**: While many designs demonstrate excellent performance in laboratory settings, scaling these designs for mass production while maintaining cost-effectiveness and reliability remains an ongoing challenge.

2.9.2 Performance Limitations

Several performance limitations have been identified in existing electroosmotic micromixer designs:

1. **Energy Efficiency**: Many designs require relatively high voltages to achieve satisfactory mixing, raising concerns about energy efficiency and potential electrolysis effects. Optimizing energy consumption while maintaining mixing performance represents an important research direction.
2. **Joule Heating**: The application of electric fields in conductive media inevitably generates Joule heating, which can affect both mixing performance and sample integrity, particularly for temperature-sensitive biological materials. Alipanah et al. (2021) investigated heat transfer effects in trapezoidal micromixers, emphasizing the importance of maintaining suitable temperatures for cell health due to Joule heating.
3. **Mixing Time**: While electroosmotic mixers often achieve high mixing efficiency, the time required to reach this efficiency may still be longer than desired for certain applications, particularly those requiring high throughput.

2.9.3 Theoretical and Computational Challenges

Several theoretical and computational challenges persist in the analysis and design of electroosmotic micromixers:

1. **Complex Multiphysics Modeling**: The coupled nature of electric fields, fluid dynamics, and concentration transport presents challenges for accurate numerical simulation. Comprehensive models must account for interactions between these phenomena, including non-linear effects and time-dependent behavior.
2. **Non-Newtonian Fluid Behavior**: While recent studies have begun addressing non-Newtonian effects in electroosmotic mixing, a comprehensive understanding of viscoelastic and shear-dependent behaviors remains limited. Mehta et al. (2022) and Haque et al. (2021) have made important contributions

in this area, but further investigation is needed, particularly for complex biological fluids.

Optimization Methodologies: The design space for electroosmotic micromixers is vast, encompassing geometric parameters, electrode configurations, and operational conditions. Developing systematic optimization methodologies to navigate this complex parameter space efficiently remains challenging.

2.9.4 Application-Specific Requirements

Different applications impose specific requirements on micromixer performance:

1. **Biological Compatibility**: Electroosmotic micromixers intended for biological applications must address concerns related to electrical effects on cells and biomolecules, as well as the biocompatibility of materials and surface treatments.
2. **Chemical Reaction Enhancement**: Applications involving chemical reactions require consideration of reaction kinetics in relation to mixing dynamics, with optimal mixing strategies potentially varying based on reaction characteristics.
3. **Integration with Analytical Systems**: Incorporating electroosmotic micromixers into comprehensive microfluidic analytical systems requires consideration of interface compatibility, control systems, and overall system performance.

2.9.5 Research Opportunities

Based on the identified challenges and gaps, several promising research directions emerge:

1. **Hybrid Mixing Approaches**: Combining electroosmotic mechanisms with other mixing strategies (passive geometrical features, acoustic excitation, etc.) may yield synergistic improvements in mixing performance. The work by Chen et al. (2022) combining passive cosine channel walls with active electroosmotic elements represents a step in this direction, but further exploration of hybrid approaches is warranted.
2. **Smart and Adaptive Mixing Systems**: Developing systems capable of real-time adjustment of electric field parameters based on feedback from mixing

performance could enhance efficiency across varying conditions and sample properties.

3. **Novel Electrode Materials and Configurations**: Exploring alternative electrode materials and innovative spatial arrangements could address fabrication challenges while improving performance. Continued investigation of fractal patterns, as initiated by Wu and Chen (2019), and three-dimensional electrode configurations present particular promise.
4. **Comprehensive Parametric Studies**: While numerous studies have examined specific parameter effects, comprehensive investigations spanning the full range of geometric, electrical, and fluid parameters would provide valuable design guidelines for application-specific optimization.
5. **Advanced Numerical Methods**: Developing more efficient and accurate numerical methods for simulating electroosmotic mixing, particularly for complex geometries and non-Newtonian fluids, would accelerate the design and optimization process.

The systematic addressing of these research gaps and opportunities will significantly advance the field of electroosmotic micromixers, enabling more efficient, reliable, and application-specific designs for a wide range of microfluidic systems.

Out of the exhaustive research opportunities discussed above, identified from an extensive literature survey of over 300 papers, this thesis focuses on the following critical aspects:

1. The design and optimization of novel electroosmotic micromixer geometries, specifically examining four distinct configurations: circular chamber, diamond chamber, diamond split-and-recombined (DSAR), and square split-and-recombined (SSAR) with non-aligned inlet-outlet arrangements.
2. The systematic investigation of operational parameters, including inlet velocity (50-500 μm/s), voltage amplitude (50-500 mV), AC frequency (2-18 Hz), and electrode configurations to maximize mixing efficiency while minimizing energy consumption.
3. The elucidation of mixing mechanisms in these chamber geometries establishes a fundamental understanding of electroosmotic vortex formation, chaotic advection, and their synergistic effects with geometric features like obstacles and chamber shapes.

4. The development of comprehensive design guidelines for the practical implementation of electroosmotic micromixers in various microfluidic applications.

These specific objectives address the most significant research gaps identified in the literature while providing a structured approach to advancing the field of electroosmotic micromixing, as detailed in **Chapter 1**.

2.10 Closure

This chapter has presented a comprehensive review of micromixing techniques with particular emphasis on electroosmotic mixing approaches. Through systematic examination of the literature, significant research gaps have been identified in the areas of chamber geometry optimization, electrode configuration, and operational parameter optimization for electroosmotic micromixers. Based on these gaps, specific research objectives and involved problems have been formulated to address the most promising opportunities for advancement in the field.

The subsequent chapters will build upon this foundation, beginning with **Chapter 3**, which details the mathematical formulation and numerical procedures employed in this research. The mathematical models governing electroosmotic flow and species transport phenomena, along with the computational approaches for solving these coupled equations, will be presented to establish the theoretical framework for the systematic investigations of different micromixer configurations in **Chapters 4** through **7**.

Chapter – 3

Mathematical Formulation and Numerical Procedure

3.1 Electroosmotic Flow Principles

Electroosmotic flow (EOF) represents a fundamental electrokinetic phenomenon that has gained significant attention in microfluidic applications due to its ability to generate fluid motion without mechanical moving parts. This section explores the theoretical foundations, governing equations, and key parameters that influence electroosmotic flow behavior in microchannels.

The electroosmotic phenomenon originates from the formation of an electric double layer (EDL) at the interface between a solid surface and an electrolyte solution. When a solid surface contacts an electrolyte solution, the surface typically acquires an electric charge through various mechanisms including:

1. **Ionization or dissociation of surface groups** (e.g., silanol groups on glass surfaces can dissociate to form negatively charged surfaces)
2. **Adsorption of ions** from the solution onto previously neutral surfaces
3. **Adsorption of polyelectrolytes, ionic surfactants, or charged macromolecules**
4. **Isomorphic substitution of atoms** within the surface crystal structure

The charged surface attracts counter-ions (ions of opposite charge) from the electrolyte solution while repelling co-ions (ions of the same charge). This redistribution of ions near the surface creates the electric double layer, which consists of two primary regions:

1. **Stern Layer**: A compact layer of immobile counter-ions directly adjacent to the surface, tightly bound by electrostatic forces.
2. **Diffuse Layer**: A region extending from the Stern layer into the bulk fluid where counter-ions are concentrated but mobile, with their concentration decreasing exponentially with distance from the surface.

The interface between these two layers is known as the shear plane, and the electric potential at this plane is termed the zeta potential (ζ). The zeta potential is a

critical parameter in electroosmotic flow as it directly influences the velocity and direction of the flow when an electric field is applied.

The thickness of the EDL is characterized by the Debye length. The Debye length typically ranges from a few nanometers in high ionic strength solutions to several hundred nanometers in dilute solutions, making it significantly smaller than typical microchannel dimensions (tens to hundreds of nanometers).

3.2 Factors Affecting Electroosmotic Flow

Several factors significantly influence electroosmotic flow characteristics in microchannels, these are discussed below.

3.2.1 Zeta Potential Variations

Spatial variations in zeta potential along channel surfaces can dramatically alter flow patterns. As demonstrated by Zhang et al. (2006), heterogeneous zeta potentials can generate complex flow structures:

- Symmetrically wavelike slip zeta potentials tend to produce symmetrical secondary electroosmotic flows
- Wave-like zeta potentials with varying phases or amplitudes generate asymmetrical vortices
- Wave-like zeta potentials with different wave numbers create asymmetrical recirculation patterns

These zeta potential variations can be deliberately engineered to enhance mixing, as shown by Wang et al. (2007), who improved mixing efficiency from approximately 50% to about 90% by adding four rectangular blocks with alternating zeta potentials along the channel.

3.2.2 Electric Field Characteristics

The nature of the applied electric field—whether DC or AC, uniform or non-uniform—significantly affects electroosmotic flow behavior:

1. **DC Electric Fields**: Traditional electroosmotic flow utilizes DC fields to generate uniform plug-like velocity profiles in channels with homogeneous

surface properties. However, as noted by Usefian and Bayareh (2019), DC fields can produce stronger vortices compared to AC fields under certain conditions.

2. **AC Electric Fields**: Alternating current fields introduce time-dependent flow patterns that can enhance mixing. Chen et al. (2013) demonstrated that AC electroosmotic (AC-EO) micromixers with asymmetric electrode pairs can generate unique three-dimensional flow patterns, achieving mixing enhancement factors between 290 and 360.
3. **Field Frequency**: The frequency of AC electric fields plays a crucial role in determining flow behavior. Huang et al. (2014) showed through numerical simulations that symmetric/asymmetric circulation zones could be generated by switching the phase-shift arrangement of microelectrodes, with the mixing performance being affected by AC frequency among other parameters.
4. **Field Amplitude**: The amplitude of the applied voltage directly influences mixing efficiency. Sasaki et al. (2010) demonstrated that higher applied voltages led to more rapid mixing in AC electroosmotic flow mixers, while Usefian et al. (2019) showed mixing efficiency increasing from 21% to 95.56% when applying DC electric fields with voltages ranging from 0 V to 40 V.

3.2.3 Fluid Properties

The characteristics of the fluid being transported also impact electroosmotic flow. These characteristics are:

1. **Ionic Concentration**: Li et al. (2019) investigated electroosmotic flow in DNA-grafted hard PDMS channels, finding that EOF velocity was size-dependent at low ionic concentrations and independent of size at high ionic concentrations. Additionally, Peng and Li (2015) observed that extremely high ionic concentrations (exceeding 1 M) significantly reduced EOF mobility, hindering channel entry.

2. **Non-Newtonian Behavior**: The rheological properties of non-Newtonian fluids introduce additional complexity to electroosmotic flows. Lv and Chen (2022) found that mixing performance was better for shear-thinning fluids compared to shear-thickening fluids, while Usefian et al. (2019) observed that circulation zones exhibited much greater intensity in shear-thinning fluids.
3. **Viscoelasticity**: The time-dependent response of viscoelastic fluids affects electroosmotic flow patterns. Chen et al. (2023) used the Oldroyd-B constitutive model to describe viscoelastic fluids like polyacrylamide (PAA) solutions, finding that the Weissenberg number significantly influenced flow rate and mixing efficiency.

3.3 Governing Equations

3.3.1 Fluid Dynamic Equations

The flow dynamics of incompressible fluids in microchannels can be described by the continuity equation and the Navier-Stokes equations:

$$\nabla.\vec{u} = 0 \tag{3.1}$$

$$\rho.\left(\frac{\partial \vec{u}}{\partial t} + \left(\vec{u}.\nabla\vec{u}\right)\right) = -\nabla p + \mu\nabla^2\vec{u} + \vec{F}_e \tag{3.2}$$

where $\vec{u}$ is the velocity vector (m/s), ρ is the fluid density (kg/m^3), p is the pressure (Pa), μ is the dynamic viscosity (Pa·s), $\vec{F}_e$ represents the electrokinetic body force (N/m^3) and t implies time (s).

3.3.2 Electric Field Equations

The electric field within the microchannel is described by the Laplace equation for the electric potential:

$$\nabla^2\phi = 0 \tag{3.3}$$

where ϕ is the electric potential (V).

For cases involving time-dependent electric fields, such as AC electroosmotic flow, the applied potential takes the form:

$$\phi = \pm\phi_0 \sin(2\pi ft + \theta) \tag{3.4}$$

where ϕ_0 is the amplitude of the applied potential (V), f is the frequency (Hz), t is time (s), and θ is the phase angle (radians).

When considering the electric double layer (EDL) formation at solid-liquid interfaces, the Poisson equation provides a more comprehensive description of the

$$\nabla^2\psi = -\frac{\rho_e}{\varepsilon\varepsilon_0} \tag{3.5}$$

where ψ is the electric potential due to the charged surface and EDL (V), ρ_e is the net charge density (C/m3), ε is the relative permittivity of the medium, and ε_0 is the permittivity of vacuum (8.854×10^{-12} F/m). The charge density ρ_e is related to the ion concentration distribution through:

$$\rho_e = F\sum_i z_i c_i \tag{3.6}$$

where F is Faraday's constant (96,485 C/mol), z_i is the valence of ion species i, and c_i is the concentration of ion species i (mol/m^3).

3.3.3 Ion Transport Equations

The distribution of ions within the electrolyte solution is governed by the Nernst-Planck equation, which accounts for ion transport through diffusion, electromigration, and convection:

$$\frac{\partial c_i}{\partial t} + \nabla\cdot\left(-D_i\nabla c_i - \frac{z_i F}{RT}D_i c_i\nabla\psi + \vec{u}c_i\right) = 0 \tag{3.7}$$

where D_i is the diffusion coefficient of ion species i (m^2/s), R is the universal gas constant (8.314 J/(mol·K)), and T is the absolute temperature (K).

3.3.4 Species Transport Equations

For analyzing the mixing performance of micromixers, the transport of a non-reactive scalar concentration field is modeled using the convection-diffusion equation:

$$\frac{\partial c}{\partial t} + \nabla\cdot(c\vec{u}) = \nabla\cdot(D\nabla c) \tag{3.8}$$

where c is the concentration of the species (mol/m^3) and D is the diffusion coefficient (m^2/s). The mass diffusivity of the Newtonian fluid for this study is assumed to be 1×10^{-11} m^2/s.

3.3.5 Electroosmotic Force and Velocity

In the Helmholtz-Smoluchowski framework, for thin electric double layers compared to the channel dimensions, the electroosmotic flow can be modeled using a slip velocity boundary condition rather than directly incorporating the electroosmotic body force in the Navier-Stokes equations. The electroosmotic slip velocity is given by:

$$\vec{u}_{eo} = -\frac{\varepsilon\varepsilon_0\zeta}{\mu}\nabla_s\phi \tag{3.9}$$

where $\vec{u}_{eo}$ is the electroosmotic slip velocity (m/s), ζ is the zeta potential (V), and $\nabla_s\phi$ represents the tangential gradient of the electric potential along the surface.

For cases where the EDL thickness is not negligible compared to the channel dimensions, the full Poisson-Nernst-Planck-Navier-Stokes (PNPNS) system must be solved, with the electroosmotic body force expressed as:

$$\vec{F}_e = \rho_e\nabla\phi \tag{3.10}$$

3.4 Boundary Conditions

Appropriate boundary conditions are essential for accurately modeling electroosmotic flow and mixing phenomena. This section details the boundary conditions applied to the governing equations described above.

3.4.1 Hydrodynamic Boundary Conditions

For fluid flow, the following boundary conditions are applied:

Inlet Condition: At the inlets, either a constant velocity or pressure is specified:

$$\vec{u} = \vec{u}_{in} \quad \text{or} \quad p = p_{in} \tag{3.11}$$

Outlet Condition: At the outlet, either a pressure condition or stress-free condition is applied:

$$p = p_{out} \quad \text{or} \quad \mathbf{n} \cdot (-p\mathbf{I} + \mu(\nabla\vec{u} + (\nabla\vec{u})^T)) = 0 \tag{3.12}$$

where $\mathbf{n}$ is the unit normal vector to the boundary.

Wall Boundary Condition: For walls without electroosmotic effects, the no-slip condition is applied:

$$\vec{u} = 0 \tag{3.13}$$

For walls with electroosmotic effects, the Helmholtz-Smoluchowski slip velocity condition is used:

$$\vec{u} = -\frac{\varepsilon\varepsilon_0\zeta}{\mu}\nabla_s\phi \tag{3.14}$$

3.4.2 Electric Field Boundary Conditions

The electric field boundary conditions depend on the specific electrode configuration:

Electrode Surfaces: At electrode surfaces, a prescribed potential is applied:

$$\phi = \phi_{applied} \tag{3.15}$$

For time-dependent potential applications (AC electroosmotic flow):

$$\phi = \pm\phi_0 \sin(2\pi ft + \theta) \tag{3.16}$$

Insulating Walls: For electrically insulating walls, a zero normal current density condition is applied:

$$\mathbf{n} \cdot \nabla\phi = 0 \tag{3.17}$$

Inlet and Outlet Boundaries: Typically, electrical insulation conditions are also applied at inlet and outlet boundaries:

$$\mathbf{n} \cdot \nabla\phi = 0 \tag{3.18}$$

3.4.3 Concentration Field Boundary Conditions

For species concentration, the following boundary conditions are used:

Inlet Condition: At inlets, specified concentrations are prescribed. For a two-inlet micromixer with different solutions:

$$\begin{aligned} c &= c_1 \quad \text{at inlet 1} \\ c &= c_2 \quad \text{at inlet 2} \end{aligned} \tag{3.19}$$

Typically, normalized concentrations of 1 and 0 are used for the two inlets to facilitate analysis of mixing performance.

Outlet Condition: At the outlet, a convective flux boundary condition is applied, assuming no diffusive flux in the normal direction:

$$\mathbf{n} \cdot D\nabla c = 0 \tag{3.20}$$

Wall Boundary Condition: At wall boundaries, a no-flux condition is typically applied:

$$\mathbf{n} \cdot (D\nabla c + \vec{u}c) = 0 \tag{3.21}$$

3.5 Performance Metrics

Several metrics are employed to evaluate the performance of electroosmotic micromixers:

Mixing Efficiency: The primary performance metric is the mixing efficiency (η), which quantifies the degree of homogenization achieved:

$$\eta = \left(1 - \sqrt{\frac{\sigma^2}{\sigma_{\max}^2}}\right) \times 100\% \tag{3.22}$$

where σ^2 is the variance of the concentration distribution at a given cross-section:

$$\sigma^2 = \frac{1}{A}\int_A (c - \bar{c})^2 dA \tag{3.23}$$

and $\sigma_{\max}^2$ is the maximum possible variance corresponding to completely unmixed fluids:

$$\sigma_{\max}^2 = \bar{c}(1 - \bar{c}) \tag{3.24}$$

with $\bar{c}$ being the mean concentration.

Relative Mixing Efficiency: To isolate the effect of electroosmotic actuation, the relative change in mixing efficiency with respect to the steady state (without electric field) is also calculated:

$$\Delta\eta = \eta - \eta_0 \tag{3.25}$$

where η_0 is the mixing efficiency at the fully developed steady state (t = 0 s).

Both of the above-mentioned performance metrics (mixing efficiency and relative mixing efficiency) are utilized to comprehensively evaluate and compare different micromixer designs and operating conditions.

3.6 Numerical Methods and Solution Procedure

The coupled system of partial differential equations governing electroosmotic flow and mixing requires robust numerical methods for accurate solutions. This section outlines the numerical approaches employed in this study.

3.6.1 Finite Element Method

The finite element method (FEM) is utilized as the primary numerical approach for discretizing and solving the governing equations. FEM offers several advantages for microfluidic simulations, including:

1. Ability to handle complex geometries
2. Flexibility in implementing boundary conditions
3. Natural treatment of second-order derivatives
4. High accuracy for smoothly varying solutions

In the FEM framework, the computational domain is discretized into a collection of elements (typically triangular or tetrahedral), and the governing equations are transformed into their weak form. The solution variables are approximated using basis functions defined on these elements, resulting in a system of algebraic equations.

For the velocity and pressure fields, we employ the Taylor-Hood elements with quadratic basis functions for velocity (P2) and linear basis functions for pressure (P1). This combination satisfies the Ladyzhenskaya-Babuska-Brezzi (LBB) stability condition, preventing spurious pressure modes.

The electric potential and concentration fields are discretized using quadratic (P2) basis functions to ensure an accurate representation of gradients, which are particularly important for electroosmotic flow calculations.

3.6.2 *Simulation Workflow*

The numerical simulations follow a structured workflow designed to efficiently and accurately capture the electroosmotic mixing phenomena:

1. **Geometry creation:** The micromixer geometry is created based on the design parameters, including channel dimensions, electrode configurations, and obstruction features.
2. **Mesh generation:** A computational mesh is generated following the strategy described in Section 3.4, with appropriate refinement in regions of interest.
3. **Steady-state initialization:** A steady-state solution without electric field activation is obtained to establish the initial flow field and concentration distribution.
4. **Transient simulation:** Using the steady-state solution as the initial condition, a time-dependent simulation is performed with activated electric fields to capture the electroosmotic mixing process.
5. **Post-processing and analysis:** The simulation results are analyzed to evaluate mixing performance, flow characteristics, and other quantities of interest.

3.6.3 *Computational Approach*

The computational approach is specifically tailored to the challenges of electroosmotic mixing simulations:

Two-Stage Solution Strategy: To reduce computational requirements, a two-stage solution strategy is implemented:

1. **Stage 1:** A fully developed steady-state solution is obtained by solving the continuity, momentum, and convection-diffusion equations without electric field effects.
2. **Stage 2:** Using the results from Stage 1 as initial conditions, a time-dependent simulation is performed, incorporating the electric field equations along with the Navier-Stokes and convection-diffusion equations. This stage captures the electroosmotic effects and mixing enhancement.

Solver Settings: The MUMPS direct solver is employed with a memory allocation factor of 1.2. For the non-linear solver, a Newton method with a damping factor of 0.9 is used. The relative tolerance for convergence is set to 10^{-6}.

Discretization Schemes: The following discretization schemes are employed:

- Quadratic (P2) elements for velocity field
- Linear (P1) elements for pressure field
- Quadratic (P2) elements for species transport and electric potential

Time Stepping: An adaptive time-stepping scheme is implemented with the following characteristics:

- Initial time step: 0.001 s
- Minimum time step: 0.0001 s
- Maximum time step: 0.01 s
- Time step adjustment based on solution behavior and convergence rate

For simulations with AC electric fields, the time step is further restricted to ensure adequate resolution of the voltage oscillations:

- Maximum time step ≤ 1/(20f), where f is the AC frequency

3.6.4 *Parametric Study Approach*

To thoroughly investigate the behavior and performance of electroosmotic micromixers, systematic parametric studies are conducted. The parameter space explored includes:

Geometric Parameters:

- Mixing chamber diameter/dimensions
- Electrode size and positioning
- Channel aspect ratio
- Obstruction geometry and placement

Electric Field Parameters:

- Voltage amplitude
- AC frequency
- Phase difference between electrode pairs

- Electrode polarity configurations

Flow Parameters:

- Inlet velocity
- Fluid properties (viscosity, density, diffusion coefficient)
- Reynolds number
- Péclet number

This comprehensive approach enables the identification of the key parameters influencing mixing performance and the development of optimized micromixer designs.

3.7 Mesh Generation and Independence Study

The accuracy and reliability of numerical solutions depend significantly on the quality and resolution of the computational mesh. This section describes the mesh generation strategy and the mesh independence study conducted to ensure that the numerical results are independent of the spatial discretization.

3.7.1 Mesh Generation Strategy

A structured mesh with unstructured triangular elements is employed for discretizing the computational domain. The mesh is generated with the following considerations:

1. **Refinement near walls and electrodes:** Higher mesh density is applied near walls and electrodes to accurately resolve the steep gradients in the electric field and velocity.
2. **Refinement in mixing regions:** Areas where intense mixing is expected, such as after obstacles or in the vicinity of electrode pairs, are refined to capture the complex flow patterns and concentration gradients.
3. **Graded mesh transition:** Smooth transitions between regions of different mesh densities are ensured to maintain solution accuracy and stability.
4. **Aspect ratio control:** The aspect ratio of mesh elements is controlled to prevent highly elongated elements that could degrade solution accuracy.

5. **Mesh quality metrics:** Additional quality metrics including skewness and orthogonal quality are monitored to ensure overall mesh quality.

The mesh is generated using a dedicated mesh generation algorithm that creates an initial coarse mesh and progressively refines it based on geometric features and anticipated solution characteristics.

3.7.2 Mesh Independence Study and Mesh Structure

To ensure that the numerical results are independent of the spatial discretization, a systematic mesh independence study is conducted. This involves creating a series of progressively refined meshes and comparing the solutions obtained on these meshes.

For the circular electroosmotic micromixer with cross-reciprocal electrodes as shown in Figure 3.1(a), six different mesh densities were evaluated, designated as G1, G2, G3, G4, G5, and G6, consisting of 1578, 2386, 5038, 9158, 11536, and 12736 domain elements, respectively. The mesh independence study was performed using the following operating conditions:

- Inlet velocity: u_o = 300 μm/s; Voltage amplitude: ϕ_0 = 100 mV
- AC frequency: f = 8 Hz; Mixing chamber diameter: D = 20 μm
- Length of the main channel: L = 80 μm

Table 3.1 shows the mixing efficiency at the micromixer outlet for different mesh densities. For each grid size (Gn), the percent error is computed considering the finest grid (G6 with 12736 elements) as the reference value, that is, $\%\ \text{error} = 100 \times \left| \eta(Gn) - \eta(G6) \right| / \eta(G6)\%$. The results indicate that the difference in mixing efficiency between mesh G5 (11536 elements) and G6 (12736 elements) is negligible (0.01%). Therefore, mesh G5 was selected as the optimal mesh for the simulations, balancing computational efficiency with solution accuracy. The mesh distribution of the selected mesh (G5) of the computational domain is shown in Figure 3.1(b).

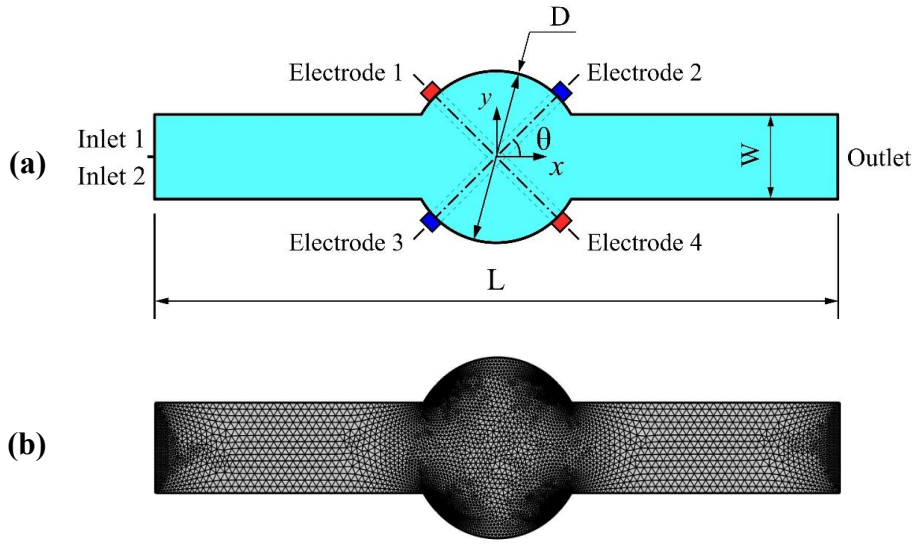

Figure 3.1 Circular electroosmotic micromixer with cross-reciprocal electrodes: (a) Schematic diagram, (b) Grid structure of the computational domain with mesh G5 for mesh study with u = 300 μm/s, ϕ_0 = 100 mV, f = 8 Hz.

Table 3.1 Mixing efficiency versus grid numbers at the micromixer outlet.

Grid	Number of domain elements	Mixing efficiency (η)	% Error in η
G1	1578	0.56082	4.12%
G2	2386	0.57162	2.27%
G3	5038	0.57751	1.26%
G4	9158	0.58018	0.81%
G5	11536	0.58481	0.01%
G6	12736	0.58489	0.00%

For the square split-and-recombined electroosmotic micromixer (SSAR) shown in Figure 3.2(a), a similar mesh independence study was conducted with mesh sizes MG1, MG2, MG3, MG4, and MG5 having 4432, 5044, 9687, 11798, and 13286 grid elements, respectively. The mesh independence study was performed using the following operating conditions:

- Inlet velocity: u_o = 200 μm/s; Voltage amplitude: ϕ_0 = 100 mV
- AC frequency: f = 8 Hz; Mixing chamber length: L_s = 30 μm
- Micromixers' total length: L = 80 μm; Obstacle length L_o = 20 μm

Table 3.2 shows the mixing efficiency at the micromixer outlet for different mesh densities. The results indicate that the difference in mixing efficiency between mesh MG4 (11798 elements) and MG5 (13286 elements) is negligible (0.01%). Therefore, mesh MG4 was selected as the optimal mesh for the simulations, balancing computational efficiency with solution accuracy. The corresponding mesh distribution plot for the selected mesh (MG4) of the computational domain is shown in Figure 3.2(b).

Table 3.2 Mixing efficiency versus grid numbers at the micromixer outlet.

Grid	Number of domain elements	Mixing efficiency (η)	% Error in η
MG1	4432	0.74134	1.11%
MG2	5044	0.74791	0.24%
MG3	9687	0.74865	0.14%
MG4	11798	0.74958	0.01%
MG5	13286	0.74968	0.00%

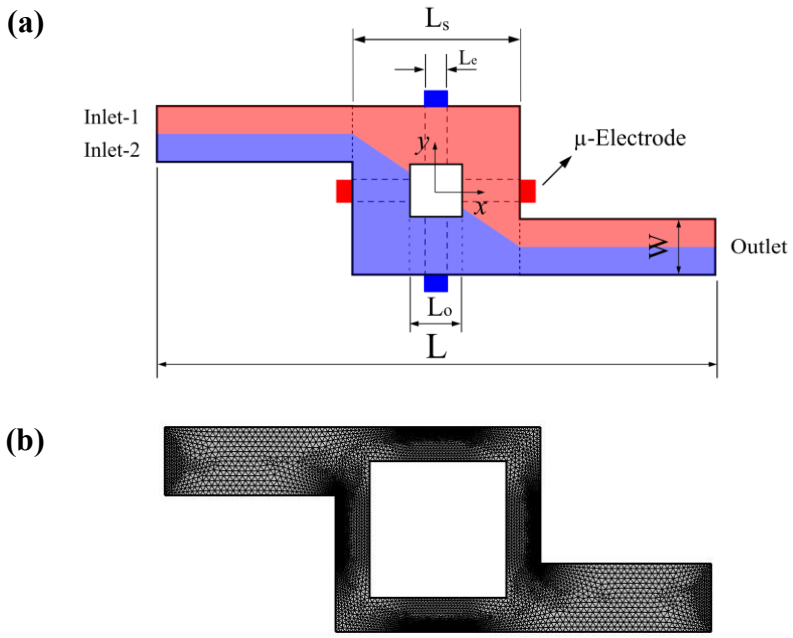

Figure 3.2 Square Split And Recombined (SSAR) electroosmotic micromixer with cross-reciprocal electrodes: (a) Schematic diagram, (b) Grid structure of the computational domain with mesh MG4 for mesh study with u = 200 μm/s, ϕ_0 = 100 mV, f = 8 Hz.

It is important to note that mesh independence studies were conducted for each distinct geometry investigated in this research, with appropriate mesh densities selected based on similar convergence criteria.

3.8 Validation of Numerical Models

Validation of the numerical models is essential to establish confidence in the simulation results. This section describes the validation studies conducted to verify the accuracy of the numerical methods employed in this research.

3.8.1 Validation of Electroosmotic Flow Model

The electroosmotic flow model was validated by comparing numerical predictions with analytical solutions for simple channel geometries. For a straight rectangular channel with uniform zeta potential and DC electric field, the velocity profile from the numerical simulation was compared with the Helmholtz-Smoluchowski analytical solution. The numerical results showed excellent agreement with the analytical solution, with relative errors below 1% throughout the domain.

3.8.2 Validation against Experimental Data

For more complex geometries and flow conditions, validation against experimental data is necessary. The numerical model was validated by comparing simulation results with experimental and numerical measurements from the literature.

Specifically, first the concentration distribution in a T-microchannel with homogeneous surface charge with experimental data of Biddiss et al. (2004) at exit, with an applied electric field strength of 70 V/cm and 280 V/cm (Figure 3.3(a)). Secondly, the concentration distribution in a microchannel with two axisymmetrically placed conducting triangle-shaped constrictions was compared with the experimental and numerical data of Wu and Li (2008) (Figure 3.3(b)). The comparison was made at an axial distance of 500 μm in the downstream direction, with an applied electric field strength of 50 V/cm. Lastly, the concentration plot of a one-ring micromixer by Shamloo et al. (2016) at the outlet (Figure 3.3(c)). These comparisons between the present numerical results and the experimental and numerical data show a good

agreement between the numerical and experimental concentration profiles, validating the accuracy of the numerical approach for the present modeling of electrokinetically driven micromixing processes.

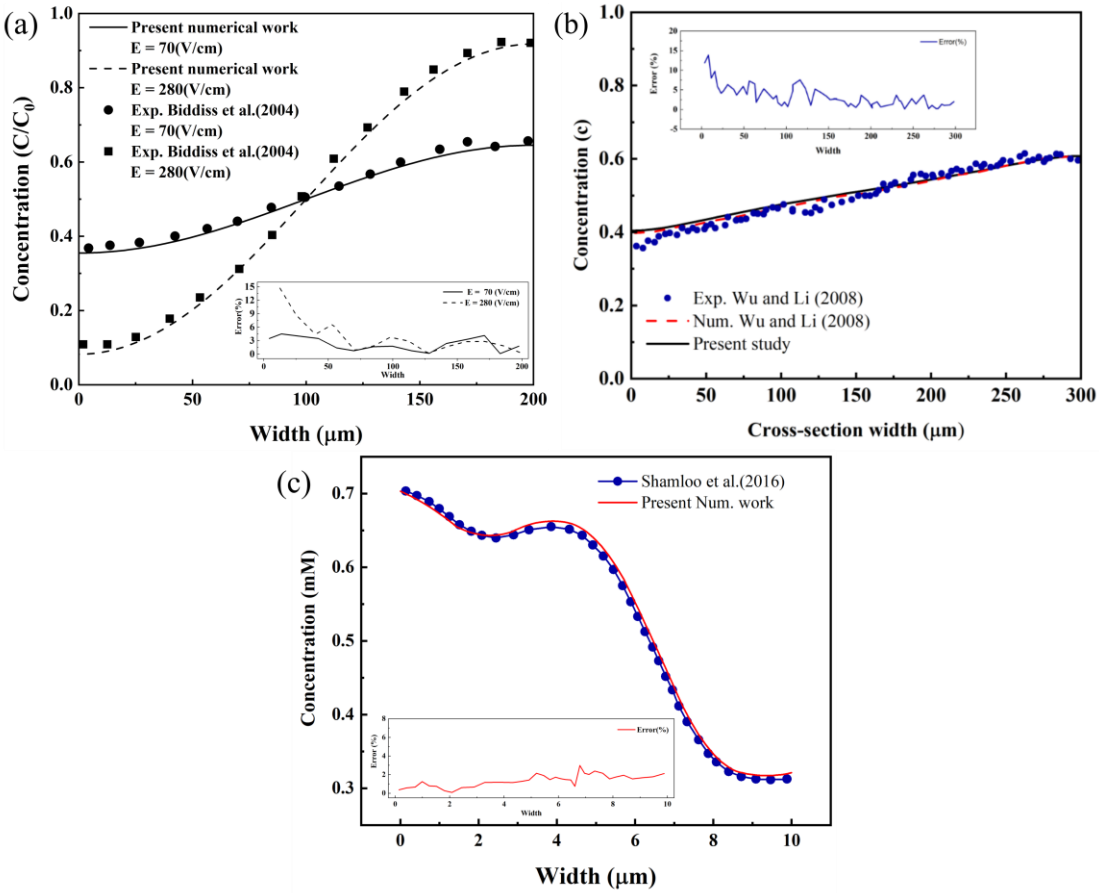

Figure 3.3 Numerical verification against the published results: (a) experimental concentration results of Biddiss et al. (2004) for applied electric field 70 and 280 V/cm; (b) experimental and numerical concentration results of Wu and Li (2008) for applied electric field 50 V/cm at 500 μm offset distance; (c) numerical concentration results of Shamloo et al. (2016) at the outlet of the micromixer.

To further assert the quantitative accuracy, the percentage deviation between the present and reference data has been plotted as an inset in the respective figures, computed using the relation Error (%) = $100 \times |(c_{num} - c_{ref}) / c_{ref}|$, where c_{num} and c_{ref} represent the present numerical and reference (experimental or published numerical) concentrations, respectively. The average percentage error between the experimental results of Biddiss et al. (2004) and the present numerical predictions is 2.25% for an

applied electric field strength of 70 V/cm and 5.17% for 280 V/cm, while the corresponding maximum deviations are 4.50% and 14.5%, respectively. The comparison with the experimental data of Wu and Li (2008) shows an average error of 3.38% and a maximum deviation of 13.87%. For the numerical model validation against Shamloo et al. (2016), the average deviation is 1.39%, with a maximum deviation of only 2.99%. These quantitative results demonstrate that the present numerical model accurately captures the electrokinetically driven micromixing behavior, with deviations well within acceptable limits for microfluidic simulations.

Additional validation was also performed by comparing the numerically predicted mixing efficiency and velocities with numerical and analytical measurements for various mixer geometries and operating conditions. In all cases, the numerical predictions fell within the experimental uncertainty bounds, further confirming the reliability of the numerical approach.

3.9 Closure

This chapter has presented a comprehensive overview of the mathematical formulation and numerical procedures employed in this research. The governing equations for electroosmotic flow and species transport have been established, including the Navier-Stokes equations for fluid dynamics, the Poisson equation for electric potential distribution, and the convection-diffusion equation for species concentration. The boundary conditions, performance metrics, and numerical solution approach using the finite element method have been detailed to provide a robust framework for the investigations that follow.

The numerical methodology is consistently applied throughout the subsequent chapters to analyze four distinct electroosmotic micromixer configurations.

Chapter – 4

Mixing Enhancement in an AC Electroosmotic Micromixer with a Circular Mixing Microchamber

4.1 Introduction

In this chapter, an attempt is made to enhance mixing in microfluidic systems through the implementation of an AC electroosmotic micromixer with a circular mixing microchamber. This design leverages the principles of electrokinetics to induce chaotic advection and improve mixing efficiency, even in low Reynolds number flows characteristic of microfluidic devices.

The circular mixing microchamber represents a novel geometric configuration that, when combined with strategically placed electrodes and AC electric fields, can potentially overcome the limitations of traditional micromixer designs. By introducing time-dependent electroosmotic flows, this approach aims to disrupt the highly ordered laminar flow typically observed in microchannels and promote rapid mixing of fluid species.

This chapter will provide a comprehensive examination of the proposed micromixer design, including its theoretical foundations, numerical modeling, and performance analysis under various operating conditions. Through this investigation, we seek to contribute to the growing body of knowledge on electrokinetic micromixing and offer insights into the design and optimization of more efficient microfluidic mixing devices.

4.2 Relevant background works

The field of microfluidic mixing has seen significant advancements over the past two decades, with researchers exploring various strategies to overcome the challenges posed by laminar flow regimes in microscale devices. This section provides a critical review of the relevant literature, focusing on the development of electrokinetic micromixers and the evolution of design strategies aimed at enhancing mixing efficiency.

Microfluidic devices have gained significant attention in recent years due to their wide-ranging applications in biomedical analysis, chemical synthesis, and environmental monitoring (Hessel et al., 2005; Chin et al., 2007). A critical component of these devices is the micromixer, which facilitates the rapid and efficient mixing of fluids at the microscale. However, achieving effective mixing in microfluidic systems poses unique challenges due to the laminar flow regime typically encountered at such small scales (Soleymani et al., 2008).

Among active mixing techniques, electrokinetic approaches have gained significant attention due to their ability to generate complex flow patterns without moving parts. Green et al. (2000) conducted pioneering work on AC electroosmotic flow, elucidating the fundamental mechanisms of fluid motion induced by non-uniform AC electric fields. This laid the groundwork for subsequent research on electrokinetic micromixers.

Chen et al. (2013) developed an AC electroosmotic micromixer using asymmetric pairs of planar electrodes, demonstrating improved mixing performance through the generation of localized vortices. Huang et al. (2007) further advanced this concept by introducing a multi-electrode configuration that enhanced mixing efficiency for both stationary and continuous fluid flows.

Recent research has focused on optimizing electrokinetic micromixer designs through advanced modeling and simulation techniques. Deng et al. (2018) employed topology optimization to determine optimal electrode patterns for electroosmotic micromixers, showcasing the potential for computational methods in device design. Nazari et al. (2020) conducted a comprehensive geometrical study on an induced-charge electrokinetic micromixer, highlighting the importance of electrode placement and configuration.

While various geometries have been explored for micromixer designs, the use of circular mixing chambers in electrokinetic systems remains relatively unexplored. Bagherabadi et al. (2019) investigated the effect of chamber aspect ratio on mixing efficiency in rectangular electrokinetic mixers, suggesting that chamber geometry plays a crucial role in device performance. However, the specific advantages and challenges associated with circular mixing chambers in the context of AC electroosmotic mixing have not been thoroughly addressed in the literature.

4.3 Research Gaps and Opportunities

Despite the significant progress in electrokinetic micromixer development, several research gaps remain:

- Limited understanding of the interplay between circular chamber geometry and AC electroosmotic effects on mixing efficiency.
- Lack of comprehensive studies on the optimization of electrode placement and AC signal parameters in circular mixing chambers.
- Insufficient exploration of the non-linear characteristics of electroosmotic flows in complex geometries.
- Need for more robust numerical models that accurately capture the multiphysics nature of electrokinetic mixing processes.

This literature review highlights the need for further investigation into AC electroosmotic micromixers with circular mixing chambers, setting the stage for the objectives and approach of the present study.

4.4 Objectives of the Study

Based on the identified research gaps and the potential advantages of circular mixing chambers in electrokinetic micromixers, this study aims to address the following objectives:

1. Design and analyze an AC electroosmotic micromixer incorporating a circular mixing microchamber to enhance mixing efficiency in microfluidic systems.
2. Investigate the influence of key geometric parameters, particularly the diameter of the circular mixing chamber, on the mixing performance of the proposed device.
3. Evaluate the effects of operational parameters, including inlet velocity, AC voltage amplitude, and frequency, on the mixing efficiency and flow characteristics within the circular chamber.
4. Develop a comprehensive understanding of the non-linear electrokinetic phenomena and their interaction with the circular chamber geometry to optimize mixing performance.

5. Identify optimal operating conditions and design guidelines for the proposed micromixer to achieve maximum mixing efficiency across a range of flow rates relevant to microfluidic applications.
6. Assess the potential advantages and limitations of the circular mixing chamber design compared to conventional rectangular geometries in the context of AC electroosmotic mixing.
7. Contribute to the broader understanding of electrokinetic mixing mechanisms in complex geometries and provide insights for the design of more efficient microfluidic mixing devices.

By addressing these objectives, this study aims to advance the field of electrokinetic micromixing and provide valuable insights for the development of next-generation microfluidic devices with enhanced mixing capabilities.

4.5 Design and Concept of Circular Mixing Microchamber

The proposed AC electroosmotic micromixer with a circular mixing microchamber represents a novel approach to enhancing mixing efficiency in microfluidic systems. This section details the design considerations, conceptual framework, and potential advantages of incorporating a circular geometry into the mixing chamber.

4.5.1 *Geometric Configuration*

The micromixer design consists of the following key components:

- ***Main microchannel:*** A straight channel with two inlets and one outlet, providing the primary flow path for the fluids to be mixed. The length (L) and width (W) of the microchannel are fixed at 80 μm and 10 μm, respectively.
- ***Circular mixing microchamber:*** A circular chamber positioned at the center of the micromixer, designed to induce complex flow patterns and enhance mixing. The diameter (D) of the mixing chamber is varied from 20 μm to 40 μm to investigate its impact on mixing efficiency.
- ***Electrode configuration:*** Two pairs of symmetrically cross-reciprocal microelectrodes positioned on the peripheral wall of the circular chamber at $\pi/4$ and $3\pi/4$ radians.

Figure 4.1 presents a schematic diagram of the proposed micromixer design, illustrating the arrangement of these components.

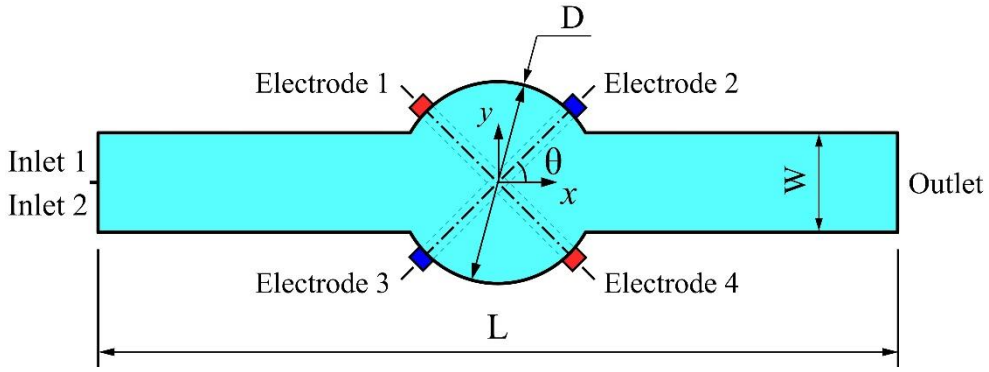

Figure 4.1 Schematic diagram of the AC electroosmotic micromixer with circular mixing microchamber, depicting the main microchannel, inlets, outlet, circular mixing chamber, and electrode positions.

4.5.2 *Rationale for Circular Chamber Design*

The incorporation of a circular mixing chamber offers several potential advantages over traditional rectangular geometries:

1. ***Symmetry and uniformity:*** The circular geometry provides radial symmetry, potentially leading to more uniform mixing across the chamber.
2. ***Elimination of corner effects:*** The absence of sharp corners reduces the likelihood of dead zones or regions of stagnant flow, which can impede mixing in rectangular chambers.
3. ***Enhanced vortex formation:*** The curved walls of the circular chamber may facilitate the formation and propagation of electroosmotic vortices, promoting chaotic advection.
4. ***Optimized electrode placement:*** The circular geometry allows for strategic positioning of electrodes to maximize the impact of electroosmotic effects on fluid motion.
5. ***Potential for scale-invariant behavior:*** The circular design may exhibit similar mixing characteristics across different size scales, offering flexibility in device fabrication and application.

4.5.3 *Electrokinetic Actuation Mechanism*

The mixing enhancement in the proposed device relies on the principles of AC electroosmosis. When an alternating electric field is applied to the electrodes, it induces time-dependent electroosmotic slip velocities at the fluid-solid interface. These slip velocities generate complex flow patterns within the circular chamber,

disrupting the traditional laminar flow with parallel streamline patterns and promoting mixing through chaotic advection.

The key features of the electrokinetic actuation mechanism include:

- ***Time-varying electric field:*** The application of an AC signal with a frequency (2–18 Hz) and a voltage amplitude (100–500 mV) creates a dynamic electric field within the chamber.
- ***Induced charge electroosmosis:*** The interaction between the applied field and the electrical double layer (EDL) at the electrode-fluid interface results in induced charges and subsequent fluid motion.
- ***Vortex generation:*** The symmetrical arrangement of electrodes promotes the formation of counter-rotating vortices within the circular chamber.
- ***Chaotic advection:*** The time-dependent nature of the AC field leads to periodic stretching and folding of fluid elements, enhancing mixing through chaotic advection.

4.5.4 *Theoretical Considerations*

The behavior of fluid within the circular mixing chamber under AC electroosmotic actuation can be described by a combination of electrokinetic and fluid dynamic principles. The key governing equations, as detailed in Chapter 3, include:

1. Navier-Stokes equations for incompressible flow
2. Continuity equation
3. Poisson equation for electric potential distribution
4. Helmholtz-Smoluchowski equation for electroosmotic slip velocity
5. Convection-diffusion equation for species transport

The circular geometry introduces additional complexities in solving these equations, particularly in terms of boundary conditions and the representation of electric field distributions. These challenges necessitate careful consideration in the numerical modeling and analysis of the proposed micromixer.

4.5.5 *Design Parameters and Variables*

The performance of the AC electroosmotic micromixer with a circular mixing chamber is influenced by several key parameters:

1. **Geometric parameters:**
    - Diameter of the circular chamber (D)
    - Width of the main microchannel (W)
    - Length of the micromixer (L)
    - Electrode size and positioning
2. **Operational parameters:**
    - Inlet velocity (u_0)
    - AC voltage amplitude (ϕ_0)
    - AC frequency (f)
3. **Fluid properties:**
    - Viscosity (μ)
    - Density (ρ)
    - Diffusion coefficient of species (D_i)
4. **Electrical properties:**
    - Electrolyte conductivity (σ)
    - Dielectric constant (ε)
    - Zeta potential at the wall-fluid interface (ζ)

The interplay between these parameters and their impact on mixing efficiency forms the basis of the investigation presented in this chapter. By systematically varying geometric and operational parameters while maintaining constant fluid and electrical properties, the study aims to optimize the micromixer design for enhanced mixing performance. The values of these parameters are summarized in Table 4.1.

Table 4.1 Constant properties and initial parameters employed in numerical modeling.

Symbol	Description	Values
ρ	Fluid density	1000 kg/m^3
μ	Dynamic viscosity of fluid	1.0×10^{-3} Pa·s
κ	Conductivity of the fluid	118.45×10^{-3} S/m
ε_0	Permittivity of vacuum	8.854×10^{-12} F/m
ε_r	Relative permittivity of fluid	80.2
ζ_0	Zeta potential	-100 mV
D_i	Diffusion coefficient of fluid	1.0×10^{-11} m²/s

c_o	Initial concentration of fluid species	1 mM
f	Alternating voltage frequency	2-18 Hz
ϕ_o	Voltage amplitude	100-500 mV

4.6 Results and Discussion

This section presents a comprehensive analysis of the performance of the AC electroosmotic micromixer with a circular mixing microchamber. The results are derived from numerical simulations based on the established theoretical model and computational framework, supported by validation studies (both experimental and numerical) described in Chapter 3.

An additional key observation from the electroosmotic micromixer with cross-reciprocal electrodes—supported by insights from both literature and the present investigation across all four configurations—reveals that vortex generation plays a pivotal role in enhancing overall mixing performance. The interaction between the alternating electric field and the induced flow field leads to the formation of counter-rotating vortex pairs within the mixing chamber. These vortices create localized recirculation zones that continuously stretch and fold the concentration interface between incoming fluid streams, thereby intensifying convective transport. The periodic disruption of flow symmetry caused by vortex motion accelerates diffusive mixing and promotes greater concentration uniformity throughout the domain. The enhancement becomes particularly prominent at frequencies where the electroosmotic and convective time scales are optimally synchronized, resulting in strong fluid deformation and rapid homogenization. This vortex-driven mechanism provides a clear physical explanation for the observed improvement in mixing efficiency and offers critical guidance for determining the optimal combinations of geometric design and operating parameters governing flow and electric field interactions.

Hence, the following discussion primarily focuses on the effects of geometric and operational parameters on mixing efficiency, flow characteristics, and overall device performance.

4.6.1 *Effect of Mixing Chamber Diameter on Micromixing Performance*

The diameter of the circular mixing chamber significantly influences the micromixing performance of the proposed device. This section presents a

comprehensive analysis of the effect of chamber diameter on mixing efficiency, fluid dynamics, and electrokinetic phenomena.

To investigate the impact of mixing chamber diameter, a set of selective parameter values are chosen with varying chamber diameters. The simulations are conducted with diameters ranging from 20 µm to 40 µm, while maintaining constant inlet velocity (u_0 = 100 µm/s), voltage amplitude (ϕ_0 = 100 mV), and frequency (f = 8 Hz). The 20 µm diameter chamber was initially considered as the base case. It is crucial to note that once fabricated, the geometry of the micromixer cannot be altered, emphasizing the importance of determining the optimal size during the design phase.

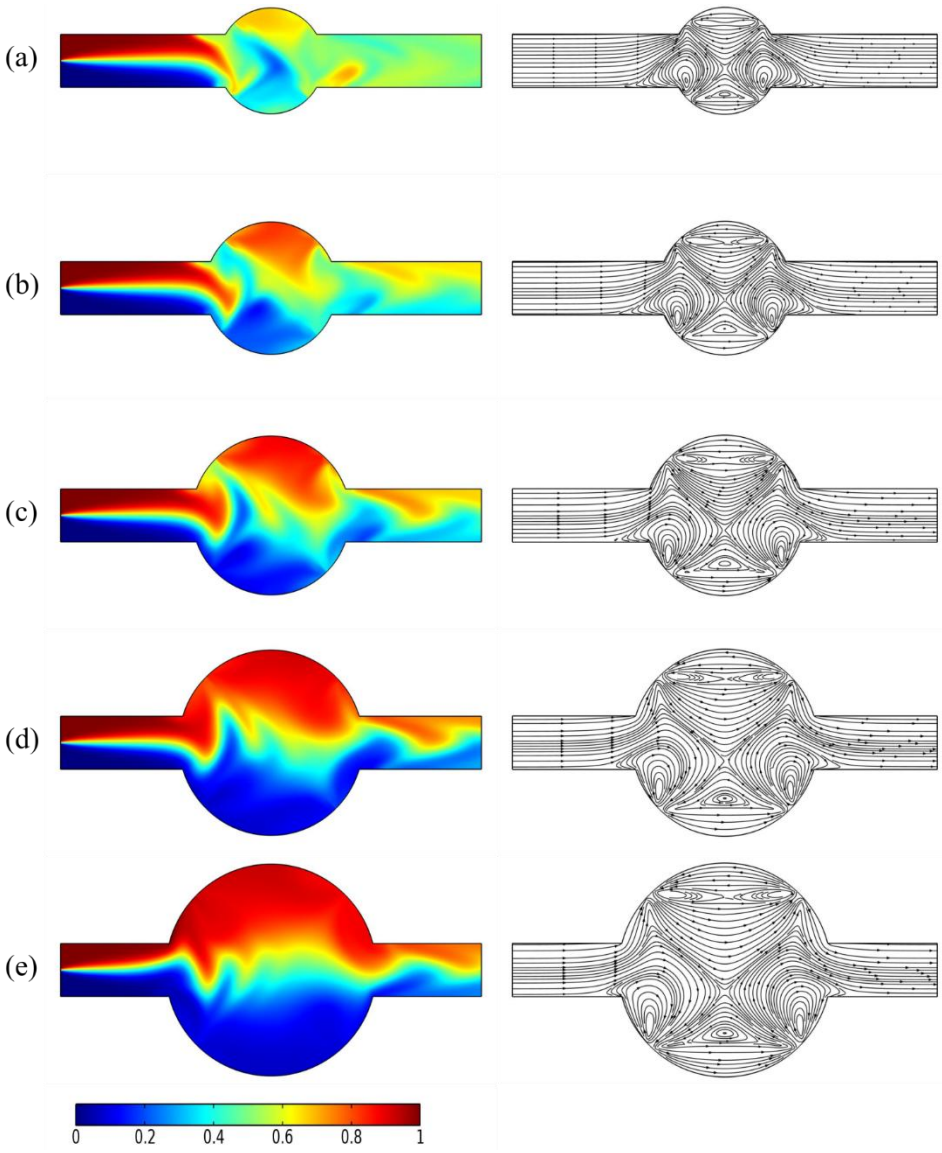

Figure 4.2 Spatial distribution of species concentration and fluid streamlines in circular mixing microchambers of varying diameters. (a) D = 20 µm, (b) D = 25 µm, (c) D = 30 µm, (d) D = 35 µm, and (e) D = 40 µm. Simulation parameters: inlet velocity (u_0) = 100 µm/s, AC voltage amplitude (ϕ_0) = 100 mV, frequency (f) = 8 Hz, at a time (t) = 0.575 s.

Figure 4.2 presents the concentration and streamline profiles within the micromixer for different chamber diameters at t = 0.575 s. Key observations from this analysis include:

1. **Mixing Mechanisms:** At the inlet section, interfacial diffusion is the primary mixing mechanism. Within the mixing chamber, mixing is predominantly driven by the alternating pull and push of fluid streams, induced by the electrical field generated by the AC electrodes.
2. **Vortex Formation:** Four distinct vortices are observed within the mixing chamber for all diameters, spanning from one electrode to the neighboring electrode. These vortices vary in size over time but remain symmetrical about the y-axis.
3. **Diameter-Dependent Mixing:** As the chamber diameter increases, the mixing of fluid species decreases. This trend is attributed to the reduced electric field strength within larger chambers, as the distance between electrodes increases.
4. **Lateral Displacement:** Smaller chamber diameters lead to increased lateral displacement of vortices in the main channel. This enhanced displacement results in closer streamlines at the intake and exit zones of the smallest diameter mixing chamber, altering the fluid velocity distribution.
5. **Electric Field Effects:** The decrease in chamber diameter intensifies the electric field strength between electrodes, contributing to stronger electrokinetic effects. This intensification significantly enhances the generation of chaotic motion within the laminar flow field, particularly for the smallest chamber diameter.

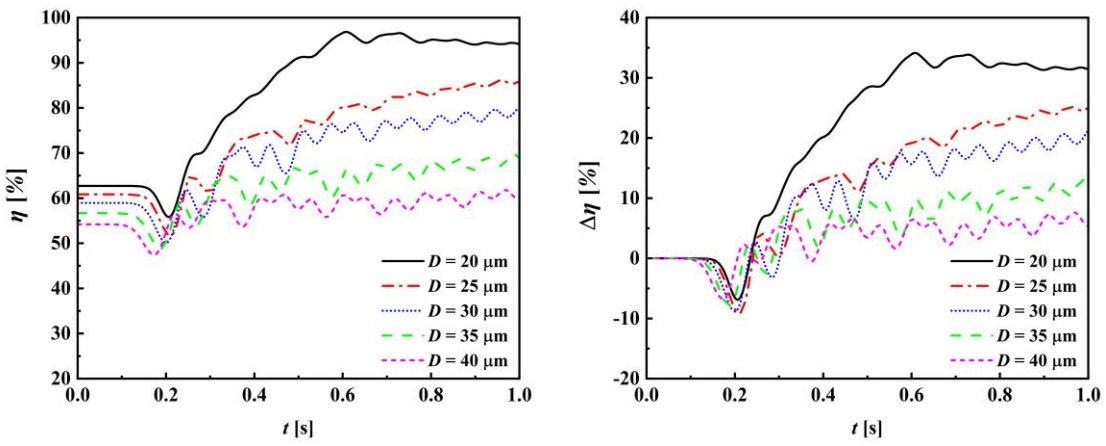

Figure 4.3 Temporal evolution of mixing efficiency for circular mixing microchambers with diameters ranging from 20 to 40 µm. (a) Absolute mixing efficiency vs. time. (b) Relative mixing efficiency with respect to steady state vs. time. Simulation parameters: inlet velocity (u_0) = 100 µm/s, AC voltage amplitude (ϕ_0) = 100 mV, frequency (f) = 8 Hz.

To quantitatively assess the micromixer's performance, the mixing efficiency at the microchannel exit was calculated for all time steps of the numerical study. Figure 4.3 illustrates the variation of mixing efficiency with time for different chamber diameters. The results reveal several important findings:

1. **Diameter-Efficiency Correlation:** The mixing efficiency consistently decreases as the mixing chamber diameter increases. This trend is observed throughout the simulation period.
2. **Temporal Evolution:** The relative mixing efficiency with respect to steady state (Figure 4.3b) demonstrates that smaller chamber diameters achieve steady-state mixing more rapidly.
3. **Optimal Performance:** The 20 µm diameter chamber consistently achieves the highest mixing efficiency throughout the simulation period. This optimal diameter effectively balances the intensification of electrokinetic effects with the residence time of fluid elements within the mixing chamber.
4. **Chaotic Motion Enhancement:** The utilization of an alternating current sinusoidal time-varying electric field applied to the electrodes significantly enhances the generation of chaotic motion within the laminar flow field. This effect is particularly pronounced for the smallest chamber diameter.
5. **Laminar Flow Disruption:** The increased volume of chaotic motion and vortices in smaller chambers effectively breaks the highly ordered laminar flow, thus enhancing the overall mixing efficiency of the micromixer.

Based on this comprehensive analysis, it can be conclude that the 20 µm diameter chamber offers the optimal mixing performance for the proposed micromixer design. This configuration maximizes the benefits of strong electrokinetic effects, enhanced vortex formation, and efficient laminar flow disruption. The selection of the 20 µm chamber diameter as the optimal design parameter has significant implications for the remainder of this study. All subsequent analyses and optimizations have been conducted using this fixed chamber diameter, allowing us to

focus on other critical parameters such as fluid flow characteristics and electric field properties.

This rigorous approach to design optimization ensures that the proposed micromixer achieves the highest possible mixing efficiency while maintaining practicality for potential fabrication and implementation in microfluidic systems.

4.6.2 *Influence of Inlet Velocity*

To identify the suitable range of inlet velocities for efficient mixing, simulations were conducted for velocities ranging from 50 μm/s to 500 μm/s, while maintaining constant chamber diameter (D = 20 μm), voltage amplitude (ϕ_0 = 100 mV), and frequency (f = 8 Hz). Figure 4.4 presents the mixing efficiency and relative mixing efficiency change with respect to steady-state for different inlet velocities. Figure 4.5 illustrates the concentration and streamline profiles within the micromixer for different inlet velocities at t = 0.55 s.

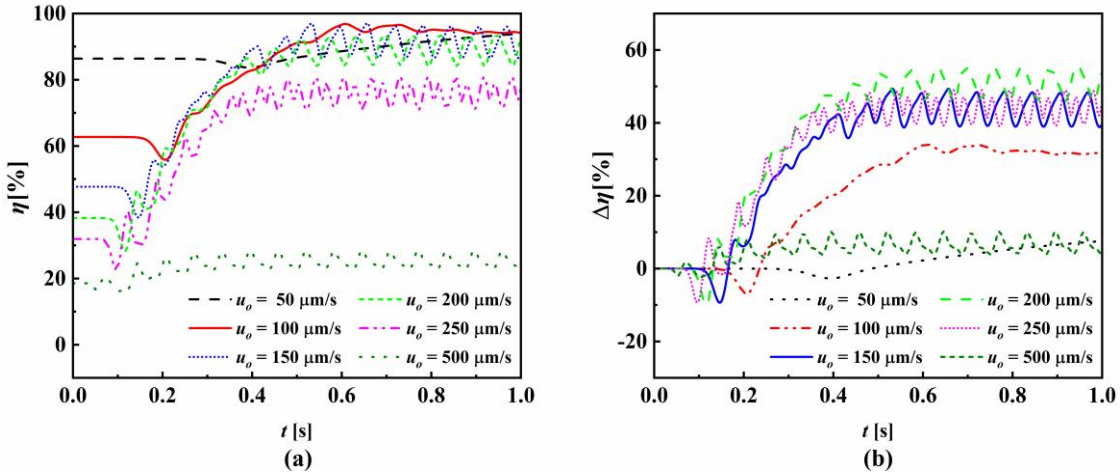

Figure 4.4 Effect of inlet velocity on mixing efficiency [D = 20 μm, ϕ_0 = 100 mV, f = 8 Hz]: (a) Mixing efficiency versus time for various inlet velocities, and (b) Relative mixing efficiency change with respect to steady state for different inlet velocities.

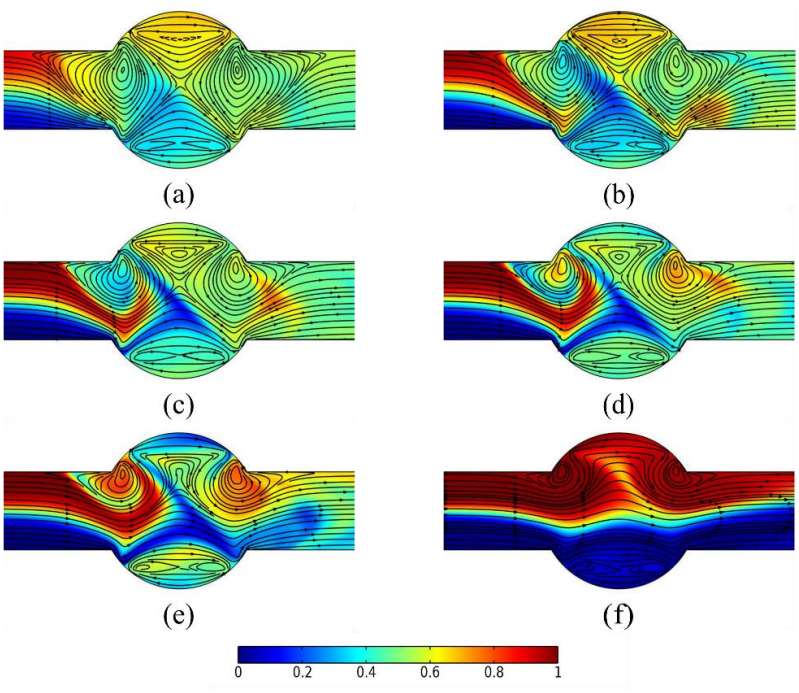

Figure 4. 5 Concentration and streamline profiles for various inlet velocities at t = 0.55 s [D = 20 µm, ϕ_0 = 100 mV, f = 8 Hz]: (a) u_0 = 50 µm/s, (b) u_0 = 100 µm/s, (c) u_0 = 150 µm/s, (d) u_0 = 200 µm/s, (e) u_0 = 250 µm/s, and (f) u_0 = 500 µm/s.

Key findings from the analysis of Figures 4.4 and 4.5 include:

1. **Optimal velocity range:** The velocity range of 100 µm/s ≤ u_0 ≤ 200 µm/s appears to be critical, indicating a balance between fluid inertia, electroosmotic forces, and species diffusion within the mixing microchamber.
2. **Non-linear behavior:** The relationship between inlet velocity and mixing efficiency is non-linear, contrary to expectations based on previous literature. After an initial decrease, there is a rapid increase in mixing efficiency with increasing velocity, with the rate of change varying for different velocities.
3. **Mixing efficiency:** The highest mixing efficiency of 94.15% is achieved at u_0 = 100 µm/s. The mixing efficiencies at the end of the simulation time for inlet velocities of 50, 100, 150, 200, 250, and 500 µm/s are 93.94%, 94.15%, 87.48%, 92.12%, 77.71%, and 22.50%, respectively.
4. **Relative mixing efficiency:** The maximum change in mixing efficiency relative to the steady-state solution (53.92%) occurs at u_0 = 200 µm/s. The relative mixing efficiency changes for inlet velocities of 50, 100, 150, 200, 250, and 500 µm/s are 7.56%, 31.43%, 39.75%, 53.92%, 45.78%, and 3.94%, respectively.

5. **Vortex formation:** Four primary vortices are generated due to the applied AC field at low inlet velocities. The volume of these vortices within the microchannel decreases with increasing inlet fluid velocity.
6. **Secondary vortices:** Within the optimal velocity range (100 μm/s ≤ u_o ≤ 200 μm/s), secondary vortices are observed near the upper wall of the mixing chamber. These secondary vortices enhance the stretching and folding of fluid streams, resulting in increased mixing at higher intake volumes.

The presence of an optimal velocity range and the observed non-linear behavior suggest a complex interplay between fluid inertia, electroosmotic forces, and species diffusion within the mixing chamber. The formation of secondary vortices within this range further supports the existence of a balance between these forces, contributing to enhanced mixing performance.

These results underscore the importance of carefully selecting the inlet velocity to optimize mixing performance in the proposed device. The identified optimal range provides a guideline for future designs and applications of similar micromixers in microfluidic systems.

4.6.3 *Impact of AC Voltage Amplitude*

The amplitude of the applied AC voltage significantly influences the strength of induced electroosmotic flow and, consequently, the mixing performance in microchannels. To investigate this effect, simulations were conducted for voltage amplitudes ranging from 100 mV to 500 mV, considering inlet velocities of 100 μm/s, 150 μm/s, and 200 μm/s, while maintaining a constant frequency of 8 Hz, as presented in Figures 4.6 and 4.7.

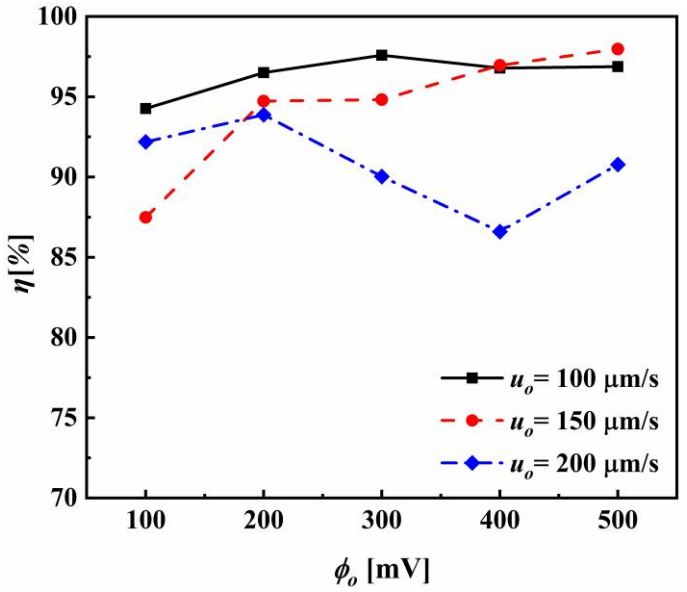

Figure 4.6 Mixing efficiency as a function of voltage amplitude for various inlet velocities at t = 1.0 s.

Figure 4.6 illustrates the mixing efficiency variation with potential amplitude at the simulation endpoint (t = 1.0 s) for different inlet velocities. The results reveal a non-linear relationship between mixing efficiency and voltage amplitude. For an inlet velocity of 100 μm/s, the mixing efficiency peaks at 97.59% with a 300 mV potential amplitude. In contrast, at 150 μm/s, the maximum mixing efficiency of 97.97% is achieved at 500 mV. For 200 μm/s, the highest efficiency of 93.88% occurs at 200 mV.

These observations indicate that the optimal voltage amplitude varies depending on the inlet velocity, suggesting a complex interplay between electroosmotic forces and fluid inertia. The non-linear relationship implies that increasing voltage does not always lead to improved mixing, as excessive electroosmotic forces may overpower fluid inertia and species diffusion.

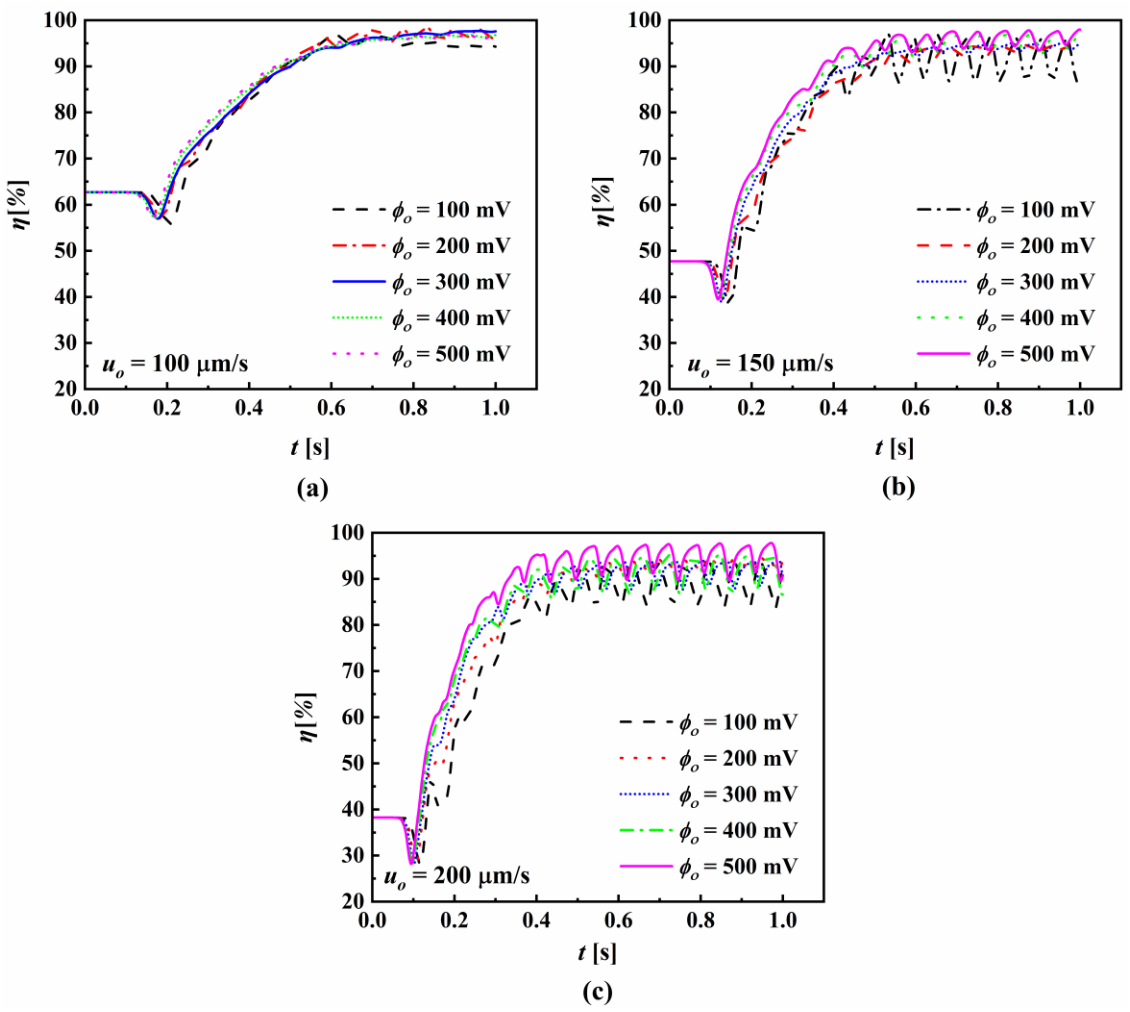

Figure 4.7 Temporal evolution of mixing efficiency for voltage amplitudes ranging from 100 mV to 500 mV at inlet velocities of (a) 100 µm/s, (b) 150 µm/s, and (c) 200 µm/s.

Figure 4.7 presents the temporal evolution of mixing efficiency for various voltage amplitudes and inlet velocities. Several key observations emerge:

1. Higher voltage amplitudes generally yield better mixing efficiency throughout most of the simulation duration.
2. Increasing inlet velocity leads to more pronounced fluctuations in mixing efficiency, likely due to the intensified competition between inertial forces and electrokinetic effects.
3. Mixing efficiency curves for higher voltages show rapid initial increases, followed by oscillations that gradually stabilize.
4. At lower velocities (100 µm/s), the mixing efficiency curves are smoother, indicating a more stable mixing process.

The fluctuations in mixing efficiency become more prominent at higher velocities, possibly due to rapid variations in inertial forces under the influence of

electrokinetic effects. This phenomenon underscores the importance of considering the entire simulation duration rather than relying solely on endpoint measurements when optimizing mixer design.

These findings suggest that while higher voltage amplitudes generally improve mixing, the optimal choice depends on the inlet velocity and desired stability of the mixing process. For applications requiring consistent mixing performance, a moderate voltage amplitude might be preferable, especially at higher inlet velocities. The results highlight the need for careful tuning of operational parameters to achieve optimal mixing in microfluidic devices.

4.6.4 *Effect of AC Frequency*

The frequency of the applied AC signal significantly influences the electroosmotic flow patterns by determining the rate of polarity switches on the microelectrodes. To investigate this effect, simulations were conducted (as shown in Figures 4.8 and 4.9) for frequencies ranging from 2 Hz to 18 Hz, maintaining a constant voltage amplitude of 500 mV. The study considered inlet velocities of 100 µm/s, 150 µm/s, and 200 µm/s.

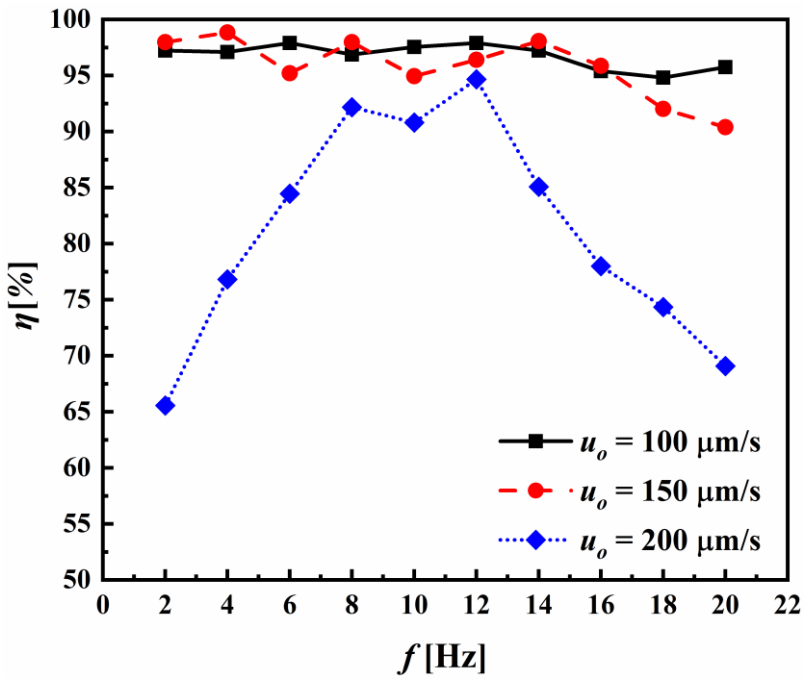

Figure 4.8 Mixing efficiency as a function of AC frequency for inlet velocities of 100, 150, and 200 µm/s at t = 1 s.

Figure 4.8 illustrates the mixing efficiency at the simulation endpoint (t = 1.0 s) for various frequencies and inlet velocities. The results reveal a complex relationship between frequency and mixing performance, with no monotonic trend observed. The highest overall mixing efficiency of 98.84% is achieved at 4 Hz for an inlet velocity of 150 µm/s. Also, for an inlet velocity of 150 µm/s, the mixing efficiency is relatively consistent.

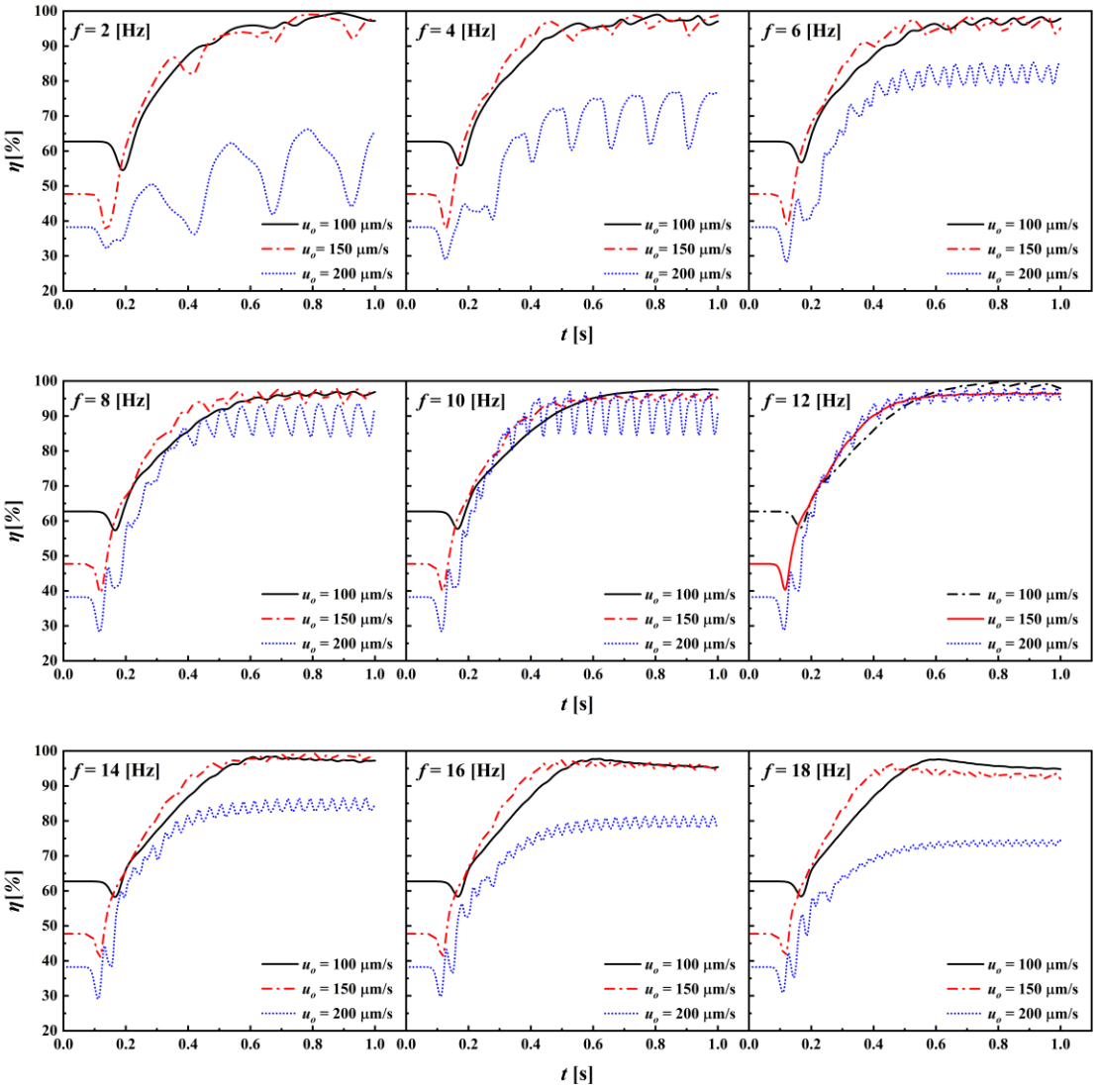

Figure 4.9 Temporal evolution of mixing efficiency for frequencies f = 2–18 Hz and inlet velocities of 100, 150, and 200 µm/s.

To gain deeper insights into the transient behavior, Figure 4.9 presents the temporal evolution of mixing efficiency for different frequencies and inlet velocities. Lower inlet velocities (100 µm/s) exhibit smoother mixing efficiency curves with fewer fluctuations across all frequencies. In contrast, higher inlet velocities (200 µm/s) show more pronounced oscillations in mixing efficiency, particularly at lower

frequencies. This observation indicates a stronger influence of inertial forces at higher velocities, leading to increased fluctuations in the mixing process.

A frequency of 12 Hz appears to provide the most stable mixing performance across all inlet velocities. At this frequency, mixing efficiencies of 97.55%, 96.40%, and 94.66% are achieved for 100 μm/s, 150 μm/s, and 200 μm/s, respectively. Notably, the mixing efficiency corresponding to the 12 Hz frequency remains above 94.66% for all inlet velocities in the range of 100–200 μm/s. This suggests that 12 Hz offers a good compromise between mixing efficiency and stability across various flow rates.

Interestingly, frequencies above 12 Hz generally lead to a deterioration in mixing efficiency. This phenomenon can be attributed to excessively rapid polarity switches, which may hinder effective mixing by not allowing sufficient time for the establishment of stable electroosmotic flow patterns.

The study also reveals that the smoothest transitions in mixing efficiency curves for inlet velocities of 100, 150, and 200 μm/s correspond to frequencies of 10, 12, and 12 Hz, respectively. This finding underscores the importance of selecting an appropriate frequency to minimize fluctuations in the mixing process, particularly at higher flow rates.

These results highlight the critical role of AC frequency in optimizing mixing performance. While lower frequencies can achieve higher peak efficiencies, they may also lead to more unstable mixing processes, especially at higher inlet velocities. The complex interplay between frequency, inlet velocity, and mixing efficiency emphasizes the need for careful tuning of these parameters to achieve optimal micromixer performance.

In conclusion, this study provides valuable insights into the design and operation of AC electroosmotic micromixers. By carefully selecting the AC frequency and considering its interaction with inlet velocity, researchers and engineers can develop more efficient and reliable microfluidic mixing devices for a wide range of applications.

4.6.5 *Optimal Conditions for Micromixer Performance*

The comprehensive analysis of various parameters influencing the micromixer's performance has yielded insights into the optimal conditions for achieving maximum mixing efficiency. Table 2 summarizes the key findings:

Table 4.2 Optimal parameters and maximum mixing efficiencies.

Parameter	Optimal Value	Maximum η
Chamber Diameter	20 μm	94.15%
Inlet Velocity	100-200 μm/s	94.15% (at 100 μm/s)
Voltage Amplitude	300 mV (for 100 μm/s)	97.59%
	500 mV (for 150 μm/s)	97.97%
	200 mV (for 200 μm/s)	93.88%
	4 Hz (for 150 μm/s)	98.84%

It is important to note here that the optimal parameters are interdependent, and the maximum mixing efficiency can vary based on the combination of parameters used. The results in Table 4.2 indicate that the smallest mixing chamber diameter (20 μm) provides the best mixing efficiency due to increased electric field strength and enhanced chaotic motion. An inlet velocity range of 100-200 μm/s demonstrates a balance between fluid inertia, electroosmotic forces, and liquid diffusivity, with peak performance at 100 μm/s. Voltage amplitude optimization varies with inlet velocity, with the highest efficiency (97.97%) observed at 500 mV for 150 μm/s. The AC frequency study revealed that 4 Hz yields the overall maximum mixing efficiency (98.84%) at 150 μm/s, while 12 Hz provides consistently high efficiency across the optimal velocity range.

These findings underscore the interdependence of parameters in optimizing mixer performance. The combination of a small mixing chamber, moderate inlet velocity, appropriately tuned voltage amplitude, and optimal AC frequency creates an environment conducive to enhanced chaotic advection and efficient mixing at the microscale.

4.6.6 *Potential Challenges and Limitations*

While the circular mixing chamber design offers several potential advantages, it also presents certain challenges that must be addressed:

1. Fabrication complexity: The circular geometry may require more sophisticated microfabrication techniques compared to rectangular designs.
2. Flow distribution: Ensuring uniform flow distribution from the inlet channels into the circular chamber may require careful design considerations.
3. Electric field non-uniformity: The curved electrode surfaces may lead to non-uniform electric field distributions, potentially affecting mixing performance.
4. Scaling effects: The optimal chamber diameter may vary with flow rate and fluid properties, necessitating careful optimization for specific applications.
5. Integration with other microfluidic components: The circular design may pose challenges in seamlessly integrating the mixer with other rectangular microfluidic elements.

By addressing these challenges through careful design and optimization, the proposed AC electroosmotic micromixer with a circular mixing chamber has the potential to offer significant improvements in mixing efficiency for a wide range of microfluidic applications.

4.7 Conclusion

This chapter presents a comprehensive investigation into the design and performance of an AC electroosmotic micromixer with a circular mixing microchamber. Through systematic numerical simulations and analysis, the effects of various geometric and operational parameters on mixing efficiency have been explored. The key findings and conclusions of this study are as follows:

1. **Electroosmotic Mixing Mechanism**: The continuous change in a potential difference between time-varying voltage signals at the micro-electrodes disrupts the highly lamellar-ordered flow lines around the micro-electrodes in the microscale domain. This perturbation varies throughout the transient process, disrupting the lamellar diffusive mixing of species concentration and enhancing the mixing ability of the microscale mixer.
2. **Microchamber Geometry**: A smaller mixing chamber diameter (20 μm) resulted in superior mixing performance. This improvement is attributed to the

reduced linear distance between cross-reciprocal-mounted micro-electrodes, which intensifies the electroosmosis force within the micro-chamber.

3. **Inlet Velocity**: An optimal range of inlet velocities (100-200 μm/s) was identified, balancing fluid inertia, electroosmotic forces, and species diffusion to achieve efficient mixing. Interestingly, the relationship between inlet velocity and mixing efficiency is not monotonic for this micromixer design, as evidenced by the highest mixing efficiency achieved at 150 μm/s.
4. **AC Voltage Amplitude**: Higher voltage amplitudes generally improve mixing efficiency, with electrokinetic disturbances becoming more prominent at higher voltage amplitudes. A voltage of 500 mV provided the best overall performance across different velocities, demonstrating the importance of this parameter in optimizing mixing.
5. **AC Frequency**: The AC-frequency variation is associated with the number of directional (polarity) switches of voltage amplitude on micro-electrodes for a specified time period of the transient study. A frequency of 12 Hz offered the most stable mixing performance across all inlet velocities, with mixing efficiencies consistently above 94.66%. This finding provides a wide range for operational control of inlet velocity in various microfluidic devices.
6. **Overall Performance**: The micromixer achieved a maximum mixing efficiency of 98.84% at an inlet velocity of 150 μm/s, corresponding to a frequency of 4 Hz and a voltage amplitude of 500 mV. This result further asserts that the relationship between velocity and mixing efficiency is complex and not simply inversely proportional to the present structure of the micromixer.

These results demonstrate the potential of circular mixing microchambers in enhancing electroosmotic mixing. The ability to achieve high mixing efficiencies (>94.66%) across a range of inlet velocities (100-200 μm/s) at 12 Hz and 500 mV provides operational flexibility for various microfluidic applications. This flexibility is particularly valuable in the design and implementation of lab-on-a-chip devices and other microfluidic systems where precise control over mixing is crucial.

The present investigation offers a new basis for the advancement of simple electroosmotic micromixers utilizing circular mixing microchambers. It contributes to the expansion and projection of concepts for future research in the domain of

electroosmotic micromixing involving mixing microchambers. Future work could focus on several areas:

1. Optimizing electrode configurations to further enhance mixing efficiency.
2. Exploring pulsed AC signals to potentially achieve even higher mixing rates.
3. Investigating the performance of the mixer with different fluid properties to broaden its applicability.
4. Conducting experimental validation of these numerical results to bridge the gap between simulation and practical implementation.

In conclusion, this study contributes significantly to the growing body of knowledge on electrokinetic micromixers. By elucidating the complex interplay between geometric parameters, operational conditions, and mixing efficiency, it provides valuable insights for the design and optimization of efficient mixing strategies in microfluidic devices. The findings herein lay a solid foundation for future advancements in microscale mixing technologies, potentially impacting fields ranging from chemical analysis to biomedical diagnostics. Future work could focus on further refining these parameters, exploring potential synergistic effects, and investigating the scalability of these optimal conditions for larger or more complex microfluidic systems. Additionally, the robustness of these optimal conditions under various fluid properties and environmental factors could be examined to broaden the applicability of this micromixer design.

Chapter – 5

Mixing Enhancement in an AC Electroosmotic Micromixer with a Diamond Mixing Microchamber

5.1 Introduction

Building upon the circular mixing chamber design presented in Chapter 4, this chapter investigates an alternative geometric configuration—a diamond mixing microchamber—to reduce the fabrication difficulties associated with curved walls and enhance mixing efficiency in electroosmotic micromixers at the same time. By utilizing a diamond-shaped chamber with strategically placed electrodes and AC electric fields, this design aims to overcome limitations identified in the circular configuration while maintaining the benefits of electrokinetic actuation.

5.2 Relevant background works

The field of microfluidic mixing has seen significant advancements over the past two decades, with researchers exploring various strategies to overcome the challenges posed by laminar flow regimes in microscale devices. This section provides a critical review of the relevant literature, focusing on the development of electrokinetic micromixers and the evolution of design strategies aimed at enhancing mixing efficiency.

Among active mixing techniques, electrokinetic approaches have gained significant attention due to their ability to generate complex flow patterns without moving parts. Green et al. (2000) conducted pioneering work on AC electroosmotic flow, elucidating the fundamental mechanisms of fluid motion induced by non-uniform AC electric fields. Chen et al. (2013) developed an AC electroosmotic micromixer using asymmetric pairs of planar electrodes, demonstrating improved mixing performance through the generation of localized vortices. Huang et al. (2007) further advanced this concept by introducing a multi-electrode configuration that enhanced mixing efficiency for both stationary and continuous fluid flows.

Recent research has focused on optimizing electrokinetic micromixer designs through advanced modeling and simulation techniques. Deng et al. (2018) employed topology optimization to determine optimal electrode patterns for electroosmotic micromixers, showcasing the potential for computational methods in device design. Nazari et al. (2020) conducted a comprehensive geometrical study on an induced-charge electrokinetic micromixer, highlighting the importance of electrode placement and configuration.

While various geometries have been explored for micromixer designs, the use of diamond mixing chambers in electrokinetic systems remains relatively unexplored. Bagherabadi et al. (2019) investigated the effect of chamber aspect ratio on mixing efficiency in rectangular electrokinetic mixers, suggesting that chamber geometry plays a crucial role in device performance. However, the specific advantages and challenges associated with diamond mixing chambers in the context of AC electroosmotic mixing have not been thoroughly addressed in the literature.

5.3 Research Gaps and Opportunities

While Chapter 4 established the performance characteristics of circular mixing chambers in electroosmotic micromixers, several specific research opportunities remain for diamond-shaped geometries. In particular, there is limited understanding of how the sharp corners and linear walls of a diamond chamber affect electroosmotic flow patterns and mixing efficiency compared to curved geometries. This chapter addresses these specific knowledge gaps through systematic investigation of a diamond mixing chamber design.

5.4 Objectives of the Study

Building upon the investigation of circular mixing chambers in Chapter 4, this chapter aims to: (1) Design and analyze an AC electroosmotic micromixer with a diamond mixing chamber; (2) Determine the effect of diamond chamber side length on mixing performance; (3) Evaluate the influence of operational parameters on the diamond configuration; (4) Compare the performance with the circular design from Chapter 4; and (5) Establish optimal operating conditions for the diamond chamber design.

5.5 Design and Concept of Diamond Mixing Microchamber

The proposed AC electroosmotic micromixer with a diamond mixing microchamber represents a novel approach to enhancing mixing efficiency in microfluidic systems. This section details the design considerations, conceptual framework, and potential advantages of incorporating a diamond geometry into the mixing chamber.

5.5.1 *Geometric Configuration*

The micromixer design consists of the following key components:

- ***Main microchannel:*** A straight channel with two inlets and one outlet, providing the primary flow path for the fluids to be mixed. The length (L) and width (W) of the microchannel are fixed at 80 μm and 10 μm, respectively.
- ***Diamond mixing microchamber:*** A diamond chamber positioned at the center of the micromixer, designed to induce complex flow patterns and enhance mixing. The side length (L_s) of the mixing chamber is varied from 20 μm to 40 μm to investigate its impact on mixing efficiency.
- ***Electrode configuration:*** Two pairs of symmetrically cross-reciprocal microelectrodes positioned on the peripheral wall of the diamond chamber at ±π/4 and ±3π/4 radians.

Figure 5.1 presents a schematic diagram of the proposed micromixer design, illustrating the arrangement of these components.

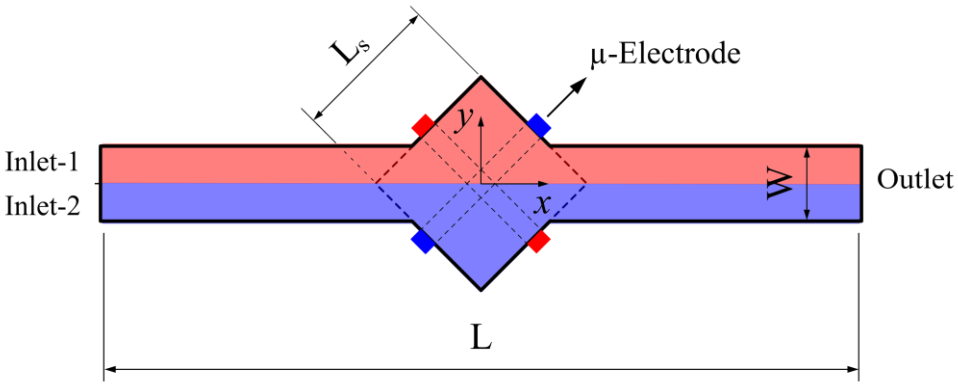

Figure 5.1 Schematic diagram of the AC electroosmotic micromixer with diamond mixing microchamber, depicting the main microchannel, inlets, outlet, diamond mixing chamber, and electrode positions.

5.5.2 *Rationale for Diamond Chamber Design*

The incorporation of a diamond mixing chamber offers several potential advantages over traditional rectangular geometries:

1. ***Symmetry and uniformity:*** The diamond geometry provides positional symmetry at the central position of the diamond wall across both the x and y axis, potentially leading to more uniform mixing across the chamber.
2. ***Elimination of curved walls:*** The absence of curved walls reduces the likelihood of failure and complexity of mounting electrodes on curved walls, which can impede the fabrication process in curved wall chambers.
3. ***Enhanced vortex formation:*** The diamond structure of the mixing chamber may facilitate the formation and propagation of electroosmotic vortices, promoting chaotic advection.
4. ***Optimized electrode placement:*** The diamond geometry allows for strategic positioning of electrodes to maximize the impact of electroosmotic effects on fluid motion.

5.5.3 *Electrokinetic Actuation Mechanism*

The mixing enhancement in the proposed diamond chamber micromixer operates through the same AC electroosmosis principles described in Chapter 3, Section 3.1. When alternating electric fields are applied to the electrodes positioned on the diamond chamber walls, they induce time-dependent electroosmotic slip velocities that generate complex flow patterns within the chamber. These patterns disrupt the laminar flow regime and promote mixing through chaotic advection. The specific geometry of the diamond chamber introduces distinct flow characteristics compared to the circular chamber examined in Chapter 4, particularly in terms of flow redirection at the angled walls and electric field distribution at the corners.

5.5.4 *Theoretical Considerations*

The behavior of fluid within the diamond mixing chamber is governed by the same set of electrokinetic and fluid dynamic principles detailed in Chapter 3, Sections 3.1-3.3. The governing equations for the Navier-Stokes equations, Poisson equation, and convection-diffusion transport remain applicable, with boundary conditions adapted to the diamond geometry.

5.5.5 *Design Parameters and Variables*

The performance of the diamond chamber micromixer is influenced by the same categories of parameters described in Chapter 4, Section 4.5.5, including geometric parameters, operational parameters, and fluid/electrical properties. For this investigation, the side length of the diamond chamber (L_s) replaces the diameter as the key geometric parameter, while all other parameters remain consistent with those listed in Table 4.1 of Chapter 4. All fluid properties and initial operational parameter values employed in this study are identical to those used for the circular chamber investigation.

5.6 Results and Discussion

This section presents a comprehensive analysis of the performance of the AC electroosmotic micromixer with a diamond mixing microchamber. The results are derived from numerical simulations based on the theoretical model and computational methods along with the appropriate validation studies (both experimental and numerical) described in Chapter 3. The discussion focuses on the effects of various geometric and operational parameters on mixing efficiency, flow characteristics, and overall device performance.

5.6.1 *Effect of Mixing Chamber Side Length on Micromixing Performance*

The side length of the diamond mixing chamber significantly influences the micromixing performance of the proposed device. This section presents a comprehensive analysis of the effect of chamber side length on mixing efficiency, fluid dynamics, and electrokinetic phenomena.

To investigate the impact of mixing chamber side lengths, a set of selective parameter values is chosen with varying chamber side lengths. The simulations are conducted with side lengths ranging from 20 μm to 40 μm, while maintaining constant inlet velocity (u_o = 100 μm/s), voltage amplitude (ϕ_o = 100 mV), and frequency (f = 8 Hz). The 30 μm side length chamber was initially considered as the base case. It is crucial to note that once fabricated, the geometry of the micromixer cannot be altered, emphasizing the importance of determining the optimal size during the design phase.

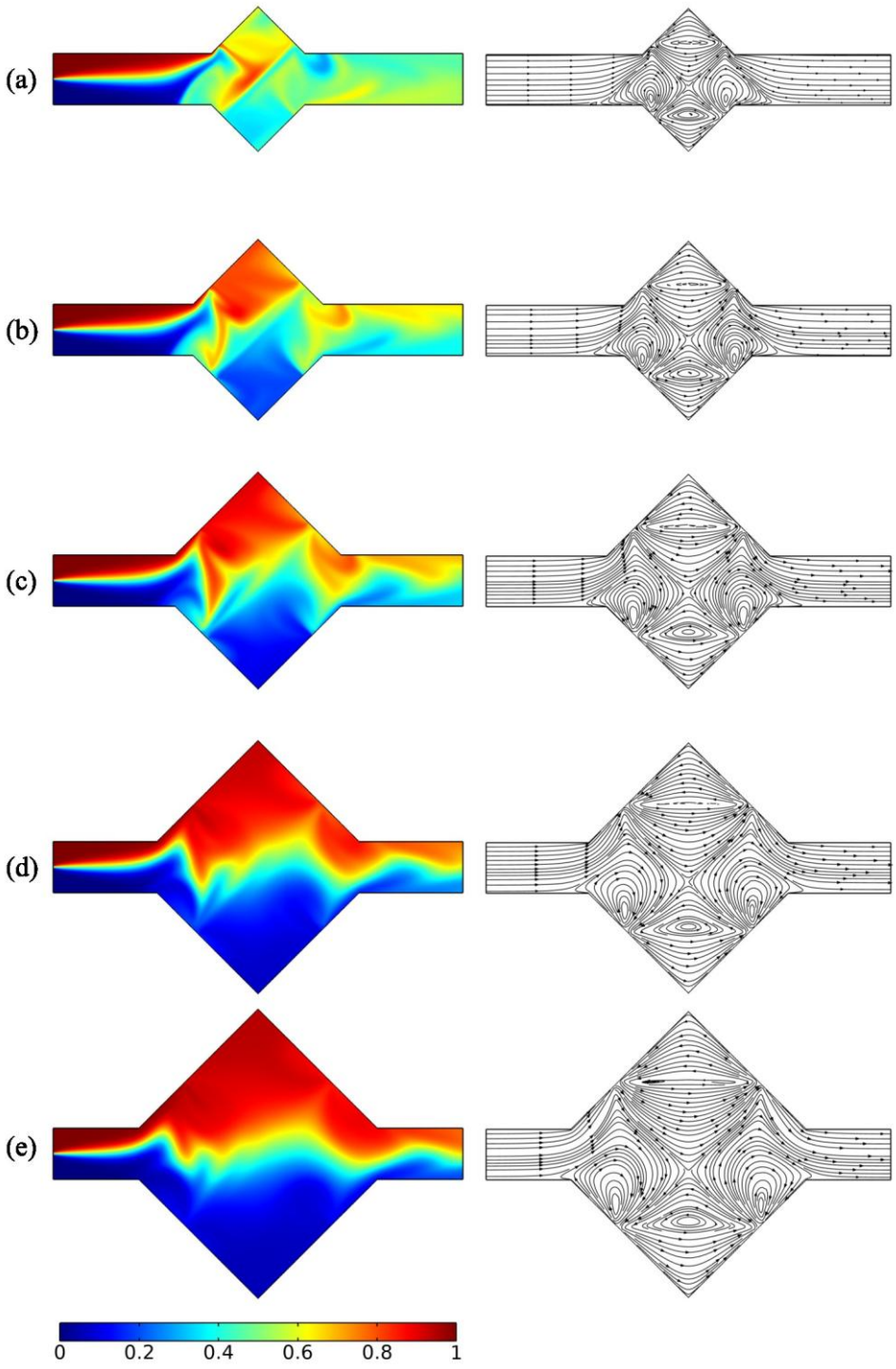

Figure 5.2 Spatial distribution of species concentration and fluid streamlines in diamond mixing microchambers of varying side lengths. (a) L_s = 20 µm, (b) L_s = 25 µm, (c) L_s = 30 µm, (d) L_s = 35 µm, and (e) L_s = 40 µm. Simulation parameters: inlet velocity (u_0) = 100 µm/s, AC voltage amplitude (ϕ_0) = 100 mV, frequency (f) = 8 Hz, at a time (t) = 0.8625 s.

Figure 5.2 presents the concentration and streamline profiles within the micromixer for different chamber side lengths at t = 0.8625 s. Key observations from this analysis include:

1. **Mixing Mechanisms:** In the inlet section, interfacial diffusion is the primary mixing mechanism. Within the mixing chamber, mixing is predominantly driven by the alternating pull and push of fluid streams, induced by the electrical field generated by the AC electrodes.
2. **Vortex Formation:** Four distinct vortices are observed within the mixing chamber for all side lengths, spanning from one electrode to the neighboring electrode. These vortices vary in size over time but remain symmetrical about the y-axis.
3. **Side Length Dependent Mixing:** As the chamber side length increases, the mixing of fluid species decreases. This trend is attributed to the reduced electric field strength within larger chambers, as the distance between electrodes increases.
4. **Lateral Displacement:** Smaller chamber side lengths lead to increased lateral displacement of vortices in the main channel. This enhanced displacement results in closer streamlines at the intake and exit zones of the smallest side length mixing chamber, altering the fluid velocity distribution, pushing more fluid from the lower half to the upper half of the microchannel and vice versa, ultimately enhancing the mixing.
5. **Electric Field Effects:** The decrease in chamber side length intensifies the electric field strength between electrodes, contributing to stronger electrokinetic effects. This intensification significantly enhances the generation of chaotic motion within the laminar flow field, particularly for the chamber with the smallest side length.

To quantitatively assess the micromixer's performance, the mixing efficiency at the microchannel exit was calculated for all time steps of the numerical study. Figure 5.3 illustrates the variation of mixing efficiency with time for different chamber side lengths. The results reveal several important findings:

1. **Side-Length-Efficiency Correlation:** The mixing efficiency consistently decreases as the mixing chamber diameter increases. This trend is observed throughout the simulation period.

2. **Temporal Evolution:** The relative mixing efficiency with respect to the steady state (Figure 5.3b) demonstrates that the smaller side length of the chamber achieves mixing more rapidly.
3. **Optimal Performance:** The 20 µm side length chamber consistently achieves the highest mixing efficiency throughout the simulation period. This optimal side length effectively balances the intensification of electrokinetic effects with the residence time of fluid elements within the mixing chamber.
4. **Chaotic Motion Enhancement:** The utilization of an alternating current sinusoidal time-varying electric field applied to the electrodes significantly enhances the generation of chaotic motion within the laminar flow field. This effect is particularly pronounced for the smallest side length of the mixing chamber.
5. **Laminar Flow Disruption:** The increased volume of chaotic motion and vortices in smaller chambers most effectively breaks the highly ordered laminar flow, thus enhancing the overall mixing efficiency of the micromixer.

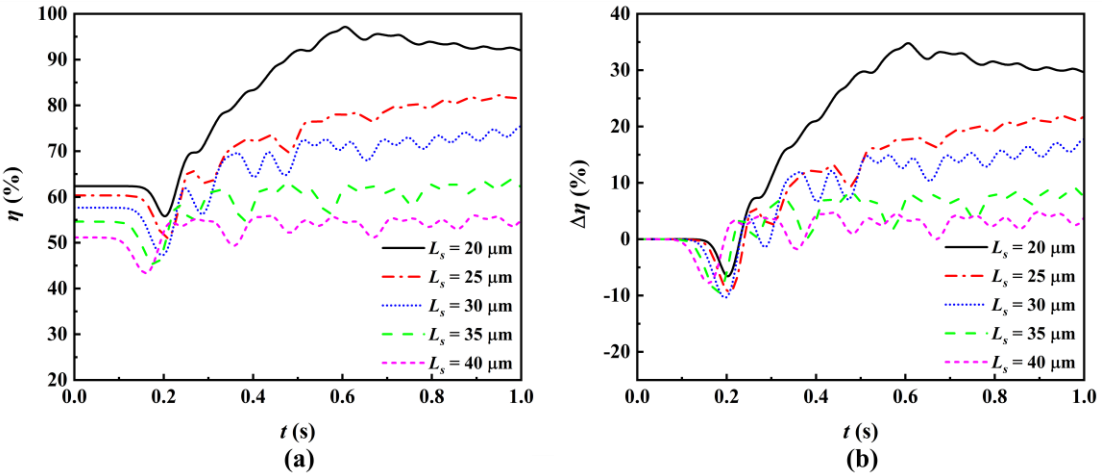

Figure 5.3 Temporal evolution of mixing efficiency for diamond mixing microchambers with side lengths ranging from 20 to 40 µm. (a) Absolute mixing efficiency vs. time. (b) Relative mixing efficiency with respect to steady state vs. time. Simulation parameters: inlet velocity (u_0) = 100 µm/s, AC voltage amplitude (ϕ_0) = 100 mV, frequency (f) = 8 Hz.

Based on this comprehensive analysis, it can be concluded that the 20 µm side length mixing chamber offers the optimal mixing performance for the proposed micromixer design. This configuration maximizes the benefits of strong electrokinetic effects, enhanced vortex formation, and efficient laminar flow disruption. The selection of the 20 µm side length mixing chamber as the optimal design parameter has significant implications for the remainder of this study. All subsequent analyses

and optimizations have been conducted using this fixed side length of the mixing chamber, allowing us to focus on other critical parameters such as fluid flow characteristics and electric field properties.

This rigorous approach to design optimization ensures that the proposed micromixer achieves the highest possible mixing efficiency while maintaining practicality for potential fabrication and implementation in microfluidic systems.

5.6.2 *Influence of Inlet Velocity*

To identify the suitable range of inlet velocities for efficient mixing, simulations were conducted for velocities ranging from 50 μm/s to 500 μm/s, while maintaining constant chamber side length (L_s = 20 μm), voltage amplitude (ϕ_0 = 100 mV), and frequency (f = 8 Hz). Figure 5.4 presents the mixing efficiency and relative mixing efficiency change with respect to steady-state for different inlet velocities. Figure 5.5 illustrates the concentration and streamline profiles within the micromixer for different inlet velocities at t = 0.92917 s.

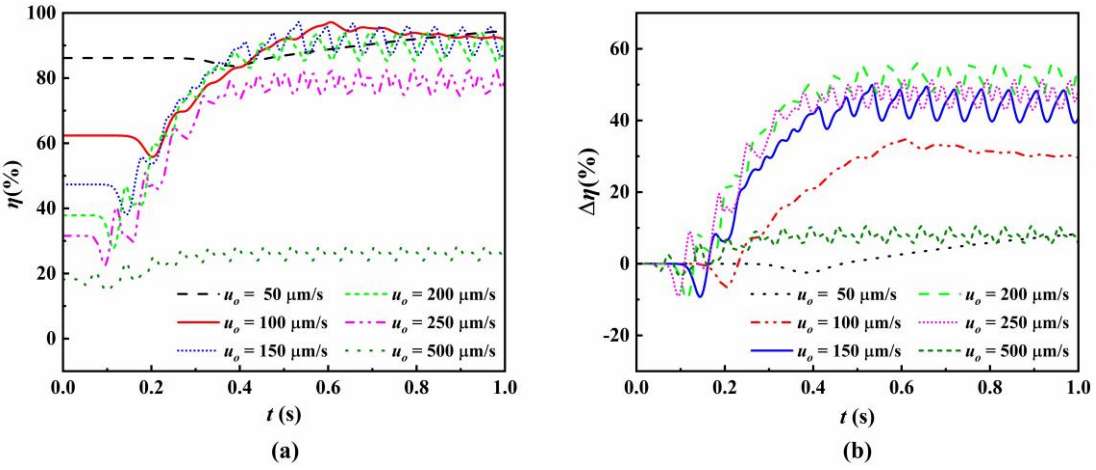

Figure 5.4 Effect of inlet velocity on mixing efficiency [L_s = 20 μm, ϕ_0 = 100 mV, f = 8 Hz]: (a) Mixing efficiency versus time for various inlet velocities, and (b) Relative mixing efficiency change with respect to steady state for different inlet velocities.

Key findings from the analysis of Figures 5.4 and 5.5 include:

1. **Optimal velocity range:** The velocity range of 100 μm/s ≤ u_0 ≤ 200 μm/s appears to be critical, indicating a balance between fluid inertia, electroosmotic forces, and species diffusion within the mixing microchamber.
2. **Non-linear behavior:** The relationship between inlet velocity and mixing efficiency is non-linear, contrary to expectations based on previous literature.

After an initial decrease, there is a rapid increase in mixing efficiency with increasing velocity, with the rate of change varying for different velocities.

3. **Mixing efficiency:** The highest mixing efficiency of 94.478% is achieved at u_0 = 50 μm/s. The mixing efficiencies at the end of the simulation time for inlet velocities of 50, 100, 150, 200, 250, and 500 μm/s are 94.478%, 92.021%, 88.042%, 92.818%, 79.924%, and 23.981%, respectively.
4. **Relative mixing efficiency:** The maximum change in mixing efficiency relative to the steady-state solution (54.959%) occurs at u_0 = 200 μm/s. The relative mixing efficiency changes for inlet velocities of 50, 100, 150, 200, 250, and 500 μm/s are 8.306%, 29.658%, 40.695%, 54.959%, 48.379%, and 5.788%, respectively.
5. **Vortex formation:** Four primary vortices are generated due to the applied AC field at low inlet velocities. The volume of these vortices within the microchannel decreases with increasing inlet fluid velocity.
6. **Secondary vortices:** Within the optimal velocity range (100 μm/s ≤ u_0 ≤ 200 μm/s), secondary vortices are observed near the upper wall of the mixing chamber. These secondary vortices enhance the stretching and folding of fluid streams, resulting in increased mixing at higher intake volumes.

The presence of an optimal velocity range and the observed non-linear behavior suggest a complex interplay between fluid inertia, electroosmotic forces, and species diffusion within the mixing chamber. The formation of secondary vortices within this range further supports the existence of a balance between these forces, contributing to enhanced mixing performance.

These results underscore the importance of carefully selecting the inlet velocity to optimize mixing performance in the proposed device. The identified optimal range provides a guideline for future designs and applications of similar micromixers in microfluidic systems.

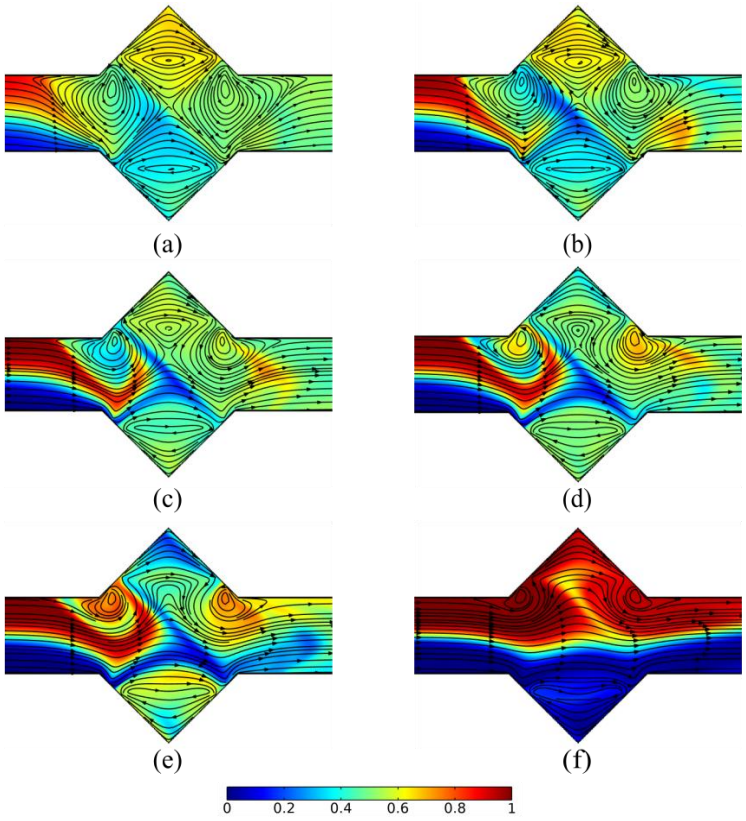

Figure 5. 5 Concentration and streamline profiles for various inlet velocities at t = 0.92917 s [L_s = 20 µm, ϕ_o = 100 mV, f = 8 Hz]: (a) u_o = 50 µm/s, (b) u_o = 100 µm/s, (c) u_o = 150 µm/s, (d) u_o = 200 µm/s, (e) u_o = 250 µm/s, and (f) u_o = 500 µm/s.

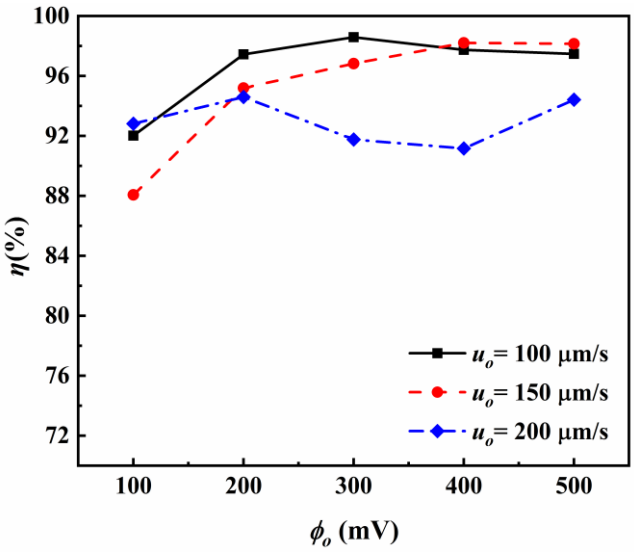

Figure 5.6 Mixing efficiency as a function of voltage amplitude for various inlet velocities at t = 1.0 s.

5.6.3 *Impact of AC Voltage Amplitude*

The amplitude of the applied AC voltage significantly influences the strength of induced electroosmotic flow and, consequently, the mixing performance in microchannels. To investigate this effect, simulations were conducted for voltage amplitudes ranging from 100 mV to 500 mV, considering inlet velocities of 100 µm/s, 150 µm/s, and 200 µm/s, while maintaining a constant frequency of 8 Hz, as presented in Figures 5.6 and 5.7.

Figure 5.6 illustrates the mixing efficiency variation with potential amplitude at the simulation endpoint (t = 1.0 s) for different inlet velocities. The results reveal a non-linear relationship between mixing efficiency and voltage amplitude. For an inlet velocity of 100 µm/s, the mixing efficiency peaks at 98.585% with a 300 mV potential amplitude. In contrast, at 150 µm/s, the maximum mixing efficiency of 98.213% is achieved at 500 mV. For 200 µm/s, the highest efficiency of 94.599% occurs at 500 mV.

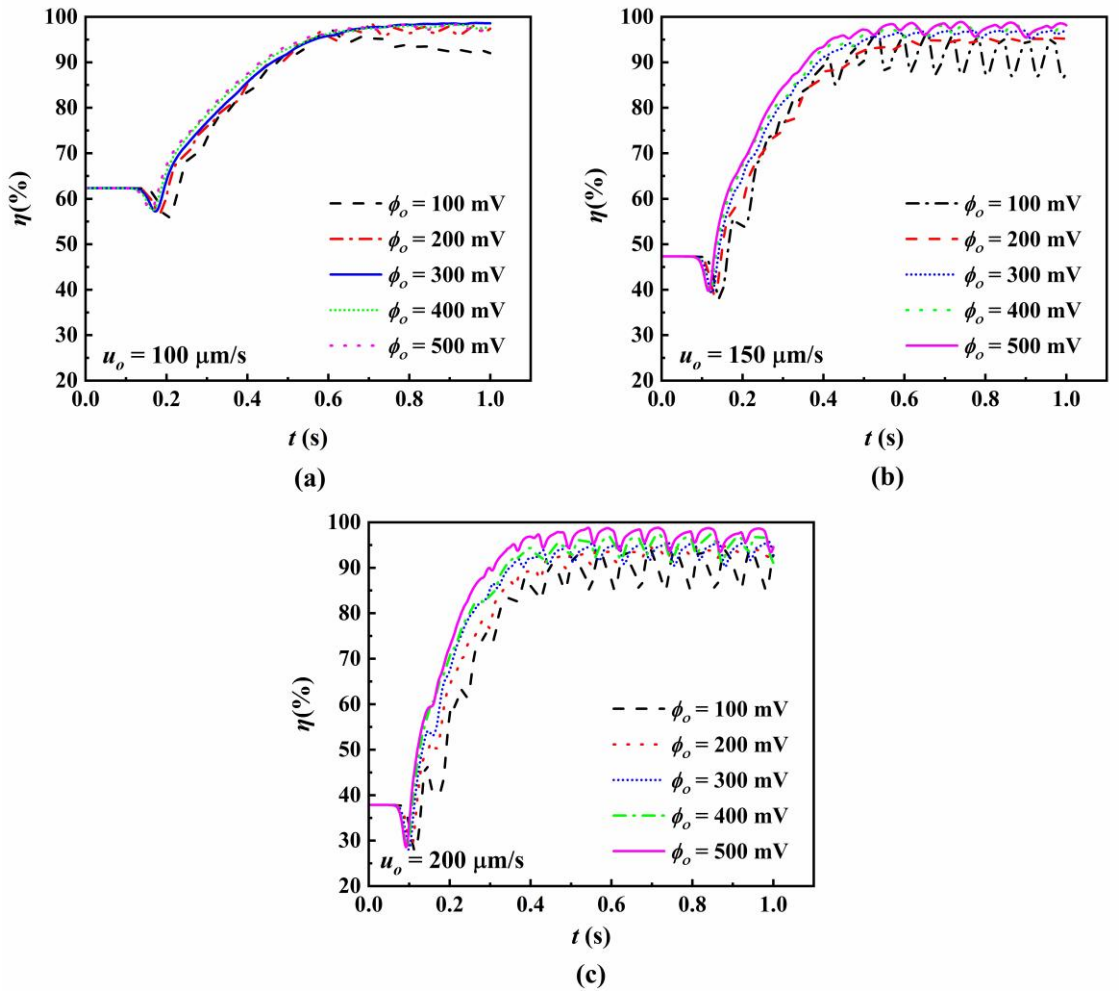

Figure 5.7 Temporal evolution of mixing efficiency for voltage amplitudes ranging from 100 mV to 500 mV at inlet velocities of (a) 100 µm/s, (b) 150 µm/s, and (c) 200 µm/s.

These observations indicate that the optimal voltage amplitude varies depending on the inlet velocity, suggesting a complex interplay between electroosmotic forces and fluid inertia. The non-linear relationship implies that increasing voltage does not always lead to improved mixing, as excessive electroosmotic forces may overpower fluid inertia and species diffusion.

Figure 5.7 presents the temporal evolution of mixing efficiency for various voltage amplitudes and inlet velocities. Several key observations emerge:

1. Higher voltage amplitudes generally yield better mixing efficiency throughout most of the simulation duration.
2. Increasing inlet velocity leads to more pronounced fluctuations in mixing efficiency, likely due to the intensified competition between inertial forces and electrokinetic effects.
3. Mixing efficiency curves for higher voltages show rapid initial increases, followed by oscillations that gradually stabilize.
4. At lower velocities (100 μm/s), the mixing efficiency curves are smoother, indicating a more stable mixing process.

The fluctuations in mixing efficiency become more prominent at higher velocities, possibly due to rapid variations in inertial forces under the influence of electrokinetic effects. This phenomenon underscores the importance of considering the entire simulation duration rather than relying solely on endpoint measurements when optimizing mixer design.

These findings suggest that while higher voltage amplitudes generally improve mixing, the optimal choice depends on the inlet velocity and desired stability of the mixing process. For applications requiring consistent mixing performance, a moderate voltage amplitude might be preferable, especially at higher inlet velocities. The results highlight the need for careful tuning of operational parameters to achieve optimal mixing in microfluidic devices.

5.6.4 *Effect of AC Frequency*

The frequency of the applied AC signal significantly influences the electroosmotic flow patterns by determining the rate of polarity switches on the microelectrodes. To investigate this effect, simulations were conducted (as shown in Figures 5.8 and 5.9) for frequencies ranging from 2 Hz to 18 Hz, maintaining a

constant voltage amplitude of 500 mV. The study considered inlet velocities of 100 µm/s, 150 µm/s, and 200 µm/s.

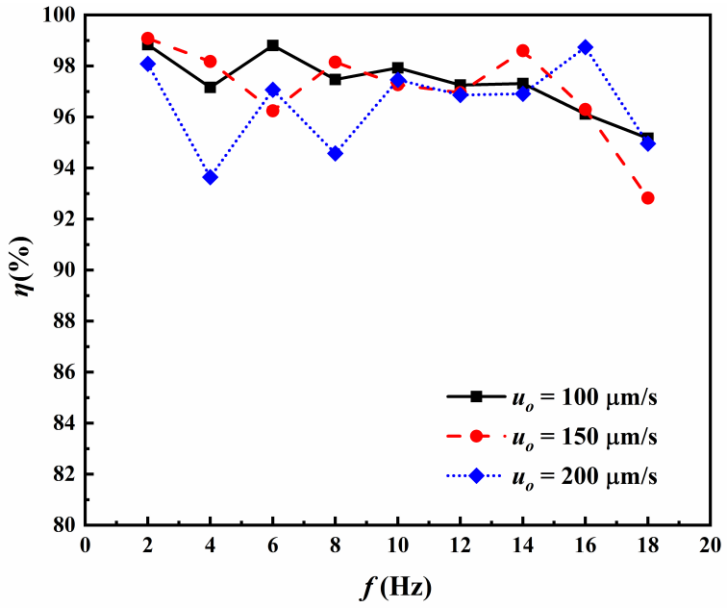

Figure 5.8 Mixing efficiency as a function of AC frequency for inlet velocities of 100, 150, and 200 µm/s at t = 1 s.

Figure 5.8 illustrates the mixing efficiency at the simulation endpoint (t = 1.0 s) for various frequencies and inlet velocities. The results reveal a complex relationship between frequency and mixing performance, with no monotonic trend observed. The highest overall mixing efficiency of 99.085% is achieved at 2 Hz for an inlet velocity of 150 µm/s. For all three inlet velocities, the mixing efficiency remains relatively inconsistent. However, the mixing efficiency has a minimum deviation corresponding to 12 Hz frequency, which is 0.391%, whereas corresponding to 10 Hz frequency the deviation is only 0.654%. The maximum mixing efficiency corresponding to 10 Hz and 12 Hz frequency is 97.924% and 97.255% respectively for 100 with an inlet velocity of 150 µm/s.

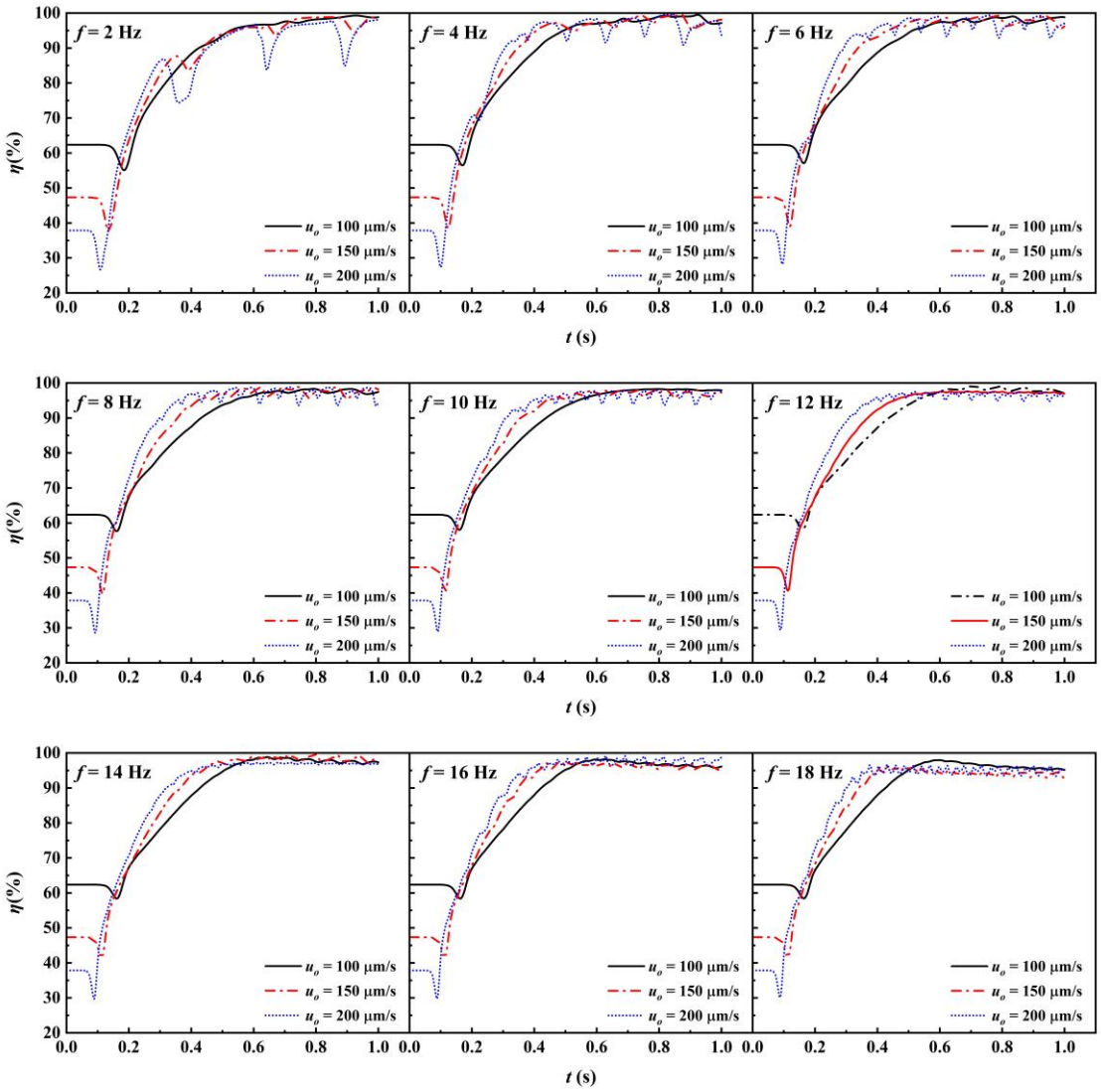

Figure 5.9 Temporal evolution of mixing efficiency for frequencies f = 2–18 Hz and inlet velocities of 100, 150, and 200 μm/s.

To gain deeper insights into the transient behavior, Figure 5.9 presents the temporal evolution of mixing efficiency for different frequencies and inlet velocities. Lower inlet velocities (100 μm/s) exhibit smoother mixing efficiency curves with fewer fluctuations across all frequencies. In contrast, higher inlet velocities (200 μm/s) show more pronounced oscillations in mixing efficiency, particularly at lower frequencies. This observation indicates a stronger influence of inertial forces at higher velocities, leading to increased fluctuations in the mixing process.

A frequency of 12 Hz appears to provide the most stable mixing performance across all inlet velocities. At this frequency, mixing efficiencies of 97.255%, 96.956%, and 96.864% are achieved for 100 μm/s, 150 μm/s, and 200 μm/s, respectively. Notably, the mixing efficiency corresponding to the 12 Hz frequency

remains above 96.864% for all inlet velocities in the range of 100–200 μm/s. This suggests that 12 Hz offers a good compromise between mixing efficiency and stability across various flow rates.

Interestingly, frequencies above 14 Hz generally lead to a deterioration in mixing efficiency. This phenomenon can be attributed to excessively rapid polarity switches, which may hinder effective mixing by not allowing sufficient time for the establishment of stable electroosmotic flow patterns.

The study also reveals that the smoothest transitions in mixing efficiency curves for inlet velocities of 100, 150, and 200 μm/s correspond to frequencies of 10, 12, and 14 Hz, respectively. This finding underscores the importance of selecting an appropriate frequency to minimize fluctuations in the mixing process, particularly at higher flow rates.

These results highlight the critical role of AC frequency in optimizing mixing performance. While lower frequencies can achieve higher peak efficiencies, they may also lead to more unstable mixing processes, especially at higher inlet velocities. The complex interplay between frequency, inlet velocity, and mixing efficiency emphasizes the need for careful tuning of these parameters to achieve optimal micromixer performance.

In conclusion, this study provides valuable insights into the design and operation of AC electroosmotic micromixers. By carefully selecting the AC frequency and considering its interaction with inlet velocity, researchers and engineers can develop more efficient and reliable microfluidic mixing devices for a wide range of applications.

Table 5.1 Optimal parameters and maximum mixing efficiencies.

Parameter	Optimal Value	Maximum η
Chamber Side Length	20 μm	92.022%
Inlet Velocity	100-200 μm/s	92.818% (at 200 μm/s)
Voltage Amplitude	300 mV (for 100 μm/s)	98.585%
	500 mV (for 150 μm/s)	98.213%
	500 mV (for 200 μm/s)	94.599%
AC Frequency	2 Hz (for 150 μm/s)	99.085%

5.6.5 *Optimal Conditions for Micromixer Performance*

The comprehensive analysis of various parameters influencing the micromixer's performance has yielded insights into the optimal conditions for achieving maximum mixing efficiency. Table 2 summarizes the key findings:

It is important to note here that the optimal parameters are interdependent, and the maximum mixing efficiency can vary based on the combination of parameters used. The results in Table 5.2 indicate that the smallest mixing chamber side length (20 μm) provides the best mixing efficiency due to increased electric field strength and enhanced chaotic motion. An inlet velocity range of 100-200 μm/s demonstrates a balance between fluid inertia, electroosmotic forces, and liquid diffusivity, with peak performance at 100 μm/s. Voltage amplitude optimization varies with inlet velocity, with the highest efficiency (98.585%) observed at 300 mV for 150 μm/s. The AC frequency study revealed that 2 Hz yields the overall maximum mixing efficiency (99.085%) at 150 μm/s, while 12 Hz provides consistently high efficiency, with minimum deviations across the optimal velocity range.

These findings underscore the interdependence of parameters in optimizing mixer performance. The combination of a small mixing chamber, moderate inlet velocity, appropriately tuned voltage amplitude, and optimal AC frequency creates an environment conducive to enhanced chaotic advection and efficient mixing at the microscale.

5.6.6 *Potential Challenges and Limitations*

While the diamond mixing chamber design offers several potential advantages, it also presents certain challenges that must be addressed:

1. Flow distribution: Ensuring uniform flow distribution from the inlet channels into the diamond chamber may require careful design considerations.
2. Electric field non-uniformity: The electrode surfaces may lead to non-uniform electric field distributions, potentially affecting mixing performance.
3. Scaling effects: The optimal chamber size may vary with flow rate and fluid properties, necessitating careful optimization for specific applications.

4. Integration with other microfluidic components: The diamond design may pose challenges in seamlessly integrating the mixer with other rectangular or circular microfluidic elements.

By addressing these challenges through careful design and optimization, the proposed AC electroosmotic micromixer with a circular mixing chamber has the potential to offer significant improvements in mixing efficiency for a wide range of microfluidic applications.

5.7 Conclusion

This chapter presents a comprehensive investigation into the design and performance of an AC electroosmotic micromixer with a diamond mixing microchamber. Through systematic numerical simulations and analysis, the effects of various geometric and operational parameters on mixing efficiency have been explored. The key findings and conclusions of this study are as follows:

1. **Electroosmotic Mixing Mechanism**: The continuous change in a potential difference between time-varying voltage signals at the micro-electrodes disrupts the highly lamellar-ordered flow lines around the micro-electrodes in the microscale domain. This perturbation varies throughout the transient process, disrupting the lamellar diffusive mixing of species concentration and enhancing the mixing ability of the microscale mixer.
2. **Microchamber Geometry**: A smaller mixing chamber side length (20 μm) resulted in superior mixing performance. This improvement is attributed to the reduced linear distance between cross-reciprocal-mounted micro-electrodes, which intensifies the electroosmosis force within the micro-chamber.
3. **Inlet Velocity**: An optimal range of inlet velocities (100-200 μm/s) was identified, balancing fluid inertia, electroosmotic forces, and species diffusion to achieve efficient mixing. Interestingly, the relationship between inlet velocity and mixing efficiency is not monotonic for this micromixer design, as evidenced by the highest mixing efficiency achieved at 150 μm/s.
4. **AC Voltage Amplitude**: Higher voltage amplitudes generally improve mixing efficiency, with electrokinetic disturbances becoming more prominent at higher voltage amplitudes. A voltage of 500 mV provided the best overall performance across different velocities, demonstrating the importance of this parameter in optimizing mixing.

5. **AC Frequency**: The AC-frequency variation is associated with the number of directional (polarity) switches of voltage amplitude on micro-electrodes for a specified time period of the transient study. A frequency of 12 Hz offered the most stable mixing performance across all inlet velocities, with mixing efficiencies consistently above 96.864%. This finding provides a wide range for operational control of inlet velocity (100-200 μm/s) in various microfluidic devices.
6. **Overall Performance**: The micromixer achieved a maximum mixing efficiency of 99.085% at an inlet velocity of 150 μm/s, corresponding to a frequency of 2 Hz and a voltage amplitude of 500 mV. This result further asserts that the relationship between velocity and mixing efficiency is complex and not simply inversely proportional to the present structure of the micromixer.

These results demonstrate the potential of diamond mixing microchambers in enhancing electroosmotic mixing. The ability to achieve high mixing efficiencies (>96.864%) across a range of inlet velocities (100-200 μm/s) at 12 Hz and 500 mV provides operational flexibility for various microfluidic applications. This flexibility is particularly valuable in the design and implementation of lab-on-a-chip devices and other microfluidic systems where precise control over mixing is crucial.

Chapter – 6

Enhanced Micromixing in a Diamond Split and Recombined (DSAR) Electroosmotic Micromixer

6.1 Introduction

Building upon the diamond-shaped mixing chamber design presented in Chapter 5, this chapter introduces an advanced configuration—a Diamond Split and Recombined (DSAR) electroosmotic micromixer—that incorporates obstacles within the diamond chamber to create a split and recombined flow pattern. By integrating principles from passive split-recombine mixers with active electrokinetic actuation, this design aims to achieve synergistic enhancement of mixing efficiency through combined flow manipulation and electroosmotically-induced chaotic advection.

6.2 Relevant background works

Building upon the comprehensive literature review presented in Chapter 2, this section focuses specifically on research developments pertinent to the Diamond Split and Recombined (DSAR) electroosmotic micromixer design.

The integration of obstacles within microchannels to enhance mixing has been explored by several researchers in the context of passive micromixers. Jeon and Shin (2009) studied the effect of obstacles in electroosmotic micromixers, demonstrating that strategically placed obstacles can disrupt fluid streamlines and promote mixing. Their work showed that obstacles create localized flow disturbances that increase the interfacial area between fluid streams, but did not explore the synergistic potential with electroosmotic actuation.

The concept of split and recombine (SAR) mixing, particularly relevant to the present DSAR design, was pioneered by Schönfeld et al. (2004), who demonstrated that repeatedly dividing and recombining fluid streams could significantly increase the interfacial area available for diffusive mixing. Xia and Wan (2008) further developed this approach by creating a multi-layer SAR mixer that achieved efficient mixing within a compact footprint by exploiting vertical splitting and horizontal

recombination of fluid streams. However, these studies focused exclusively on passive mixing mechanisms without incorporating electrokinetic effects.

In the realm of active micromixers, Chen et al. (2016) made significant progress by developing a system that integrates electroosmotic flow with passive mixing elements. Their work demonstrated the potential for synergistic enhancement of mixing efficiency through the combined effects of electrokinetic actuation and geometric flow manipulation. Similarly, Gong et al. (2018) investigated an AC electroosmotic micromixer with patterned electrodes and passive structures, showing improved mixing performance compared to either approach alone.

Of particular relevance to the present study, Yasui et al. (2011) examined the effects of nanobead embedments in electroosmotic microchannels, finding that these structures created local non-uniformities in the electric field that enhanced mixing. Their work suggests that strategically placed obstacles can interact with electrokinetic phenomena to create complex flow patterns beneficial for mixing.

Despite these advancements, the specific combination of a diamond-shaped mixing chamber with internal obstacles in an AC electroosmotic system remains unexplored. While Bagherabadi et al. (2019) investigated rectangular electrokinetic mixers with obstacles, their work did not address the unique flow dynamics that may arise in diamond geometries with strategically placed obstacles. Similarly, Bhopte et al. (2018) studied obstacle-based passive micromixers but did not examine the potential synergies with electrokinetic actuation.

The present study builds upon these foundations by investigating the DSAR design, which combines the geometric advantages of the diamond mixing chamber established in Chapter 5 with the principles of split-recombine mixing and electroosmotic actuation to potentially achieve enhanced mixing performance through synergistic mechanisms.

6.3 Research Gaps and Opportunities

While Chapters 4 and 5 established the performance characteristics of circular and diamond mixing chambers in electroosmotic micromixers, the specific integration of obstacles within these chambers to create split-and-recombine effects remains unexplored. In particular, there is limited understanding of the synergistic interaction between obstacle-induced flow manipulation and electroosmotic actuation in diamond geometries. This chapter addresses these specific knowledge gaps through a

systematic investigation of a Diamond Split and Recombined (DSAR) electroosmotic micromixer design.

6.4 Objectives of the Study

Building upon the investigation of diamond mixing chambers in Chapter 5, this chapter aims to: (1) Design and analyze a Diamond Split and Recombined (DSAR) electroosmotic micromixer that integrates obstacles within the diamond chamber; (2) Investigate the influence of obstacle size on mixing performance; (3) Determine the optimal electrode configuration for the DSAR design; (4) Evaluate the effects of operational parameters on the synergistic combination of obstacle-induced flow splitting and electroosmotic actuation; (5) Elucidate the underlying mixing mechanisms in the DSAR configuration; and (6) Compare the performance with the basic diamond chamber design from Chapter 5.

6.5 Design and Concept of Diamond Split and Recombined (DSAR) Micromixer

The proposed Diamond Split and Recombined (DSAR) electroosmotic micromixer represents an evolution of the diamond mixing chamber design presented in Chapter 5. This section details the design considerations, geometric configuration, and conceptual framework underlying the DSAR micromixer.

6.5.1 *Geometric Configuration*

The DSAR micromixer design consists of the following key components:

- ***Main microchannel:*** A straight channel with two inlets and one outlet, providing the primary flow path for the fluids to be mixed. The length (L) and width (W) of the microchannel are maintained at 80 μm and 10 μm, respectively, consistent with the design presented in Chapter 5.
- ***Diamond mixing microchamber:*** A diamond-shaped chamber positioned at the center of the micromixer, with a fixed side length (L_s) of 30 μm.
- ***Obstacles:*** Diamond obstacles are positioned at the center of the diamond chamber, extending from the top to the bottom of the chamber. The obstacle length (L_o) is varied from 0 μm (no obstacle) to 25 μm to investigate its impact on mixing performance.
- ***Electrode configuration:*** Two pairs of symmetrically positioned microelectrodes located on the peripheral walls of the diamond chamber.

The electrode length (L_e) is varied from 2 μm to 10 μm to examine its influence on electroosmotic actuation and mixing efficiency.

Figure 6.1 presents a schematic diagram of the DSAR micromixer design, illustrating the arrangement of these components.

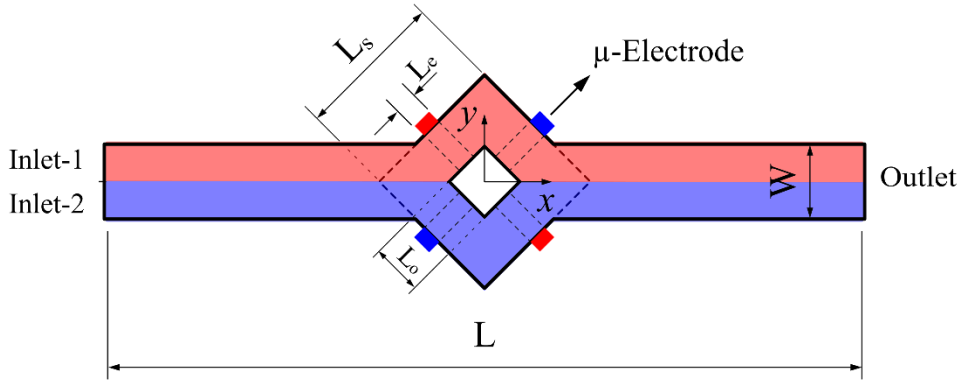

Figure 6.1 Schematic diagram of the AC electroosmotic micromixer with Diamond split and recombined (DSAR) mixing microchamber, depicting the main microchannel, inlets, outlet, diamond mixing chamber, and electrode positions.

6.5.2 *Rationale for DSAR Design*

The incorporation of obstacles within the diamond mixing chamber is motivated by several considerations:

1. **Enhanced flow manipulation**: The obstacles create a split and recombine effect by dividing the incoming fluid streams and forcing them to flow around the obstacle before recombining, thereby increasing the interfacial area between the fluids and promoting mixing.
2. **Synergistic combination of passive and active mixing**: The DSAR design integrates passive mixing elements (obstacles) with active electrokinetic actuation, potentially leading to synergistic enhancement of mixing performance through complementary mechanisms.
3. **Disruption of laminar flow patterns**: The obstacles introduce additional perturbations to the flow field, helping to disrupt the laminar flow structure and promote chaotic advection within the mixing chamber.
4. **Localized intensification of electric field-based microvortices**: The presence of obstacles increases the overall regions of induced zeta potential, increasing the number of microvortices, and potentially enhancing electroosmotic effects in critical areas of the mixing chamber.

5. **Controlled vortex formation**: The obstacles influence the formation and positioning of electroosmotically-induced vortices, potentially optimizing their contribution to the mixing process.

6.5.3 *Electrokinetic Actuation Mechanism*

The mixing enhancement in the DSAR micromixer is achieved through a combination of obstacle-induced flow manipulation and AC electroosmotic actuation. Building upon the electrokinetic principles described in Chapters Table 5.1 Optimal parameters and maximum mixing efficiencies. 82 and 5, the DSAR design incorporates obstacles that split incoming fluid streams and force them to flow around the obstacle before recombining. This process increases the interfacial area between fluids while electroosmotically-induced vortices further enhance mixing through chaotic advection. The interaction between these two mechanisms potentially leads to synergistic enhancement of mixing performance.

6.5.4 *Design Parameters and Variables*

The performance of the DSAR micromixer is influenced by the same parameter categories described in Chapters 4 and 5, with the addition of obstacle length (L_o) as a key geometric parameter. All fluid and electrical properties remain consistent with those used in previous chapters, as detailed in Table 4.1 of Chapter 4.

6.6 Results and Discussion

This section presents a comprehensive analysis of the performance of the DSAR electroosmotic micromixer based on numerical simulations. The discussion focuses on the effects of various geometric and operational parameters on mixing efficiency, flow characteristics, and overall device performance.

6.6.1 *Effect of Obstacle Size on Micromixing Performance*

The size of the obstacle within the diamond mixing chamber significantly influences the micromixing performance of the DSAR micromixer. This section presents an analysis of the effect of obstacle length (L_o) on mixing efficiency, fluid dynamics, and electrokinetic phenomena.

To investigate the impact of obstacle size, simulations were conducted with obstacle lengths ranging from 0 μm (no obstacle) to 25 μm, while maintaining constant diamond chamber side length (L_s = 30 μm), electrode length (L_e = 2 μm),

inlet velocity (u_o = 100 µm/s), voltage amplitude (ϕ_o = 100 mV), and frequency (f = 8 Hz).

Figure 6.2 presents the concentration and streamline profiles within the micromixer for different obstacle lengths at t = 0.775 s.

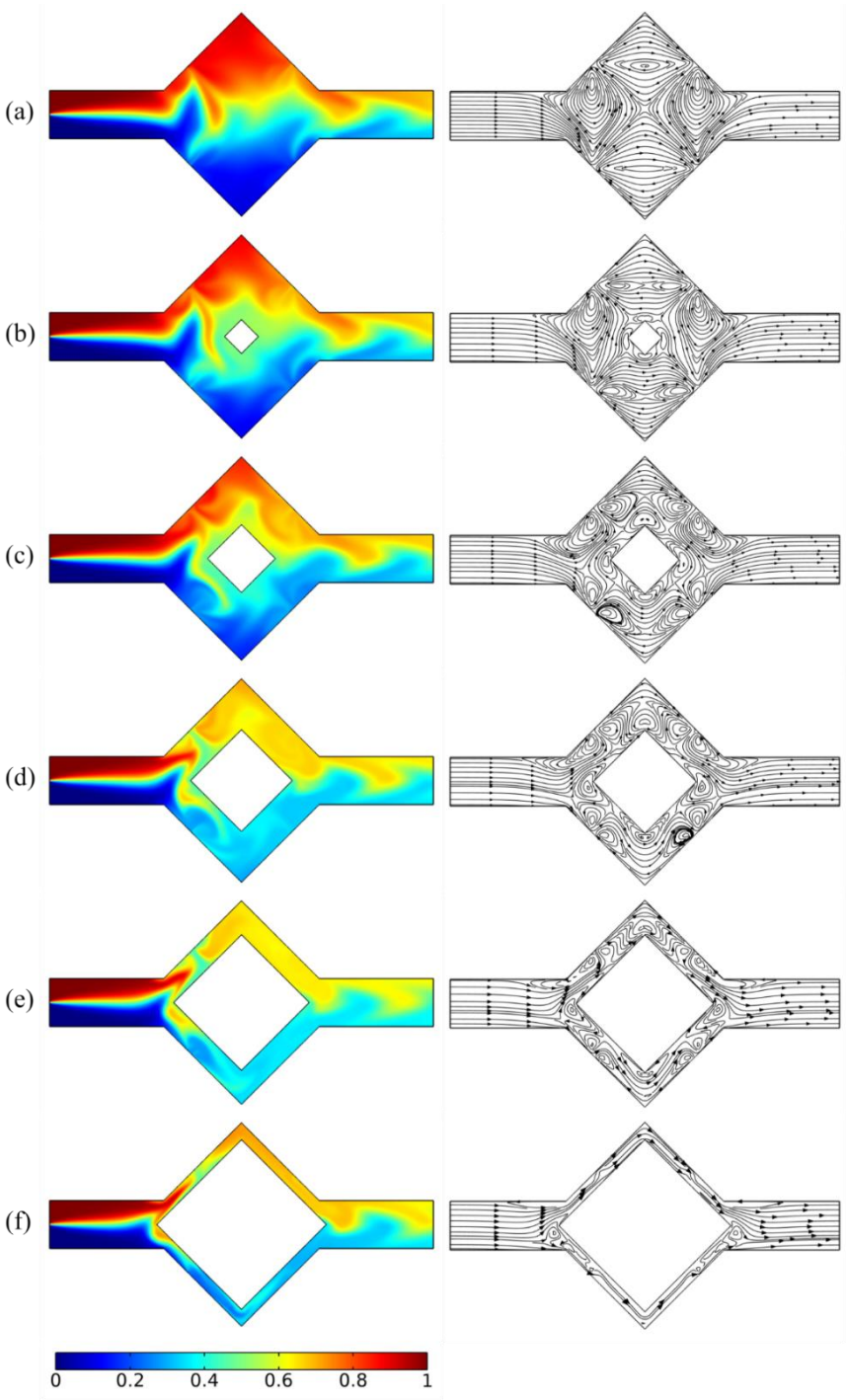

Figure 6.2 Spatial distribution of species concentration and fluid streamlines in Diamond split and recombined (DSAR) mixing microchamber of varying obstacle sizes. (a) L_o = 0 µm, (b) L_o = 5 µm, (c) L_o = 10 µm, (d) L_o = 15 µm, (e) L_o = 20 µm, (f) L_o = 25 µm, Simulation parameters: inlet

velocity (u_0) = 100 µm/s, AC voltage amplitude (ϕ_0) = 100 mV, frequency (f) = 8 Hz electrode length (L_e) = 2 µm, at a time (t) = 0.775.

In Figure 6.2, the concentration and streamline profiles reveal several important observations:

1. **Flow splitting and recombination**: The introduction of obstacles within the diamond chamber clearly demonstrates the splitting of fluid streams as they encounter the obstacle, followed by recombination downstream. This effect becomes more pronounced with increasing obstacle length.
2. **Vortex formation**: In the absence of obstacles (Figure 6.2a), four primary vortices are observed within the mixing chamber, consistent with the findings from Chapter 5. As obstacle length increases, the vortex patterns are significantly modified, with the formation of additional, smaller vortices in the regions adjacent to the obstacles,
3. **Streamline disruption**: Larger obstacles (Figure 6.2e-f) cause more significant disruption of the streamlines, forcing fluid elements to take more circuitous paths through the mixing chamber and potentially enhancing mixing through increased path length and interfacial area.
4. **Concentration gradients**: The concentration profiles indicate more effective mixing in configurations with moderate obstacle lengths (Figure 6.2d-e), as evidenced by the more uniform concentration distribution at the outlet. Very small obstacles (Figure 6.2b) show limited improvement over the basic diamond chamber, while excessively large obstacles (Figure 6.2f) appear to impede fluid flow and may reduce the effectiveness of electroosmotic actuation.

To quantitatively assess the impact of obstacle size on mixing performance, Figure 6.3 presents the temporal evolution of mixing efficiency for different obstacle lengths.

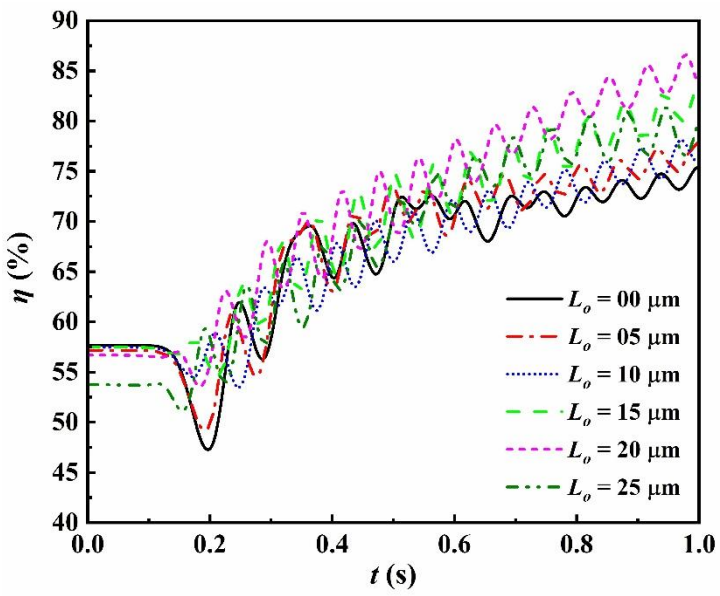

Figure 6.3 Temporal evolution of absolute mixing efficiency for Diamond Split and Recombined (DSAR) mixing microchamber with obstacles size ranging from 0 to 25 μm. Simulation parameters: inlet velocity (u_o) = 100 μm/s, AC voltage amplitude (ϕ_o) = 100 mV, frequency (f) = 8 Hz, electrode length (L_o = 2 μm).

The mixing efficiency profiles in Figure 6.3 provide several key insights:

1. **Optimal obstacle length**: An obstacle length of 20 μm achieves the highest mixing efficiency throughout most of the simulation period, reaching approximately 84% efficiency at the end state. This represents a significant improvement over the basic diamond chamber (0 μm obstacle) which achieves approximately 75% efficiency under the same conditions.
2. **Non-monotonic relationship**: The relationship between obstacle length and mixing efficiency is non-monotonic, with performance initially improving as obstacle length increases from 0 μm to 20 μm, but then declining for larger obstacles (25 μm). This suggests the existence of a critical obstacle size that optimally balances flow splitting/recombination effects with electroosmotic actuation.
3. **Temporal response**: The configurations with moderate obstacle lengths (10-20 μm) not only achieve higher ultimate mixing efficiencies but also reach a steady state more rapidly, indicating enhanced mixing kinetics.
4. **Performance degradation with excessive obstacle size**: The significant decrease in mixing efficiency observed with the 25 μm obstacle suggests that excessively large obstacles may impede fluid flow and restrict the

development of electroosmotically-induced vortices, counteracting the benefits of the split and recombine effect.

The observed enhancement in mixing performance with the optimal obstacle length (20 μm) can be attributed to several factors:

- Effective balance between flow obstruction and electroosmotic actuation
- Creation of optimal flow path lengths for fluid elements traversing the mixing chamber
- Formation of secondary vortices that complement the primary electroosmotically-induced vortices
- Increased interfacial area between fluid streams due to the split and recombine effect
- Enhanced strain and stretching of fluid elements as they navigate around the obstacle

These findings demonstrate that the introduction of appropriately sized obstacles within the diamond mixing chamber can significantly enhance mixing performance compared to the basic diamond chamber design. However, obstacles influence the electric field distribution. This distribution can also be altered by introducing variations in electrode lengths. Therefore, we will exclude the most unfavorable mixing efficiency cases (i.e., no-obstacle configuration and the largest obstacle case) in the subsequent section, which examines the impact of electrode length on mixing performance.

6.6.2 *Effect of Electrode Length on Mixing Performance*

The length of the electrodes positioned on the peripheral walls of the diamond chamber plays a crucial role in determining the strength and distribution of the electroosmotically-induced flow field. This section investigates the influence of electrode length (L_e) on the mixing performance of the DSAR micromixer, considering its interaction with obstacle size.

Simulations were conducted for electrode lengths ranging from 2 μm to 10 μm, in combination with obstacle lengths of 5 μm, 10 μm, 15 μm, and 20 μm, while maintaining constant inlet velocity (u_0 = 100 μm/s), voltage amplitude (ϕ_0 = 100 mV), and frequency (f = 8 Hz).

Figure 6.4 presents the concentration and streamline profiles for selected combinations of electrode length and obstacle size at t = 0.725 s..

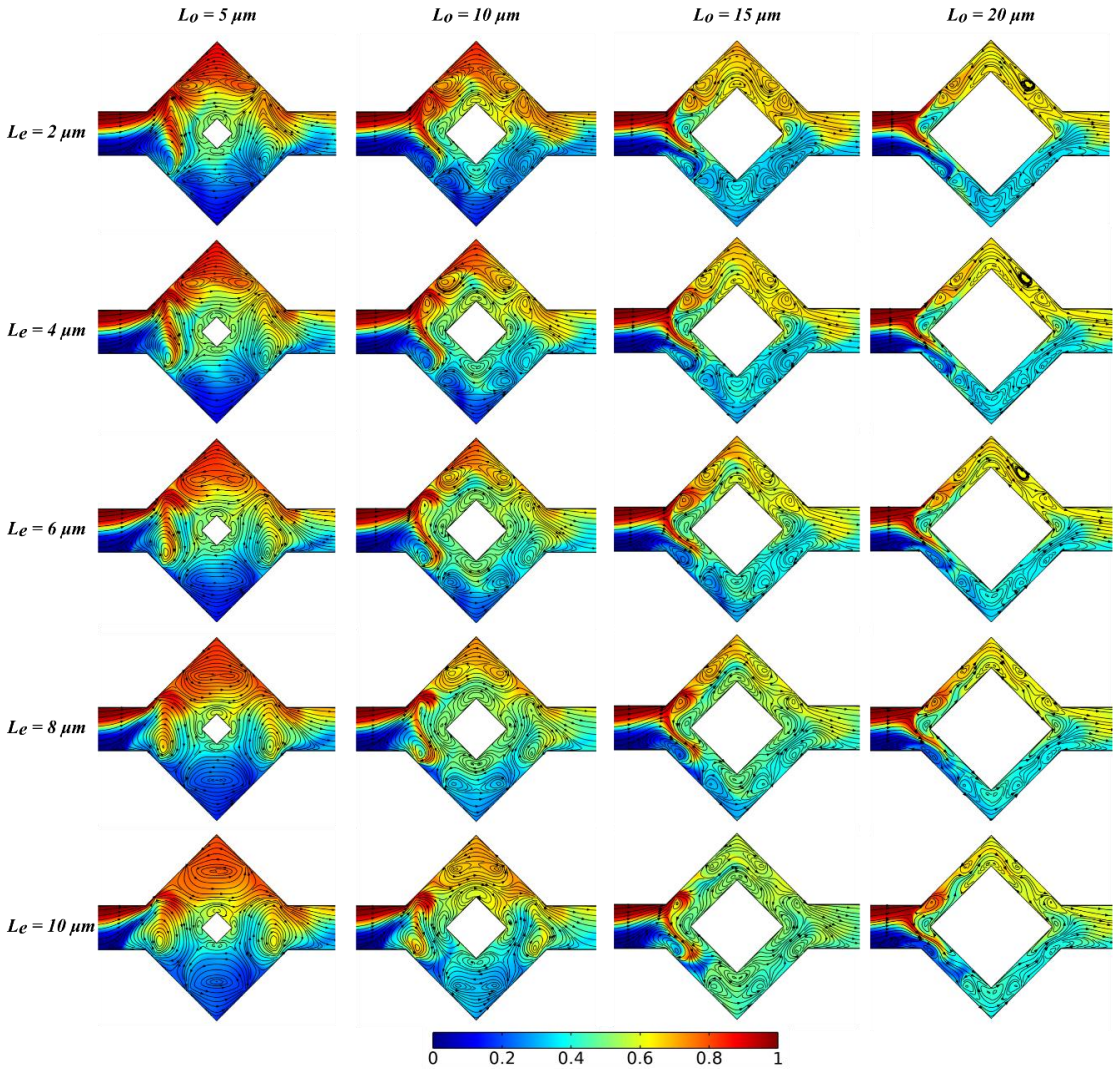

Figure 6.4 Combined spatial distribution of species concentration and fluid streamlines in Diamond split and recombined (DSAR) mixing microchamber of varying obstacle sizes and electrode length. Simulation parameters: inlet velocity (u_0) = 100 μm/s, AC voltage amplitude (ϕ_0) = 100 mV, frequency (f) = 8 Hz, at a time (t) = 0.725 s.

In Figure 6.4, the concentration and streamline profiles reveal the complex interaction between electrode length and obstacle size:

1. **Electroosmotic actuation strength**: Longer electrodes (10 μm) generate stronger electroosmotic flows, as evidenced by the more pronounced vortices and greater disturbance of the concentration field compared to shorter electrodes (2 μm).
2. **Synergistic effects**: The combination of longer electrodes with optimal obstacle sizes (15 μm) appears to produce synergistic enhancement of mixing,

with more uniform concentration distributions at the outlet than either feature alone.

3. **Vortex characteristics**: The size, position, and strength of the electroosmotically-induced vortices are significantly influenced by both electrode length and obstacle size, with longer electrodes generally producing larger, more powerful vortices.
4. **Flow field complexity**: The interaction between obstacle-induced flow splitting and electroosmotic actuation creates complex flow patterns, particularly with longer electrodes, which may contribute to enhanced chaotic advection and improved mixing.

To quantitatively assess the relationship between electrode length and mixing performance, Figure 6.5 presents the mixing efficiency as a function of electrode length for different obstacle sizes.

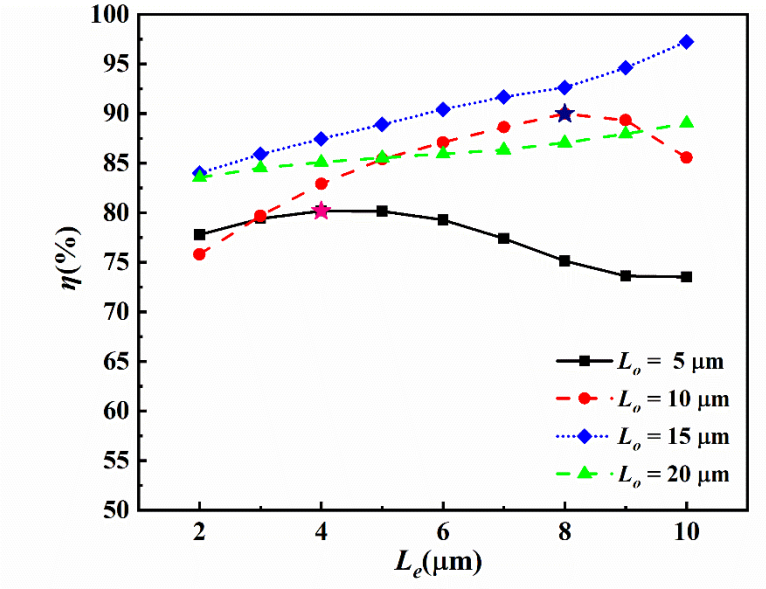

Figure 6.5 Absolute mixing efficiency versus electrode length (L_e) for diamond mixing microchamber with obstacle sizes ranging from 5 to 20 μm. Simulation parameters: inlet velocity (u_0) = 100 μm/s, AC voltage amplitude (ϕ_0) = 100 mV, frequency (f) = 8 Hz.

The results demonstrate several important trends:

1. **Positive correlation**: For relatively larger obstacle sizes (15 and 20 μm), increasing the electrode length generally leads to improved mixing efficiency, indicating that stronger electroosmotic actuation enhances the mixing process.
2. **Obstacle-dependent response**: The sensitivity of mixing efficiency to electrode length varies with obstacle size. For the 15 μm obstacle, mixing

efficiency increases significantly with electrode length, reaching approximately 97% with 10 μm electrodes. In contrast, the 5 μm and 20 μm obstacles show more modest improvements with increasing electrode length.

3. **Optimal configuration**: The combination of 15 μm obstacle length and 10 μm electrode length achieves the highest mixing efficiency among all tested configurations, suggesting this represents an optimal balance between flow splitting/recombination and electroosmotic actuation.
4. **Diminishing returns**: For the 5 μm and 10 μm obstacles, the benefit of increasing electrode length appears to plateau beyond 4 μm and 8 μm, suggesting that there may be limits to the improvements achievable through electrode lengthening, depending on the obstacle configuration.

The enhanced performance observed with longer electrodes can be attributed to several factors:

- Increased area for electroosmotically induced slip velocity generation
- Stronger and more extensive electrokinetic vortices
- Greater penetration of electroosmotic effects into the central regions of the mixing chamber
- More effective interaction between electroosmotic flows and obstacle-induced flow patterns
- Enhanced disruption of laminar flow structure through stronger electrokinetic actuation

These findings indicate that the combination of appropriately sized obstacles (15 μm) with extended electrodes (10 μm) provides the most effective configuration for the DSAR micromixer, achieving significantly higher mixing efficiency than either feature alone. This optimal configuration will be used as the basis for subsequent investigations of operational parameters.

6.6.3 *Identification of Suitable Inlet Velocity*

The inlet velocity significantly influences the balance between convective transport, diffusive mixing, and electrokinetic effects in the DSAR micromixer. This section investigates the effect of inlet velocity on mixing performance, focusing on the optimal geometric configuration identified in the previous sections (obstacle length L_o = 15 μm, electrode length L_e = 10 μm).

Simulations were conducted for inlet velocities ranging from 50 µm/s to 500 µm/s, while maintaining constant voltage amplitude (ϕ_o = 100 mV) and frequency (f = 8 Hz). Figure 6.6 presents the concentration and streamline profiles for different inlet velocities at t = 0.975 s.

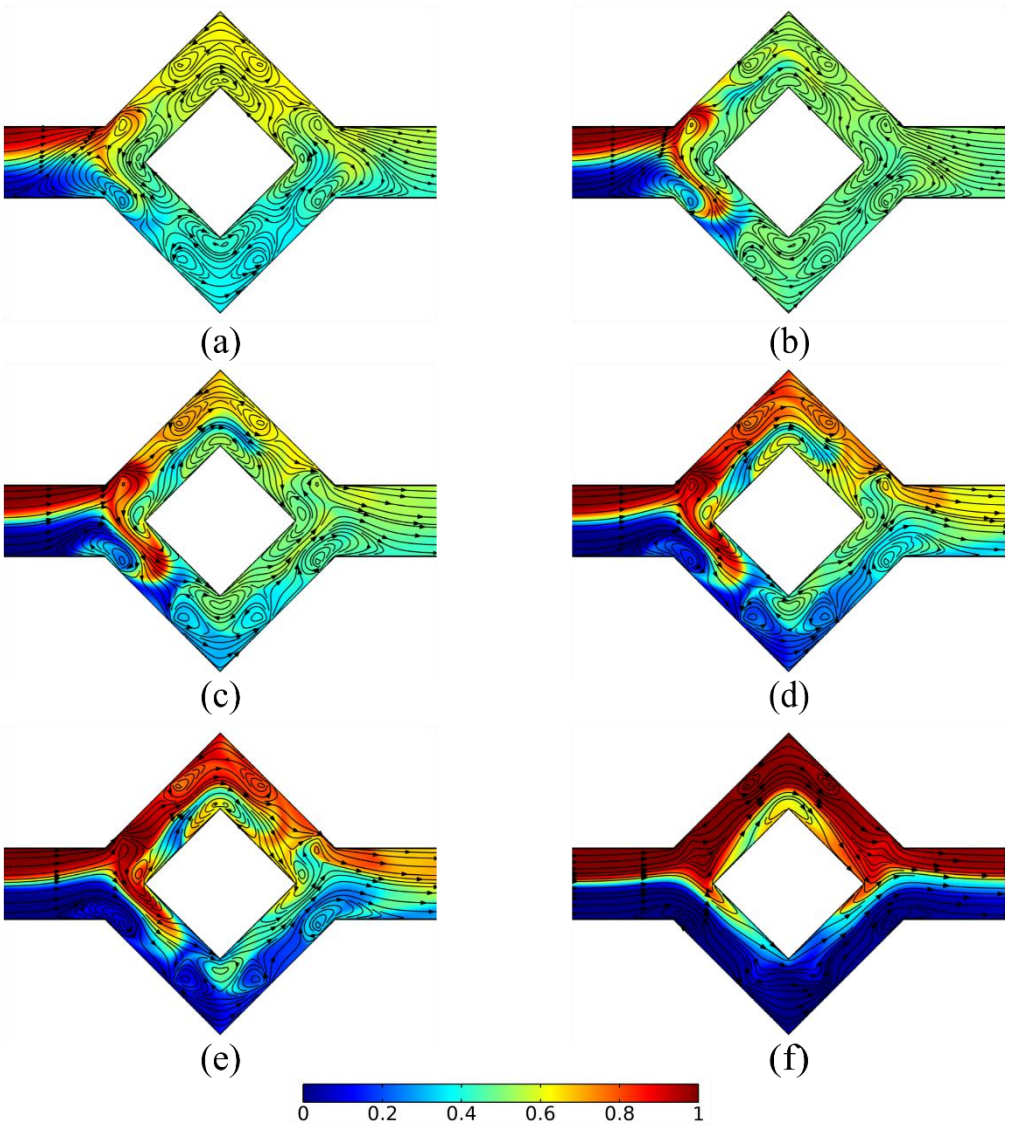

Figure 6.6 Concentration and streamline profiles for various inlet velocities at t = 0.975 s [L_o = 15 µm, ϕ_o = 100 mV, f = 8 Hz]: (a) u_o = 50 µm/s, (b) u_o = 100 µm/s, (c) u_o = 150 µm/s, (d) u_o = 200 µm/s, (e) u_o = 250 µm/s, and (f) u_o = 500 µm/s.

The concentration and streamline profiles reveal several important observations:

1. **Velocity-dependent vortex formation**: At lower velocities (50-100 µm/s), well-defined vortices are observed both upstream and downstream of the obstacle, contributing to effective mixing. As velocity increases, the

downstream vortices become less prominent, while the upstream vortices become compressed against the obstacle.

2. **Flow penetration**: At lower velocities, the electroosmotically-induced flow patterns penetrate farther into the main channel, affecting a larger portion of the fluid domain. This effect diminishes with increasing velocity as inertial forces begin to dominate.
3. **Residence time effects**: Lower velocities provide longer residence times within the mixing chamber, allowing more time for diffusive mixing and electrokinetic effects to act on the fluid elements.
4. **High-velocity limitations**: At very high velocities (500 μm/s), the flow becomes predominantly convective, with minimal influence from electroosmotic effects, resulting in poor mixing as evidenced by the distinct separation between the two fluid streams at the outlet.

To quantitatively assess the effect of inlet velocity on mixing performance, Figure 6.7 presents the temporal evolution of mixing efficiency and the relative mixing efficiency change with respect to steady state for different inlet velocities.

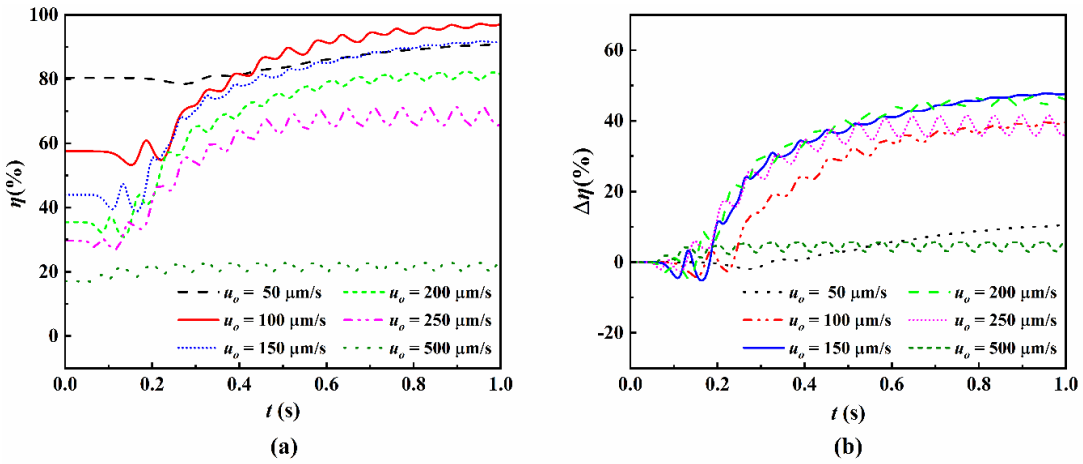

Figure 6.7 Effect of inlet velocity on mixing efficiency [L_o = 15 μm, L_e = 10 μm, ϕ_o = 100 mV, f = 8 Hz]: (a) Mixing efficiency versus time for various inlet velocities, and (b) Relative mixing efficiency change with respect to steady state for different inlet velocities.

In Figure 6.7, The mixing efficiency profiles provide several key insights:

1. **Optimal velocity range**: The highest mixing efficiencies are achieved within the velocity range of 50-150 μm/s, with the 100 μm/s configuration reaching approximately 97% efficiency at steady state.
2. **Enhanced performance at intermediate velocities**: Unlike the basic diamond chamber, the DSAR micromixer shows consistently superior performance (both mixing rate and efficiency) at intermediate velocities (100 μm/s), suggesting that the obstacle-enhanced design is effective as the number of vortices generated is maximized.
3. **Relative enhancement**: The relative mixing efficiency change with respect to steady state (Figure 6.7b) shows that the 150 μm/s and 200 μm/s configurations achieve the greatest improvement relative to their steady-state baseline, indicating that the DSAR design is particularly effective at enhancing mixing at these moderate velocities.
4. **Sharp decline at high velocities**: Beyond 200 μm/s, mixing efficiency decreases rapidly, with the 500 μm/s configuration achieving only about 22% efficiency. This decline is more pronounced than in the basic diamond chamber (25%), suggesting that the obstacle-based design is more sensitive to velocity variations.

The superior performance of the DSAR micromixer at moderate velocities can be attributed to several factors:

- Enhanced interaction between obstacle-induced flow patterns and electroosmotic effects when convective transport is less dominant
- More effective development of vortices both upstream and downstream of the obstacle
- Increased residence time allows for more complete development of the split and recombine effect
- Greater influence of secondary flows and vortical fluid motion
- More effective stretching and folding of fluid elements due to the combined action of obstacles and electroosmotic actuation

These findings suggest that the DSAR micromixer is particularly well-suited for applications requiring high mixing efficiency at moderate flow rates, such as

chemical reactions with slow kinetics or biological assays requiring gentle fluid handling.

6.6.4 *Impact of AC Voltage Amplitude*

The amplitude of the applied AC voltage directly influences the strength of the induced electroosmotic flow and, consequently, the mixing performance of the DSAR micromixer. This section investigates the effect of voltage amplitude on mixing efficiency, focusing on the optimal geometric configuration (obstacle length L_o = 15 µm, electrode length L_e = 10 µm) and the velocity range identified as most effective (100-200 µm/s).

Simulations were conducted for voltage amplitudes ranging from 50 mV to 300 mV, considering inlet velocities of 100 µm/s, 150 µm/s, and 200 µm/s, while maintaining a constant frequency of 8 Hz. Figure 6.8 illustrates the mixing efficiency as a function of voltage amplitude at the simulation endpoint (t = 1.0 s) for different inlet velocities.

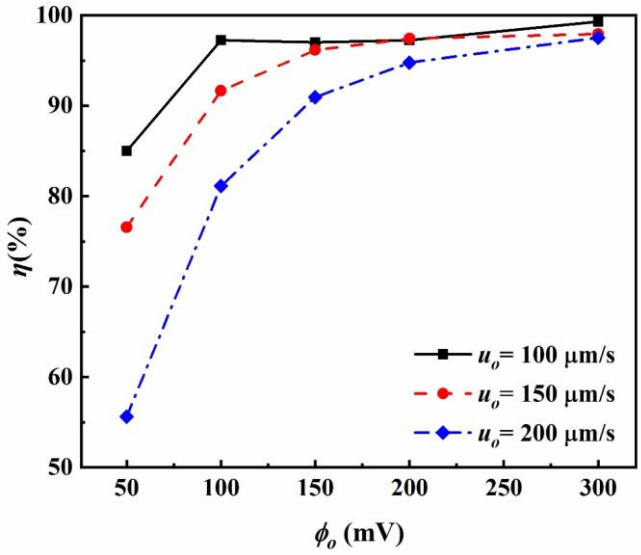

Figure 6.8 Mixing efficiency as a function of voltage amplitude for various inlet velocities at t = 1.0 s.

In Figure 6.8, The results reveal several important trends:

1. **Positive correlation**: For all inlet velocities, mixing efficiency generally increases with voltage amplitude, indicating that stronger electroosmotic actuation enhances the mixing process in the DSAR micromixer.
2. **Velocity-dependent response**: The sensitivity of mixing efficiency to voltage amplitude varies with inlet velocity. At lower velocities (100 µm/s), a

relatively modest voltage (100 mV) is sufficient to achieve near-complete mixing (>97%). In contrast, higher velocities (200 µm/s) require higher voltages to achieve comparable performance.

3. **Optimal voltage-velocity combinations**: The highest mixing efficiency (99.3%) is achieved with 300 mV at 100 µm/s, while 300 mV provides the best performance of 97.9% and 97.5% at 150 µm/s and 200 µm/s respectively. This shows that using 300 mV cuts energy requirements by 40% to achieve similar mixing levels compared to using 500 mV in setups without obstacles (like diamond and circular chamber configurations).

To examine the temporal evolution of mixing efficiency under different voltage conditions, Figure 6.9 presents the mixing efficiency as a function of time for various voltage amplitudes and inlet velocities.

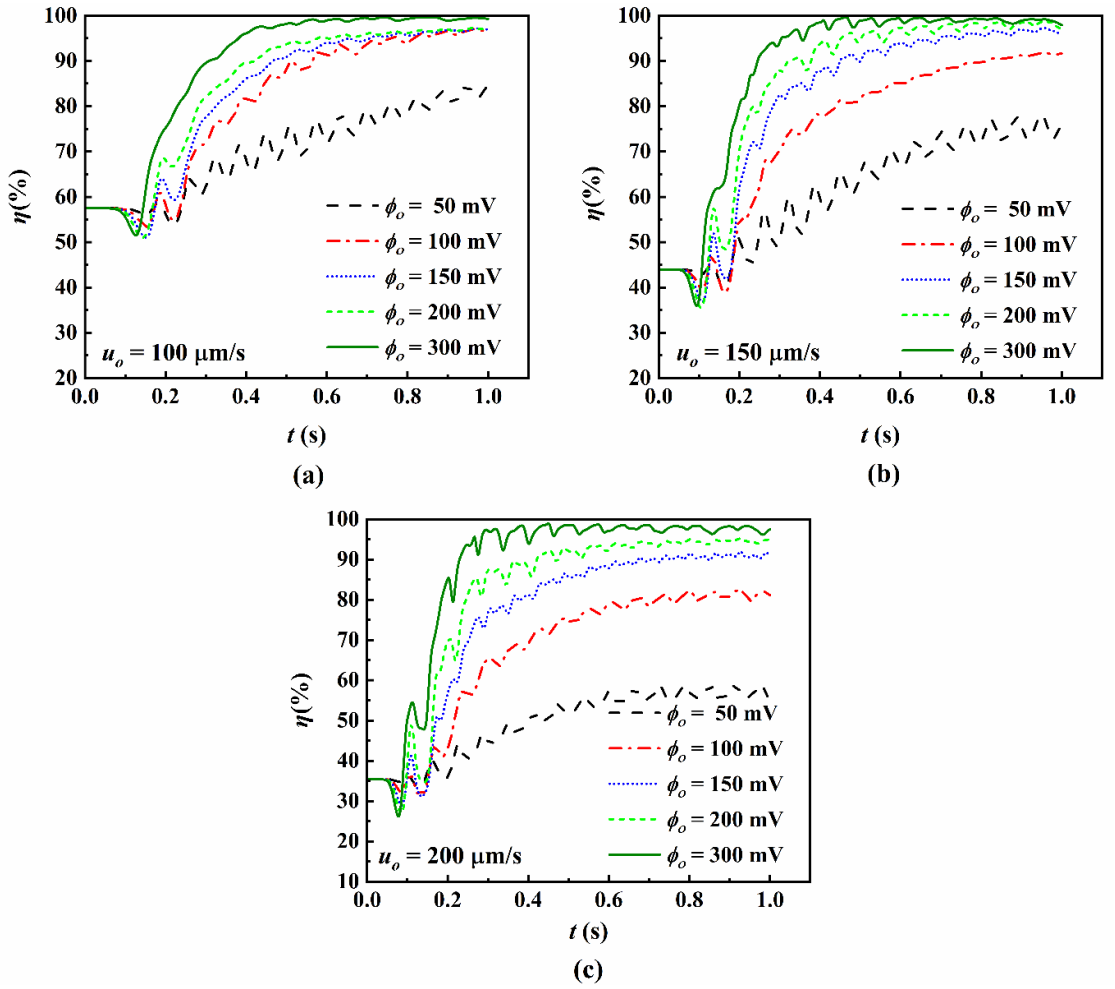

Figure 6.9 Temporal evolution of mixing efficiency for voltage amplitudes ranging from 50 mV to 300 mV at inlet velocities of (a) 100 µm/s, (b) 150 µm/s, and (c) 200 µm/s.

The temporal evolution profiles provide additional insights:

1. **Enhanced mixing kinetics**: Higher voltage amplitudes not only improve ultimate mixing efficiency but also accelerate the mixing process, as evidenced by the steeper initial slopes of the mixing efficiency curves for higher voltages.
2. **Fluctuation characteristics**: At higher velocities and voltages, the mixing efficiency exhibits more pronounced oscillations, reflecting the dynamic competition between convective transport and electroosmotic effects.
3. **Steady-state behavior**: For lower velocities (100 μm/s), the system reaches a stable steady state more rapidly and with fewer fluctuations compared to higher velocities, particularly at moderate to high voltage amplitudes (150-300 mV).

The enhanced performance observed with higher voltage amplitudes can be attributed to several factors:

- Stronger electroosmotic slip velocities at the electrode surfaces
- More powerful vortices capable of overcoming convective transport
- Enhanced chaotic advection due to stronger time-dependent flows
- More effective interaction between electroosmotic flows and obstacle-induced flow patterns
- Greater penetration of electrokinetic effects into the main channel

These findings highlight the importance of voltage amplitude as a key operational parameter for optimizing the performance of the DSAR micromixer. The ability to achieve near-complete mixing (> 99%) with moderate voltages (300 mV) at practical flow rates (100 μm/s) demonstrates the effectiveness of the DSAR design in enhancing microfluidic mixing through the synergistic combination of electroosmotic actuation and obstacle-induced flow manipulation. Furthermore, the DSAR design has proven to be more energy-efficient compared to the two previous cases (diamond and circular mixing chamber design with no obstacle).

6.6.5 *Effect of AC Frequency*

The frequency of the applied AC signal determines the rate of polarity switching at the electrodes and significantly influences the electroosmotic flow

patterns within the DSAR micromixer. This section investigates the effect of frequency on mixing efficiency, focusing on the optimal geometric configuration (obstacle length L_o = 15 µm, electrode length L_e = 10 µm) and voltage amplitude (300 mV).

Simulations were conducted for frequencies ranging from 2 Hz to 18 Hz, considering inlet velocities of 100 µm/s, 150 µm/s, and 200 µm/s. Figure 6.10 illustrates the mixing efficiency as a function of frequency at the simulation endpoint (t = 1.0 s) for different inlet velocities.

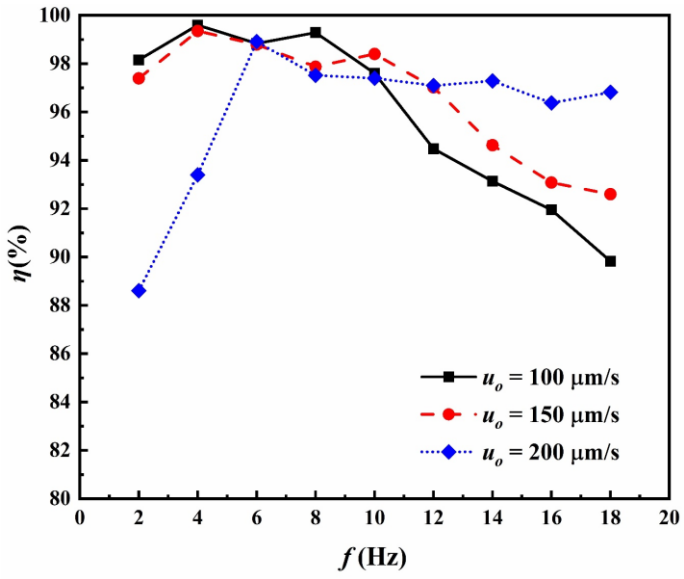

Figure 6.10 Mixing efficiency as a function of AC frequency for inlet velocities of 100, 150, and 200 µm/s at t = 1 s.

The results reveal several important observations:

1. **Complex frequency dependence**: The relationship between frequency and mixing efficiency is non-monotonic, with multiple local maxima and minima observed across the frequency range. This complex behavior suggests intricate interactions between the time-dependent electroosmotic flows and the obstacle-induced flow patterns.
2. **Velocity-specific optimal frequencies**: Each inlet velocity exhibits distinct optimal frequencies for maximum mixing efficiency. For 100 µm/s, the highest efficiency (99.5% and 99.3%) is achieved at 4 Hz and 8 Hz; for 150 µm/s, optimal performance (99.4%) occurs at 4 Hz; and for 200 µm/s, the best results (98.2) are observed at 6 Hz.

3. **High performance at moderate frequencies**: Across all velocities, the frequency range of 6-10 Hz generally provides high mixing efficiency, suggesting this represents a practical operating range for the DSAR micromixer.
4. **Consistent performance at specific frequencies**: At 6 Hz, all three velocity conditions achieve high mixing efficiency (>98%), indicating that this frequency may offer operational flexibility across different flow rates.

To gain deeper insights into the transient behavior, Figure 6.11 presents the temporal evolution of mixing efficiency for different frequencies and inlet velocities.

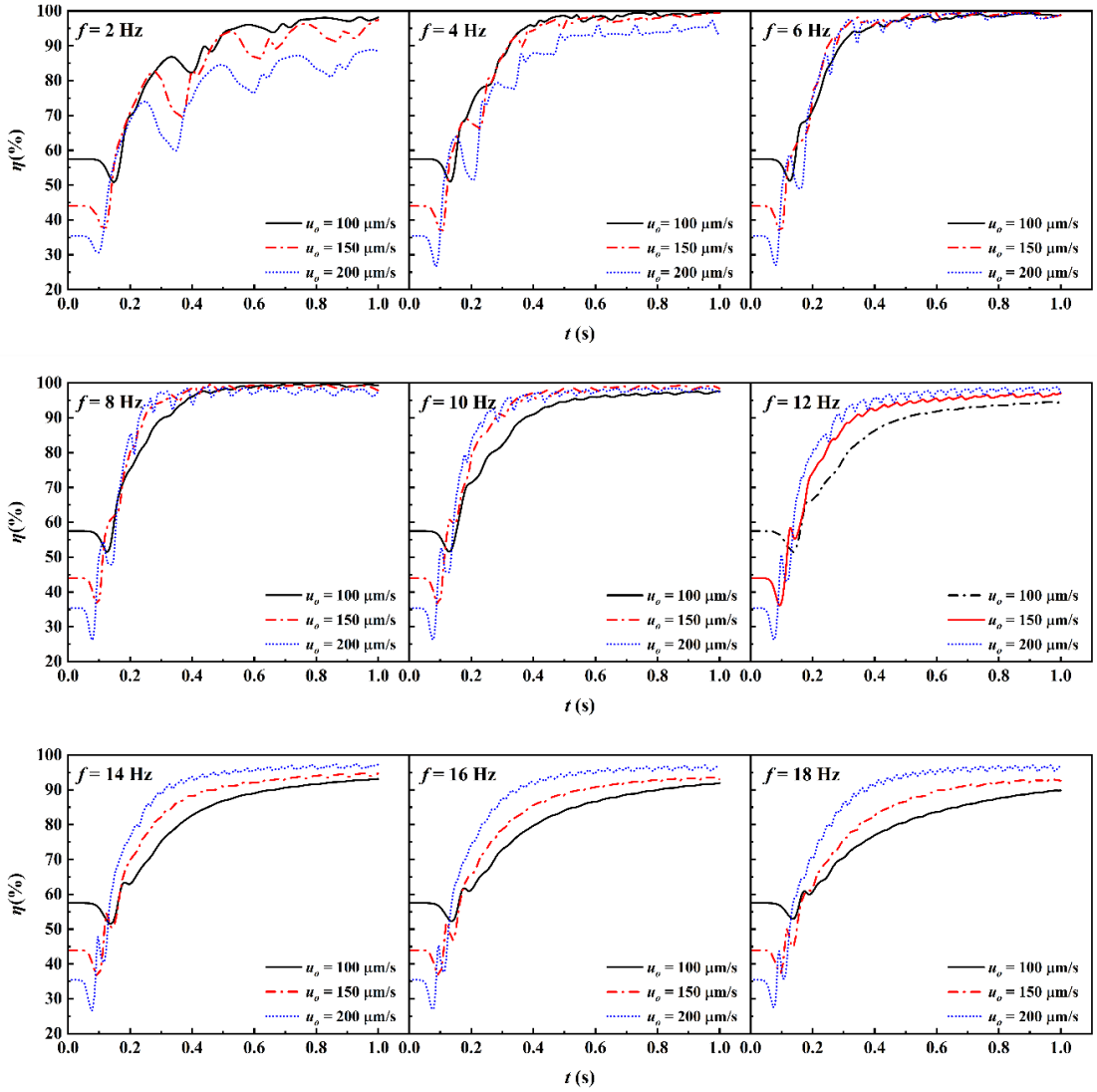

Figure 6.11 Temporal evolution of mixing efficiency for frequencies f = 2–18 Hz and inlet velocities of 100, 150, and 200 μm/s.

In Figure 6.11, the temporal evolution profiles provide additional insights:

1. **Frequency-dependent mixing dynamics**: Lower frequencies (2-4 Hz) generally exhibit larger amplitude fluctuations in mixing efficiency, particularly at higher inlet velocities, indicating less stable mixing processes.
2. **Stabilization effect of moderate frequencies**: The frequency range of 6-12 Hz tends to produce smoother mixing efficiency curves with smaller fluctuations, suggesting more stable and reliable mixing performance.
3. **Initial mixing rate**: Moderate frequencies generally lead to more rapid initial increases in mixing efficiency, potentially beneficial for applications requiring quick mixing responses.
4. **Steady-state behavior**: For velocities of 100–200 μm/s, a frequency of 10 Hz achieves both stable and efficient steady-state performance with minimal fluctuations, while at higher frequencies (≥12 Hz), a smoother transition is attained, and a reversal in the mixing trend with velocity is observed.

The complex frequency dependence observed in the DSAR micromixer can be attributed to several factors:

- Resonance effects between the electrode switching frequency, the characteristic timescales of fluid motion and species diffusion timescale within the mixing chamber
- Interaction between the frequency-dependent electroosmotic vortices and the obstacle-induced flow patterns
- Time-dependent stretching and folding of fluid elements under the influence of both obstacle effects and oscillating electrokinetic flows
- Vortex formation and dissipation cycles that may synchronize or interfere with the applied AC signal
- Varying degrees of penetration of electroosmotic effects into the main channel at different frequencies

These findings highlight the importance of frequency selection in optimizing the performance of the DSAR micromixer. The identification of frequency ranges that provide high and stable mixing efficiency across different inlet velocities (particularly around 10 Hz) offers valuable guidance for practical implementation of this micromixer design.

6.6.6 *Optimal Conditions for DSAR Micromixer Performance*

Based on the comprehensive parametric analysis presented in the preceding sections, we can identify the optimal conditions for maximizing the performance of the DSAR electroosmotic micromixer. Table 6.1 summarizes the key findings:

Table 6.1 Optimal parameters and maximum mixing efficiencies for the DSAR micromixer.

Parameter	Optimal Value	Maximum Mixing Efficiency
Obstacle Length	15 μm	84% (with L_e = 2 μm, u_o = 100 μm/s, ϕ_o = 100 mV, f = 8 Hz)
Electrode Length	10 μm	97.25% (with L_o = 15 μm, u_o = 100 μm/s, ϕ_o = 100 mV, f = 8 Hz)
Inlet Velocity (u_o)	100 μm/s	99.3% (with L_o = 15 μm, L_e = 10 μm, ϕ_o = 300 mV, f = 8 Hz)
Voltage Amplitude	300 mV (for 100 μm/s)	99.3%
	300 mV (for 150 μm/s)	97.7%
	300 mV (for 200 μm/s)	97.5%
AC Frequency	4 Hz and 8 Hz (for 100 μm/s)	> 99%
	4 Hz (for 150 μm/s)	> 99%
	6 Hz (for 200 μm/s)	> 98%

These optimal conditions are interrelated, and the maximum mixing efficiency can vary based on the specific combination of parameters employed. The results indicate that the DSAR micromixer can achieve exceptionally high mixing efficiency (> 99%) under optimal conditions, representing a significant improvement over the basic diamond chamber design presented in Chapter 5.

The key insights from this optimization study include:

1. **Geometric optimization**: An obstacle length of 15 μm (approximately 50% of the diamond chamber side length) and an electrode length of 10 μm provide the optimal geometric configuration for maximizing mixing efficiency.

2. **Operational parameters**: An inlet velocity of 100 μm/s, combined with a voltage amplitude of 300 mV and a frequency of either 4 Hz or 8 Hz, yields the highest mixing performance (>99% efficiency).
3. **Enhanced performance**: Under optimal conditions, the DSAR micromixer achieves substantially higher mixing efficiency (99.3%) compared to the basic diamond chamber presented in Chapter 5 (maximum efficiency of 99.1% under its optimal conditions).
4. **Operational flexibility**: The DSAR design maintains high mixing efficiency (>96%) across a broader range of operational parameters, particularly with respect to frequency variations, offering flexibility for practical applications.
5. **Energy efficiency**: The ability to achieve near-complete mixing at moderate voltage amplitudes (300 mV) suggests potential energy savings compared to alternative micromixer designs requiring higher actuation voltages.

These findings demonstrate that the integration of optimally sized obstacles within a diamond mixing chamber, combined with appropriately configured electrodes and operational parameters, can substantially enhance mixing performance in electroosmotic micromixers. The DSAR design effectively leverages the synergistic benefits of obstacle-induced flow manipulation and electrokinetic actuation to achieve exceptional mixing efficiency under practical operating conditions.

6.6.7 *Potential Challenges and Limitations*

While the DSAR micromixer demonstrates exceptional performance under optimal conditions, several challenges and limitations must be considered for practical implementation:

1. **Fabrication complexity**: The introduction of obstacles within the diamond chamber increases fabrication complexity compared to the basic design. Precise positioning and dimensioning of the obstacles are critical for achieving optimal performance, potentially requiring advanced microfabrication techniques.
2. **Electrode integration**: The elongated electrodes (10 μm) identified as optimal may present challenges for integration and electrical connection within a

practical microfluidic device, potentially requiring specialized fabrication approaches.

3. **Sensitivity to parameter variations**: The DSAR design exhibits complex dependencies on multiple parameters, with optimal performance occurring within specific ranges. This sensitivity may necessitate precise control of operational conditions in practical applications.
4. **Scaling considerations**: The optimal geometric parameters identified in this study may not scale linearly with overall device dimensions, potentially requiring re-optimization for different scale implementations.
5. **Material limitations**: The performance of the DSAR micromixer depends on the electrokinetic properties of the channel surfaces and electrodes, which may vary with different materials or fabrication techniques.

Addressing these challenges will require careful design considerations, advanced fabrication techniques, and potentially the development of robust control systems for maintaining optimal operational conditions. Despite these challenges, the significant performance advantages offered by the DSAR design warrant further investigation and development for practical microfluidic applications.

6.7 Conclusion

This chapter presents a comprehensive investigation into the design and performance of a Diamond Split and Recombined (DSAR) electroosmotic micromixer, which integrates obstacles within a diamond mixing chamber to enhance mixing through the combined effects of electrokinetic actuation and flow manipulation. Through systematic numerical simulations and analysis, we have explored the effects of various geometric and operational parameters on mixing efficiency, leading to the following key findings:

1. **Enhanced Mixing Mechanism**: The DSAR micromixer leverages a synergistic combination of obstacle-induced flow splitting/recombination and AC electroosmotic actuation to achieve exceptionally high mixing efficiency. The obstacles disrupt laminar flow patterns and create additional interfacial area between fluid streams, while the electroosmotic effects generate time-dependent vortices that promote chaotic advection.

2. **Optimal Geometric Configuration**: An obstacle length of 15 μm (approximately 50% of the diamond chamber side length) and an electrode length of 10 μm represent the optimal geometric configuration for maximizing mixing performance. This configuration achieves a balance between flow obstruction, split-recombine effects, and electroosmotic actuation that significantly enhances mixing efficiency.
3. **Operational Parameter Optimization**: Under optimal conditions (inlet velocity of 100 μm/s, voltage amplitude of 300 mV, and frequency of 4 Hz or 8 Hz), the DSAR micromixer achieves near-complete mixing (99.3% efficiency), representing a significant improvement over the basic diamond chamber design presented in Chapter 5.
4. **Energy Efficiency**: The DSAR design requires substantially lower voltage amplitudes (300 mV vs. 500 mV) to achieve optimal performance compared to the basic diamond chamber, representing a 40% reduction in voltage requirements. This enhanced energy efficiency has significant implications for the integration of DSAR micromixers with low-power microfluidic systems.
5. **Operational Flexibility**: The DSAR micromixer maintains high mixing efficiency across multiple frequencies and a range of inlet velocities, offering greater flexibility for practical applications compared to the basic diamond chamber design.

These findings demonstrate that the DSAR design represents a significant advancement in electroosmotic micromixer technology, offering substantial improvements in mixing efficiency, energy efficiency, and operational flexibility. The integration of optimally sized obstacles within a diamond mixing chamber effectively leverages the benefits of both passive (obstacle-induced) and active (electroosmotic) mixing strategies, resulting in enhanced performance across multiple metrics.

Chapter – 7

Analysis of a Square Split-and-Recombined (SSAR) Electroosmotic Micromixer with offset Inlet-Outlet Microchannels

7.1 Introduction

Building upon the Diamond Split and Recombined (DSAR) micromixer design presented in Chapter 6, this chapter introduces an advanced configuration—a Square Split and Recombined (SSAR) electroosmotic micromixer with non-aligned inlet-outlet microchannels. This design aims to enhance mixing efficiency while offering improved compactness and fabrication ease through the use of flat walls and perpendicular turns. By increasing the mean flow path while maintaining the benefits of obstacle integration and electrokinetic actuation, the SSAR design represents a further evolution in electroosmotic micromixers' design and development.

The SSAR electroosmotic micromixer represents an advancement in micromixer design, combining the benefits of electrokinetic actuation present in DSAR with increased compactness of design and a further improvement in fabrication ease. It also provides increased steady-state mixing by increasing the mean flow path, which may lead to reduced active energy requirements while attaining the same mixing efficiency level as that of the DSAR electroosmotic micromixer.

This chapter presents a comprehensive analysis of the SSAR electroosmotic micromixer, focusing on the influence of key geometric parameters (obstacle size and electrode length) and operational conditions (inlet velocity, voltage amplitude, and frequency) on mixing performance. Through systematic numerical simulations, we aim to elucidate the underlying mixing mechanisms, identify optimal design configurations, bring down the operational cost by reducing the active energy (voltage amplitude) cost to make it energy efficient and establish guidelines for maximizing mixing efficiency and minimizing the energy requirements in practical applications.

7.2 Relevant background works

Building upon the comprehensive literature reviews presented in previous chapters, this section focuses specifically on research developments pertinent to the Square Split and Recombined (SSAR) electroosmotic micromixer with non-aligned inlet-outlet microchannels.

The concept of non-aligned or offset inlet-outlet arrangements in microfluidic devices has received limited attention despite its potential benefits for mixing enhancement. Zhou et al. (2020) investigated an electroosmotic micromixer with an asymmetrically designed mixing chamber, demonstrating that geometric asymmetry can enhance fluid layer interactions and improve mixing performance compared to symmetric configurations. However, their work did not specifically address square geometries or the integration of obstacles with offset channels.

Square mixing chambers offer several advantages for microfabrication due to their planar features and straight walls. Chen and Cho (2022) proposed a novel micromixing scheme by introducing a chaotic field inside a square chamber with a main T-shaped microchannel. By incorporating two pairs of meandering electrodes on the upper and lower walls, they achieved high mixing efficiency, demonstrating the potential of square geometries for effective electroosmotic mixing.

The integration of obstacles within microchannels has been explored by Seo et al. (2018), who analyzed split and recombine (SAR) circular-type electroosmotic microscale mixers with different obstacle shapes. Their findings indicated that obstacles enhance mixing through stretching and folding of the fluid flow field, but they did not investigate the potential synergies with non-aligned channel arrangements.

Particularly relevant to the present SSAR design is the work of Lim and Lam (2024), who demonstrated a T-shaped micromixer with constrictions. Their study showed that phase-lagged AC potential could create crescent patterns that increase the contact interface between fluid streams, suggesting potential benefits from manipulating flow paths in electroosmotic systems.

The concepts of energy efficiency and compactness in microfluidic systems were addressed by Saravanakumar et al. (2024), who designed a direct current electroosmosis (DCEO) micromixer with hexagonal cross-section channels. Their approach achieved high mixing efficiency within a compact footprint, highlighting the importance of geometric optimization for practical applications.

Despite these advancements, the specific combination of a square mixing chamber with obstacles and non-aligned (offset) inlet-outlet microchannels remains unexplored in the context of AC electroosmotic actuation. The SSAR micromixer investigated in this chapter builds upon these foundations and the findings from previous chapters to potentially achieve enhanced mixing efficiency with improved compactness and energy consumption characteristics.

7.3 Research Gaps and Opportunities

While previous chapters have established the performance characteristics of circular, diamond, and DSAR mixing chambers, the potential benefits of a square chamber with non-aligned inlet-outlet channels remain unexplored. Specific research opportunities include: (1) Investigating the effect of offset channel arrangement on mean flow path and mixing efficiency; (2) Examining how square geometry affects fabrication ease and system compactness; and (3) Determining whether this design can achieve comparable mixing performance with reduced energy requirements.

7.4 Objectives of the Study

Building upon the micromixer designs investigated in Chapters 4-6, this chapter aims to: (1) Design and analyze a Square Split-and-Recombined electroosmotic micromixer with non-aligned inlet-outlet microchannels; (2) Investigate how the offset channel arrangement affects flow patterns and mixing performance; (3) Determine the optimal geometric and operational parameters for the SSAR configuration; (4) Evaluate the potential benefits in terms of energy efficiency and fabrication simplicity; and (5) Compare the performance with previously studied designs to establish comprehensive design guidelines.

7.5 Design Concept of SSAR with Offset Inlet-Outlet Channels

The proposed Square Split and Recombined (SSAR) electroosmotic micromixer represents an evolution of the DSAR electroosmotic micromixer design presented in Chapter 6, combining geometric innovation with electroosmotic principles. This section details the design rationale, geometric configurations, and conceptual framework underlying the offset SSAR electroosmotic micromixer.

7.5.1 *Geometric Configuration*

The SSAR micromixer design consists of the following key components:

- **Square mixing microchamber**: A square-shaped chamber positioned at the center of the micromixer, with a fixed side length (L_s) of 30 µm. This represents a rotation of the diamond chamber design from Chapter 5 by 45°, converting it into a square orientation.
- **Obstacles**: Square obstacles positioned at the center of the square chamber, extending from the top to the bottom of the chamber. The obstacle length (L_o) is varied from 0 µm (no obstacle) to 25 µm to investigate its impact on mixing performance.
- **Offset inlet-outlet microchannel**: One straight channel with two inlets and one straight channel with one outlet placed in an offset position at square mixing chamber walls, providing the connecting flow path for the fluids to be mixed. The length of each connecting channel (L_c) and width (W) of the microchannel are maintained at 25 µm ((making total linear length the same, 25 + 30 + 25 = 80 µm) and 10 µm, respectively, consistent with previous designs.
- **Electrode configuration**: Two pairs of symmetrically positioned microelectrodes located on the peripheral walls of the square chamber. The electrode length (L_e) is varied from 2 µm to 9 µm to examine its influence on electroosmotic actuation and mixing efficiency.

Figure 7.1 presents a schematic diagram of the offset SSAR micromixer design, illustrating the arrangement of these components.

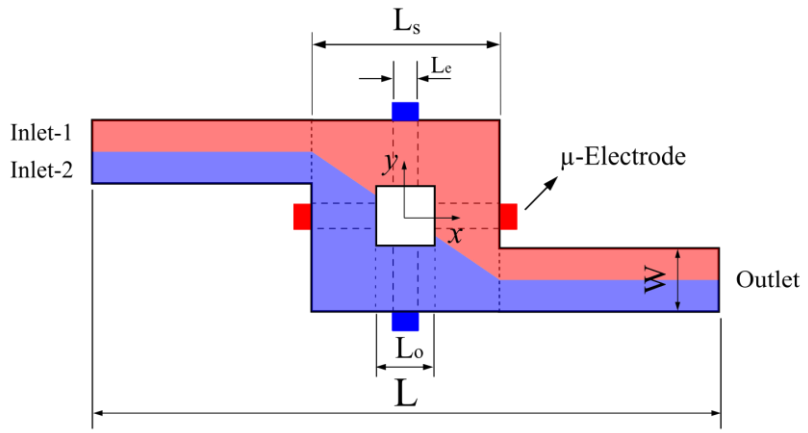

Figure 7.1 Schematic diagram of the AC electroosmotic micromixer with Square split and recombined (SSAR) mixing microchamber, depicting the offset connecting microchannel, inlets, outlet, square mixing chamber, and electrode positions.

7.5.2 *Rationale for SSAR Design*

1. The design improvement achieved by rotating the diamond mixing chamber by 45° to attain the square split and recombined mixing chamber and offsetting the connecting inlet-outlet microchannel is motivated by several considerations:
2. **Enhanced mean flow path**: The offset design increases the mean flow path of the fluid while maintaining the linear length of the micromixer, thereby further increasing the interfacial area between the fluids and promoting mixing.
3. **Reduction of electric energy consumption**: The SSAR design integrates increased mean path leading to enhanced passive mixing without losing effects of obstacles and active electrokinetic actuation as in the DSAR micromixer, potentially leading to synergistic enhancement of mixing performance through aided complementary design-led strategy, resulting in reduced active energy consumption.
4. **More compact design**: The proposed SSAR micromixer has a reduced overall width (30 μm) compared to the width (30√2 μm) of the DSAR micromixer, improving the compactness of the design without affecting the cross-reciprocal positioning of microelectrodes and hence the electric field distribution and associated electroosmotic effects in critical areas of the mixing chamber.
5. **Fabrication considerations**: The use of flat walls, perpendicular turns, and straight channels facilitates easier manufacturing compared to curved or angular designs.

7.5.3 *Electrokinetic Actuation Mechanism*

The SSAR micromixer employs the same electrokinetic actuation principles described in Chapter 6, with electroosmotic slip velocities generated at electrode surfaces in response to applied AC electric fields. The interaction between obstacle-induced flow splitting and electroosmotic actuation creates complex flow patterns that enhance mixing through increased interfacial area and chaotic advection. The square geometry and offset channels modify these flow patterns compared to previously

studied designs, potentially affecting the formation and interaction of electroosmotically-induced vortices with obstruction-induced flow splitting.

7.5.4 *Design Parameters and Variables*

The performance of the SSAR micromixer is influenced by the same parameter categories described in Chapters 4-6, including geometric parameters, operational parameters, and fluid/electrical properties. For this investigation, the square chamber geometry and offset inlet-outlet arrangement represent key geometric modifications, while the obstacle length (L_o) and electrode length (L_e) remain important design variables. All fluid and electrical properties remain consistent with those used in previous investigations, as detailed in Table 4.1 of Chapter 4

7.6 Results and Discussion

This section presents a comprehensive analysis of the performance of the SSAR electroosmotic micromixer based on numerical simulations. The discussion focuses on the effects of various geometric and operational parameters on mixing efficiency, flow characteristics, and overall device performance.

7.6.1 *Effect of Obstacle Size on Micromixing Performance*

The size of the obstacle within the square mixing chamber significantly influences the micromixing performance of the SSAR micromixer. This section presents an analysis of the effect of obstacle length (L_o) on mixing efficiency, fluid dynamics, and electrokinetic phenomena.

To investigate the impact of obstacle size, simulations were conducted with obstacle lengths ranging from 0 μm (no obstacle) to 25 μm, while maintaining constant square chamber side length (L_s = 30 μm), electrode length (L_e = 2 μm), inlet velocity (u_0 = 100 μm/s), voltage amplitude (ϕ_0 = 100 mV), and frequency (f = 8 Hz).

Figure 7.2 presents the concentration and streamline profiles within the micromixer for different obstacle lengths at t = 0.9625 s.

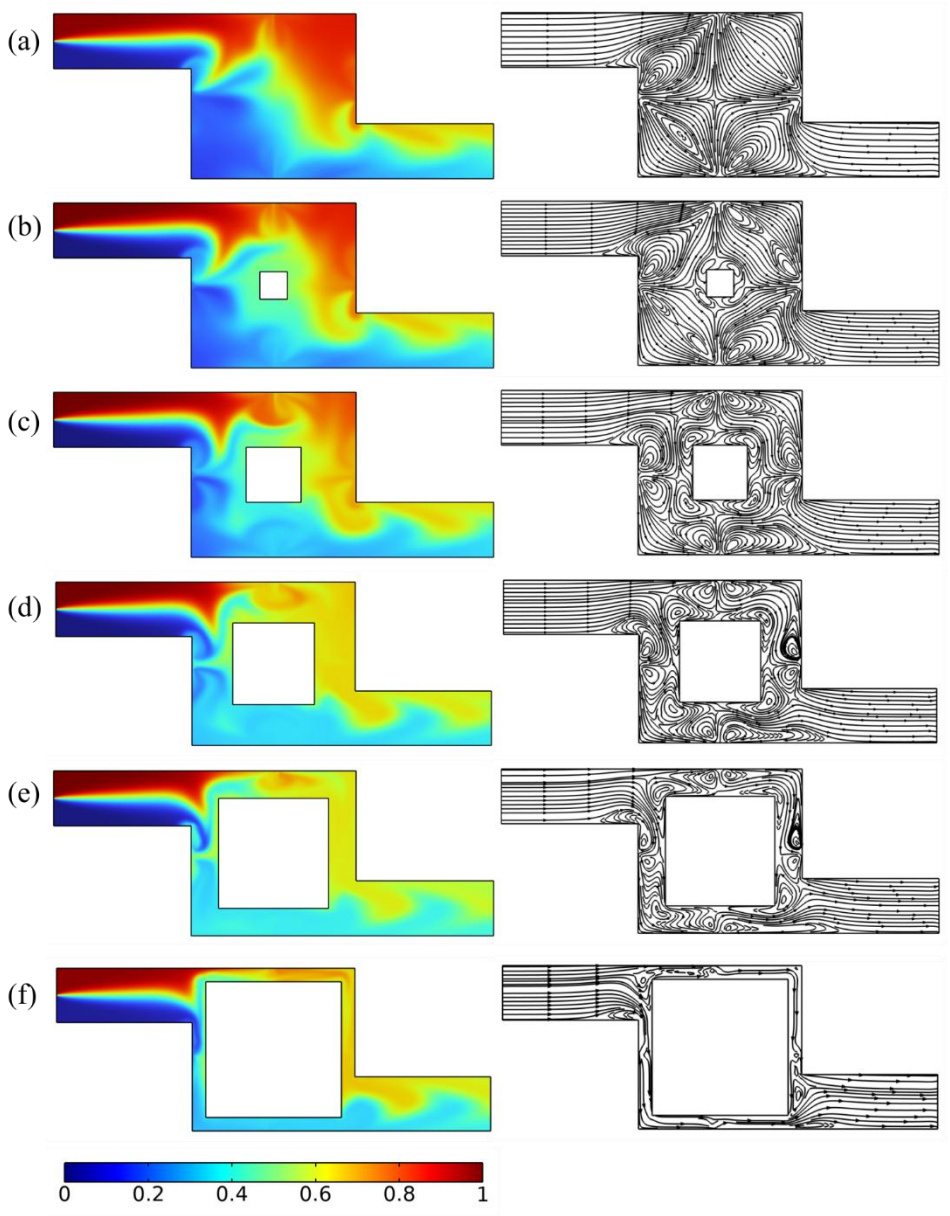

Figure 7.2 Spatial distribution of species concentration and fluid streamlines in Square split and recombined (SSAR) electroosmotic micromixer of varying obstacle sizes. (a) L_o = 0 µm, (b) L_o = 5 µm, (c) L_o = 10 µm, (d) L_o = 15 µm, (e) L_o = 20 µm, (f) L_o = 25 µm, Simulation parameters: inlet velocity (u_0) = 100 µm/s, AC voltage amplitude (ϕ_0) = 100 mV, frequency (f) = 8 Hz electrode length (L_e) = 2 µm, at a time (t) = 0.9625 s.

In Figure 7.2, the concentration and streamline profiles reveal several important observations:

1. **Flow splitting and recombination**: The introduction of obstacles within the square chamber demonstrates the splitting of fluid streams as they encounter the obstacle, followed by recombination downstream. This effect becomes more pronounced with increasing obstacle length.

2. **Vortex formation**: In the absence of obstacles (Figure 7.2a), four primary vortices are observed within the mixing chamber. As obstacle size increases, the vortex patterns are significantly modified, with the formation of additional, smaller vortices in the regions adjacent to the obstacles.
3. **Streamline disruption**: Larger obstacles (Figure 7.2e-f) cause more significant disruption of the streamlines, forcing fluid elements to take more circuitous paths through the mixing chamber and potentially enhancing mixing through increased path length and interfacial area.
4. **Concentration gradients**: The concentration profiles indicate more effective mixing in configurations with moderate obstacle lengths (Figure 7.2d-e), as evidenced by the more uniform concentration distribution at the outlet. Very small obstacles (Figure 7.2b) show limited improvement over the basic square chamber, while excessively large obstacles (Figure 7.2f) appear to impede fluid flow and may reduce the effectiveness of electroosmotic actuation.
5. Many of these findings are consistent with our earlier observations noted in the previous chapter.

To quantitatively assess the impact of obstacle size on mixing performance, Figure 7.3 presents the temporal evolution of mixing efficiency for different obstacle lengths.

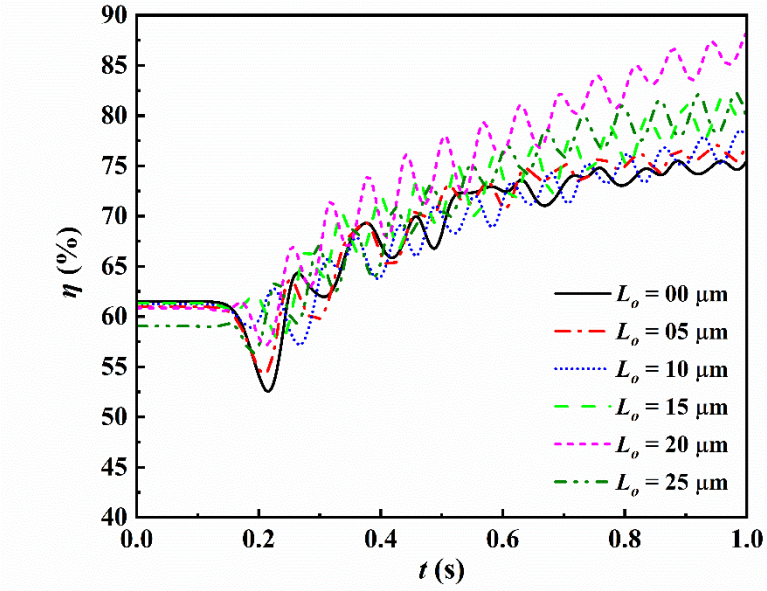

Figure 7.3 Temporal evolution of absolute mixing efficiency for Square split and recombined (SSAR) electroosmotic micromixer with obstacle sizes ranging from 0 to 25 µm. Simulation parameters: inlet velocity (u_0) = 100 µm/s, AC voltage amplitude (ϕ_0) = 100 mV, frequency (f) = 8 Hz, electrode length (L_o = 2 µm).

The mixing efficiency profiles in Figure 7.3 provide several key insights:

1. **Optimal obstacle length**: An obstacle length of 20 μm achieves the highest mixing efficiency throughout most of the simulation period, reaching approximately 89% efficiency at the end state. This represents a significant improvement over the basic diamond chamber (0 μm obstacle) which achieves approximately 75% efficiency under the same conditions.
2. **Non-monotonic relationship**: The relationship between obstacle length and mixing efficiency is non-monotonic, with performance initially improving as obstacle length increases from 0 μm to 20 μm, but then declining for larger obstacles (25 μm). This suggests the existence of a critical obstacle size that optimally balances flow splitting/recombination effects with electroosmotic actuation which is consistent with the findings from Chapter 6.
3. **Temporal response**: The configurations with moderate obstacle lengths (10-20 μm) not only achieve higher ultimate mixing efficiencies but also reach a steady state more rapidly, indicating enhanced mixing kinetics, which is consistent with the findings from Chapter 6.
4. **Performance degradation with excessive obstacle size**: The significant decrease in mixing efficiency observed with the 25 μm obstacle suggests that excessively large obstacles may impede fluid flow and restrict the development of electroosmotically-induced vortices, counteracting the benefits of the split and recombine effect, which is again consistent with the findings from Chapter 6.

The observed enhancement in mixing performance with the optimal obstacle length (20 μm) can be attributed to several factors:

- Effective balance between flow obstruction and electroosmotic actuation
- Creation of optimal flow path lengths for fluid elements traversing the mixing chamber
- Formation of secondary vortices that complement the primary electroosmotically-induced vortices
- Increased interfacial area between fluid streams due to the split and recombine effect
- Enhanced strain and stretching of fluid elements as they navigate around the obstacle

The optimal obstacle length of 20 µm represents approximately 66.66% of the square chamber side length (30 µm), suggesting a design guideline for similar SSAR micromixers. As found in the previous chapter (i.e., Chapter 6), obstacles and electrode length, both influence the electric field distribution. Therefore, as we did in the previous chapter, we will exclude the most unfavorable mixing efficiency cases (i.e., no-obstacle configuration and the largest obstacle case) from the subsequent section that examines the impact of electrode length on mixing performance.

7.6.2 *Effect of Electrode Length on Mixing Performance*

The length of the electrodes positioned on the peripheral walls of the square chamber plays a crucial role in determining the strength and distribution of the electroosmotically-induced flow field. This section investigates the influence of electrode length (L_e) on the mixing performance of the SSAR micromixer, considering its interaction with obstacle size.

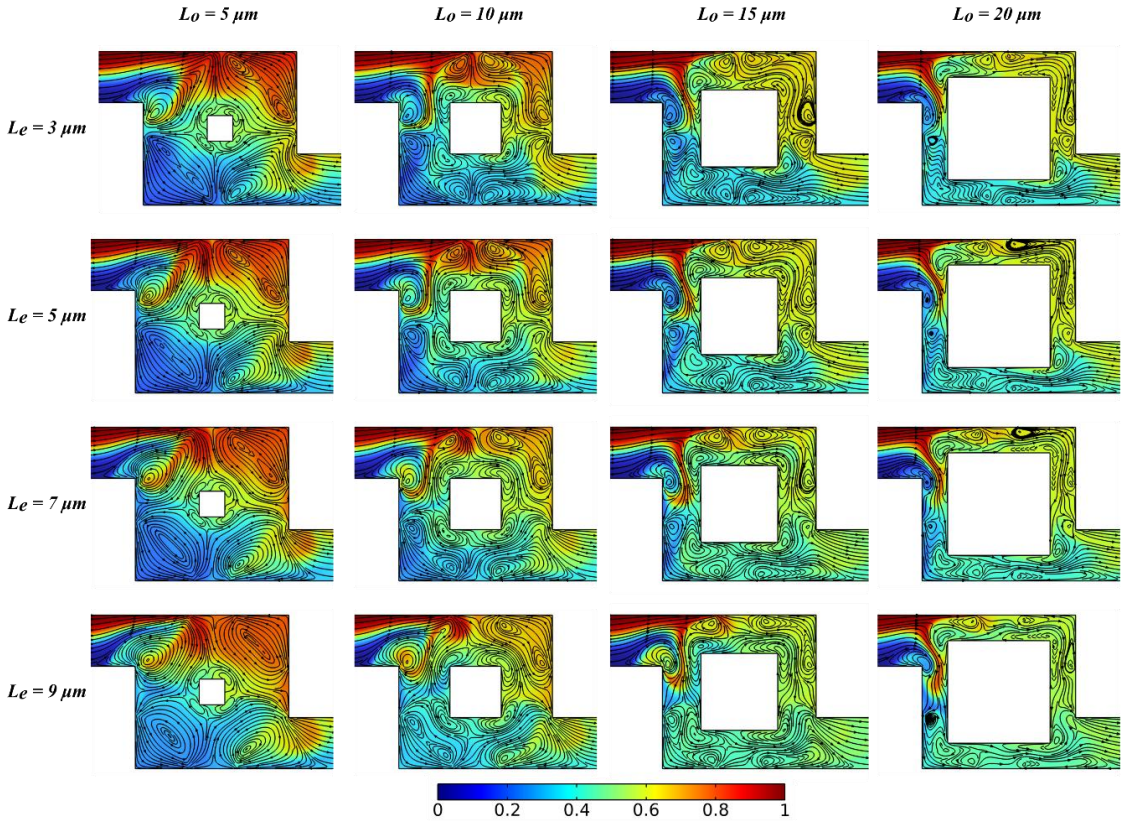

Figure 7.4 Combined spatial distribution of species concentration and fluid streamlines in square split and recombined (SSAR) mixing microchamber of varying obstacle sizes and electrode length. Simulation parameters: inlet velocity (u_0) = 100 µm/s, AC voltage amplitude (ϕ_0) = 100 mV, frequency (f) = 8 Hz, at a time (t) = 0.98333 s.

Simulations were conducted for electrode lengths ranging from 2 μm to 9 μm, in combination with obstacle lengths of 5 μm, 10 μm, 15 μm, and 20 μm, while maintaining constant inlet velocity (u_0 = 100 μm/s), voltage amplitude (ϕ_0 = 100 mV), and frequency (f = 8 Hz).

Figure 7.4 presents the concentration and streamline profiles for selected combinations of electrode length and obstacle size at t = 0.98333 s.In Figure 7.4, the concentration and streamline profiles reveal the complex interaction between electrode length and obstacle size:

1. **Electroosmotic actuation strength**: Longer electrodes (9 μm) generate stronger electroosmotic flows, as evidenced by the more pronounced vortices and greater disturbance of the concentration field compared to shorter electrodes (3 μm).
2. **Synergistic effects**: The combination of longer electrodes with optimal obstacle sizes (20 μm) appears to produce synergistic enhancement of mixing, with more uniform concentration distributions at the outlet than either feature alone.
3. **Vortex characteristics**: The size, position, and strength of the electroosmotically-induced vortices are significantly influenced by both electrode length and obstacle size, with longer electrodes generally producing larger, more powerful vortices, which is consistent with findings in Chapter 6.
4. **Flow field complexity**: The interaction between obstacle-induced flow splitting and electroosmotic actuation creates complex flow patterns, particularly with longer electrodes, which may contribute to enhanced chaotic advection and improved mixing.

To quantitatively assess the relationship between electrode length and mixing performance, Figure 7.5 presents the mixing efficiency as a function of electrode length for different obstacle sizes.

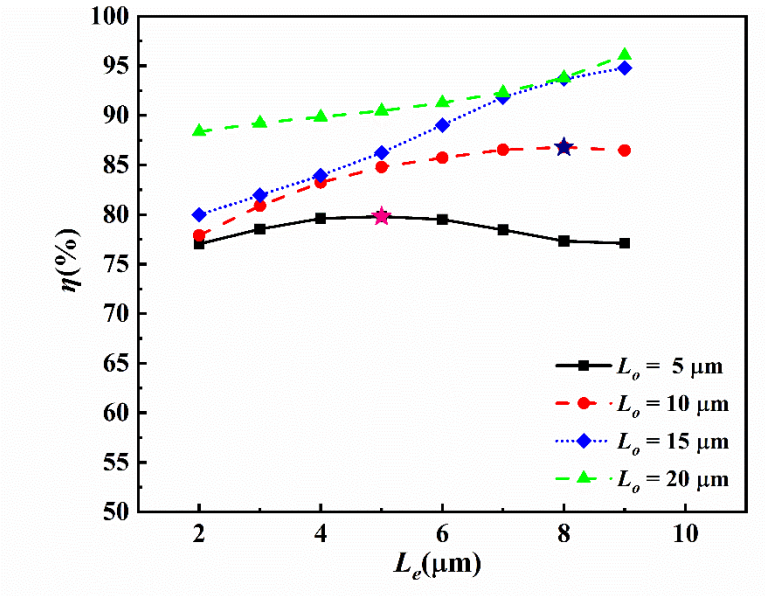

Figure 7.5 Absolute mixing efficiency versus electrode length (L_e) for square mixing microchamber with obstacle sizes ranging from 5 to 20 μm. Simulation parameters: inlet velocity (u_0) = 100 μm/s, AC voltage amplitude (ϕ_0) = 100 mV, frequency (f) = 8 Hz.

The results demonstrate several important trends:

1. **Positive correlation**: For relatively larger obstacle sizes (15 and 20 μm), increasing the electrode length generally leads to improved mixing efficiency, indicating that stronger electroosmotic actuation enhances the mixing process, which is consistent with Chapter 6.

2. **Obstacle-dependent response**: The sensitivity of mixing efficiency to electrode length varies with obstacle size. For the 15 μm obstacle, mixing efficiency increases significantly with electrode length, reaching approximately 94% with a 9 μm electrode, though the slope of mixing efficiency corresponding to the 20 μm obstacle is less than that of the 15 μm case. The mixing efficiency is consistently higher than that of the 15 μm obstacle, and it also reaches approximately 96% with the same electrode size of 9 μm. In contrast, the 5 μm and 20 μm obstacles show more modest improvements with increasing electrode length.

3. **Optimal configuration**: The combination of 20 μm obstacle length and 9 μm electrode length achieves the highest mixing efficiency among all tested configurations, suggesting this represents an optimal balance between flow splitting/recombination and electroosmotic actuation.

4. **Diminishing returns**: For the 5 μm and 10 μm obstacles, the benefit of increasing electrode length appears to plateau beyond 5 μm and 8 μm, suggesting that there may be limits to the improvements achievable through electrode lengthening, depending on the obstacle configuration.

The enhanced performance observed with longer electrodes can be attributed to factors as discussed in Chapter 6.

The findings indicate that the combination of appropriately sized obstacles (20 μm) with extended electrodes (9 μm) provides the most effective configuration for the SSAR micromixer, achieving significantly higher mixing efficiency than either feature alone. This optimal configuration will be used as the basis for subsequent investigations of operational parameters, also, this is not totally consistent with Chapter 6, where the optimal obstacle size found was 15 μm.

7.6.3 *Identification of Suitable Inlet Velocity*

The inlet velocity significantly influences the balance between convective transport, diffusive mixing, and electrokinetic effects in the SSAR micromixer. This section investigates the effect of inlet velocity on mixing performance, focusing on the optimal geometric configuration identified in the previous sections (obstacle length L_o = 20 μm, electrode length L_e = 9 μm).

Simulations were conducted for inlet velocities ranging from 50 μm/s to 500 μm/s, while maintaining constant voltage amplitude (ϕ_0 = 100 mV) and frequency (f = 8 Hz). Figure 7.6 presents the concentration and streamline profiles for different inlet velocities at t = 0.83333 s.

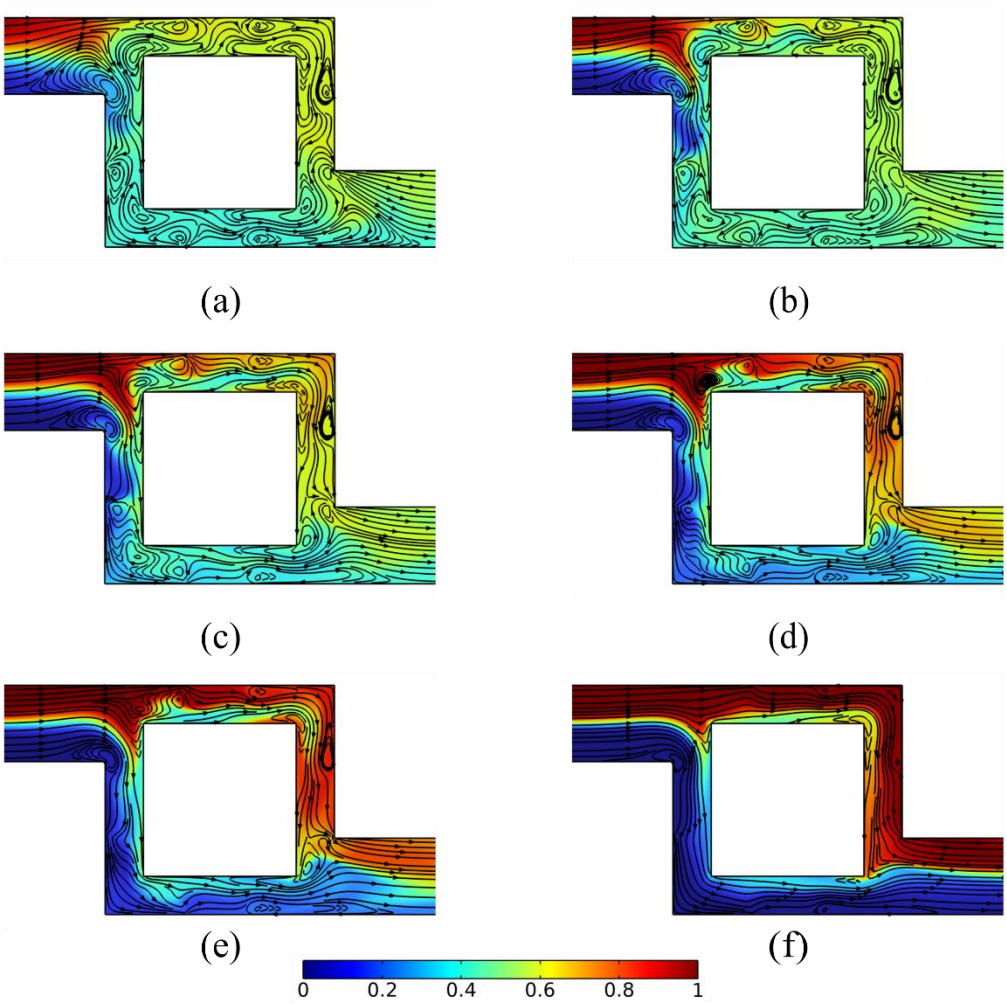

Figure 7.6 Concentration and streamline profiles for various inlet velocities at t = 0.83333 s [L_o = 20 µm, ϕ_o = 100 mV, f = 8 Hz]: (a) u_o = 50 µm/s, (b) u_o = 100 µm/s, (c) u_o = 150 µm/s, (d) u_o = 200 µm/s, (e) u_o = 250 µm/s, and (f) u_o = 500 µm/s.

The concentration and streamline profiles reveal several important observations (which are primarily consistent with Chapter 6:

1. **Velocity-dependent vortex formation**: At lower velocities (50-100 µm/s), well-defined vortices are observed both upstream and downstream of the obstacle, contributing to effective mixing. As velocity increases, the downstream vortices become less prominent, while the upstream vortices become compressed against the obstacle.
2. **Flow penetration**: At lower velocities, the electroosmotically-induced flow patterns penetrate farther into the main channel, affecting a larger portion of the fluid domain. This effect diminishes with increasing velocity as inertial forces begin to dominate.

3. **Residence time effects**: Lower velocities provide longer residence times within the mixing chamber, allowing more time for diffusive mixing and electrokinetic effects to act on the fluid elements.
4. **High-velocity limitations**: At very high velocities (500 μm/s), the flow becomes predominantly convective, with minimal influence from electroosmotic effects, resulting in poor mixing as evidenced by the distinct separation between the two fluid streams at the outlet.

To quantitatively assess the effect of inlet velocity on mixing performance, Figure 7.7 presents the temporal evolution of mixing efficiency and the relative mixing efficiency change with respect to steady state for different inlet velocities.

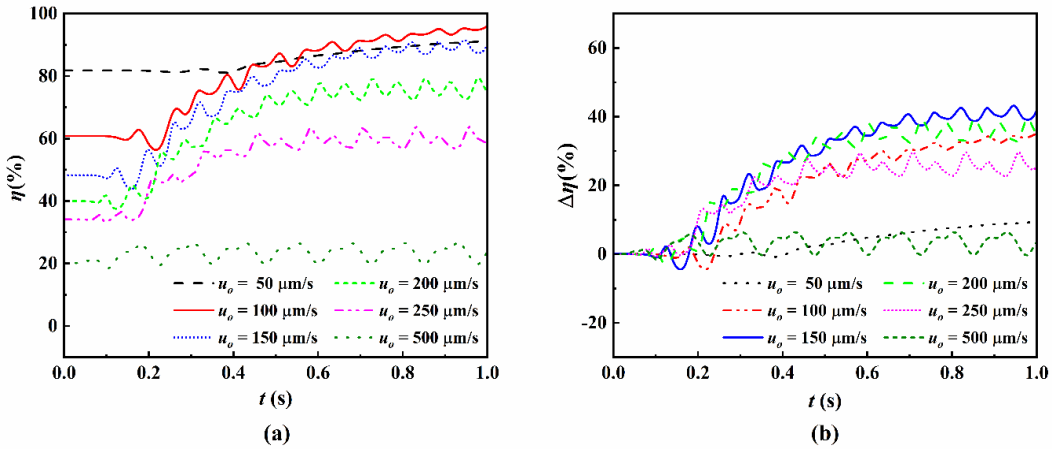

Figure 7.7 Effect of inlet velocity on mixing efficiency [L_o = 20 μm, L_e = 9 μm, ϕ_0 = 100 mV, f = 8 Hz]: (a) Mixing efficiency versus time for various inlet velocities, and (b) Relative mixing efficiency change with respect to steady state for different inlet velocities.

In Figure 7.7, The mixing efficiency profiles provide several key insights:

1. **Optimal velocity range**: The highest mixing efficiencies are achieved within the velocity range of 50-150 μm/s, with the 100 μm/s configuration reaching approximately 96% efficiency at steady state.
2. **Enhanced performance at low velocities**: Likely of DSAR micromirer the SSAR micromixer also shows consistently superior performance at moderate velocities (100 μm/s), suggesting that the obstacle-enhanced design is particularly effective as the number of vortices generated is maximized.
3. **Relative enhancement**: The relative mixing efficiency change with respect to steady state (Figure 7.7b) shows that the 150 μm/s and 200 μm/s

configurations achieve the greatest improvement relative to their steady-state baseline, indicating that the SSAR design is particularly effective at enhancing mixing at these moderate velocities, which is again consistent with DSAR micromixer investigated in Chapter 6.

4. **Sharp decline at high velocities**: Beyond 200 μm/s, mixing efficiency decreases rapidly, with the 500 μm/s configuration achieving only about 24% efficiency. This decline is a bit less pronounced than in the DSAR chamber, suggesting that the SSAR design is relatively more stable than the DSAR design due to velocity variations.

The superior performance of the SSAR micromixer at moderate velocities can be attributed to factors as described in Chapter 6 for the DSAR micromixer.

These findings suggest that the SSAR micromixer is well-suited for applications requiring high mixing efficiency at moderate flow rates, and it is almost as efficient as the DSAR micromixer, although it has a more compact design than the DSAR micromixer.

7.6.4 *Impact of AC Voltage Amplitude*

The amplitude of the applied AC voltage directly influences the strength of the induced electroosmotic flow and, consequently, the mixing performance of the SSAR micromixer. This section investigates the effect of voltage amplitude on mixing efficiency, focusing on the optimal geometric configuration (obstacle length L_o = 20 μm, electrode length L_e = 9 μm) and the velocity range identified as most effective (100-200 μm/s).

Simulations were conducted for voltage amplitudes ranging from 50 mV to 250 mV, considering inlet velocities of 100 μm/s, 150 μm/s, and 200 μm/s, while maintaining a constant frequency of 8 Hz. Figure 7.8 illustrates the mixing efficiency as a function of voltage amplitude at the simulation endpoint (t = 1.0 s) for different inlet velocities.

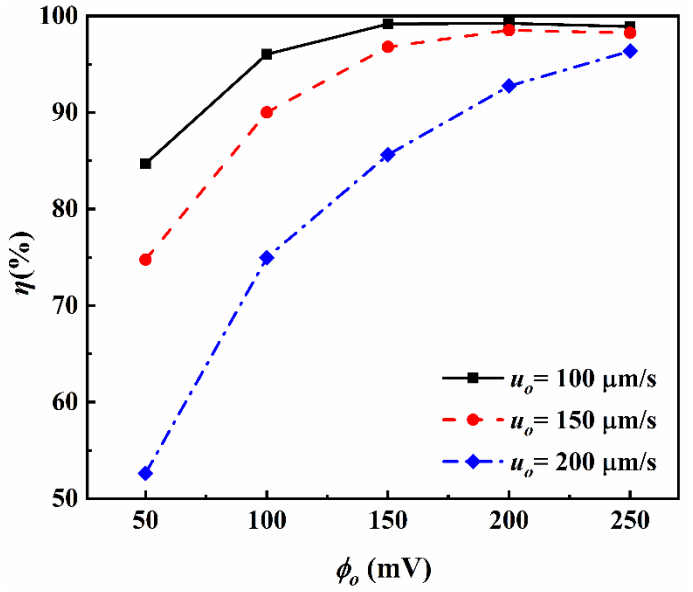

Figure 7.8 Mixing efficiency as a function of voltage amplitude for various inlet velocities at t = 1.0 s.

In Figure 7.8, the results reveal several important trends:

1. **Positive correlation**: For all inlet velocities, mixing efficiency generally increases with voltage amplitude, indicating that stronger electroosmotic actuation enhances the mixing process in the SSAR micromixer, which is consistent with the DSAR micromixer investigated in Chapter 6.
2. **Velocity-dependent response**: The sensitivity of mixing efficiency to voltage amplitude varies with inlet velocity. At lower velocities (100 μm/s), a relatively modest voltage (150 mV) is sufficient to achieve near-complete mixing (>99%). In contrast, higher velocities (200 μm/s) require higher voltages to achieve comparable performance.
3. **Optimal voltage-velocity combinations**: The highest mixing efficiency (99.2%) is achieved with 200 mV at 100 μm/s, while 250 mV provides the best performance of 98.24% and 97% at 150 μm/s and 200 μm/s respectively. This shows that using 250 mV further cuts energy requirements by approximately 16.67% to achieve similar mixing levels compared to using 300 mV in setup i.e., the DSAR micomixer.

To examine the temporal evolution of mixing efficiency under different voltage conditions, Figure 7.9 presents the mixing efficiency as a function of time for various voltage amplitudes and inlet velocities.

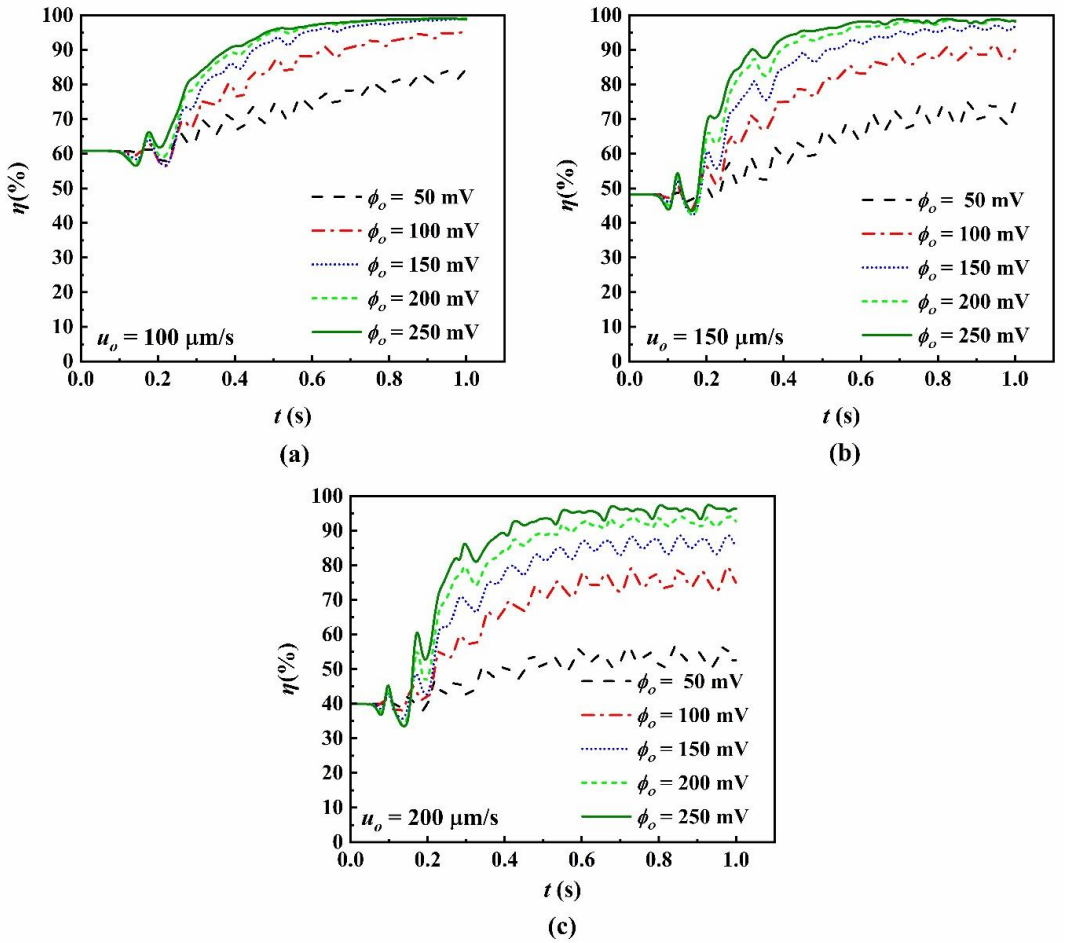

Figure 7.9 Temporal evolution of mixing efficiency for voltage amplitudes ranging from 50 mV to 250 mV at inlet velocities of (a) 100 μm/s, (b) 150 μm/s, and (c) 200 μm/s.

The temporal evolution profiles provide additional insights, which are primarily similar to those of the DSAR micromixer:

1. **Enhanced mixing kinetics**: Higher voltage amplitudes not only improve ultimate mixing efficiency but also accelerate the mixing process, as evidenced by the steeper initial slopes of the mixing efficiency curves for higher voltages.
2. **Fluctuation characteristics**: At higher velocities and voltages, the mixing efficiency exhibits more pronounced oscillations, reflecting the dynamic competition between convective transport and electroosmotic effects.
3. **Steady-state behavior**: For lower velocities (100 μm/s), the system reaches a stable steady state more rapidly and with fewer fluctuations compared to higher velocities, particularly at moderate to high voltage amplitudes (150-250 mV).

The enhanced performance observed with higher voltage amplitudes can be attributed to several factors:

- Stronger electroosmotic slip velocities at the electrode surfaces
- More powerful vortices capable of overcoming convective transport
- Enhanced chaotic advection due to stronger time-dependent flows
- More effective interaction between electroosmotic flows and obstacle-induced flow patterns
- Greater penetration of electrokinetic effects into the main channel

These findings highlight the importance of voltage amplitude as a key operational parameter for optimizing the performance of the SSAR micromixer. The ability to achieve near-complete mixing (>99%) with moderate voltages (150 mV) at practical flow rates (100 μm/s) and good mixing (>97%) with high voltages (250 mV) for higher flow rates (150-200 μm/s) demonstrate the effectiveness of the SSAR design in enhancing microfluidic mixing. Furthermore, the SSAR design is found to be more compact and energy-efficient compared to the DSAR micromixer.

7.6.5 *Effect of AC Frequency*

The frequency of the applied AC signal determines the rate of polarity switching at the electrodes and significantly influences the electroosmotic flow patterns within the SSAR micromixer. This section investigates the effect of frequency on mixing efficiency, focusing on the optimal geometric configuration (obstacle length L_o = 20 μm, electrode length L_e = 9 μm) and voltage amplitude (250 mV).

Simulations were conducted for frequencies ranging from 2 Hz to 18 Hz, considering inlet velocities of 100 μm/s, 150 μm/s, and 200 μm/s. Figure 7.10 illustrates the mixing efficiency as a function of frequency at the simulation endpoint (t = 1.0 s) for different inlet velocities.

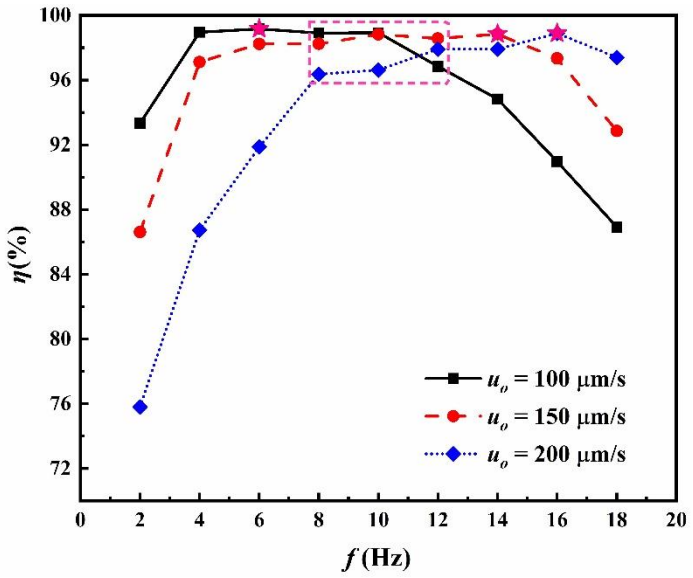

Figure 7.10 Mixing efficiency as a function of AC frequency for inlet velocities of 100, 150, and 200 μm/s at t = 1 s.

The results reveal several important observations:

1. **Complex frequency dependence**: The relationship between frequency and mixing efficiency is non-monotonic, with separate plateaus observed across different velocities. This behavior suggests intricate interactions between the time-dependent electroosmotic flows, the obstacle, and mixing chamber design-induced flow patterns.
2. **Velocity-specific optimal frequencies**: Each inlet velocity exhibits distinct optimal frequencies for maximum mixing efficiency. For 100 μm/s, the highest efficiency (99.2%) is achieved at 6 Hz; for 150 μm/s, optimal performance (98.99%) occurs at 14 Hz; and for 200 μm/s, the best results (98.99) are observed at 16 Hz.
3. **High and consistent performance at moderate frequencies**: Across all velocities, the frequency range of 8-12 Hz generally provides high mixing efficiency (≥ 96%), suggesting this represents a practical operating range for the SSAR micromixer.

To gain deeper insights into the transient behavior, Figure 7.11 presents the temporal evolution of mixing efficiency for different frequencies and inlet velocities.

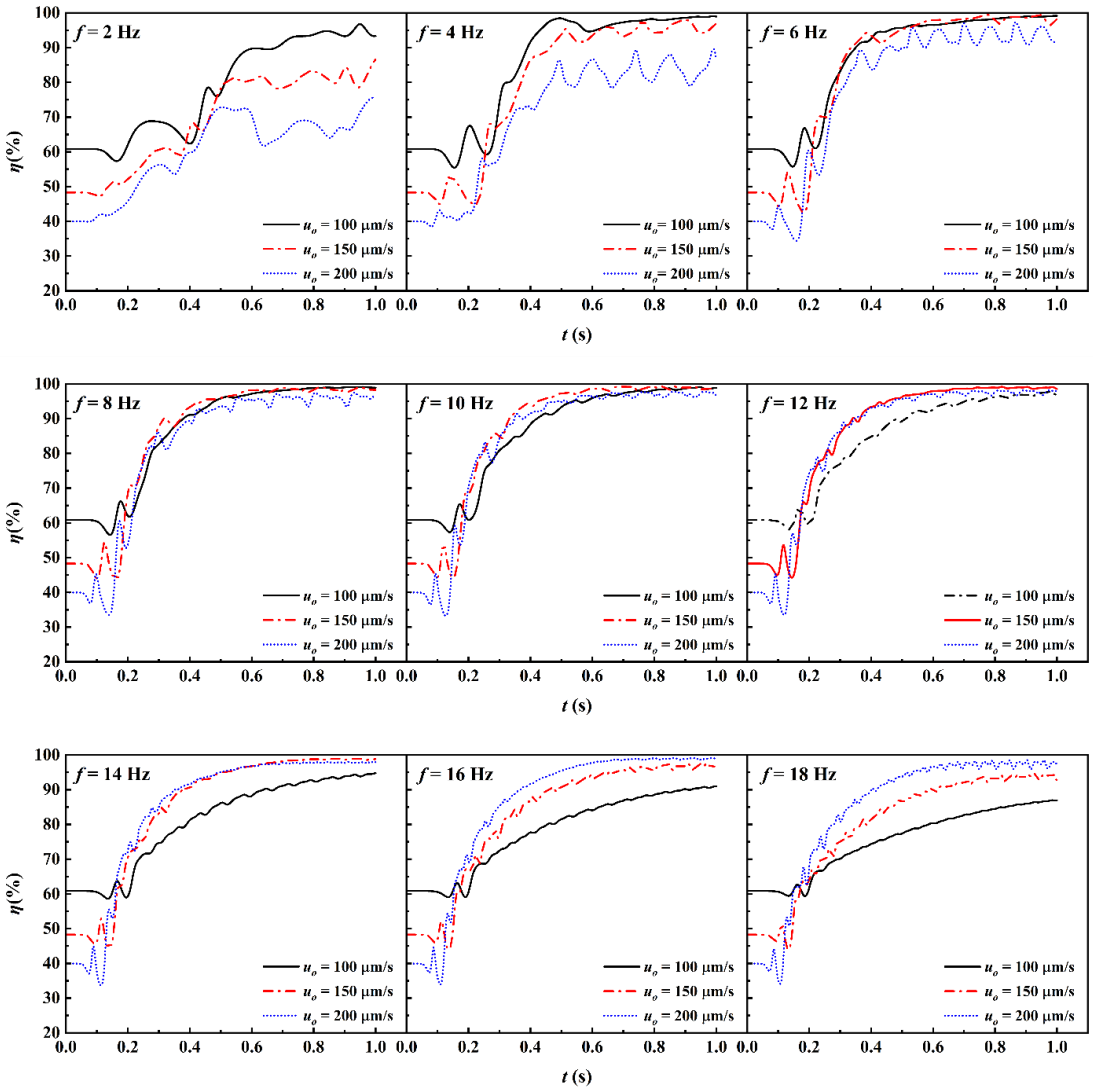

Figure 7.11 Temporal evolution of mixing efficiency for frequencies f = 2–18 Hz and inlet velocities of 100, 150, and 200 μm/s.

In Figure 7.11, the temporal evolution profiles provide additional insights:

1. **Frequency-dependent mixing dynamics**: Lower frequencies (2-4 Hz) generally exhibit larger amplitude fluctuations in mixing efficiency, particularly at higher inlet velocities, indicating less stable mixing processes, which is consistent with the DSAR micromixer investigated in Chapter 6.
2. **Stabilization effect of moderate frequencies**: The frequency range of 10-14 Hz tends to produce smoother mixing efficiency curves with smaller fluctuations, suggesting more stable and reliable mixing performance.
3. **Initial mixing rate**: Moderate frequencies generally lead to more rapid initial increases in mixing efficiency, potentially beneficial for applications requiring quick mixing responses.

4. **Steady-state behavior**: For velocities of 100–200 μm/s, a frequency of 10 Hz achieves both stable and efficient steady-state performance with minimal fluctuations, while at higher frequencies (≥14 Hz), a smoother transition is attained, and a reversal in the mixing trend with velocity is observed.

The complex frequency dependence observed in the SSAR micromixer can be attributed to several factors that are primarily consistent with the DSAR micromixer from a physics point of view.

These findings highlight the importance of frequency selection in optimizing the performance of the SSAR micromixer. The identification of frequency ranges that provide high and stable mixing efficiency across different inlet velocities (particularly around the 8-12 Hz range) offers valuable guidance for the practical implementation of this micromixer design.

7.6.6 *Optimal Conditions for SSAR Micromixer Performance*

Based on the comprehensive parametric analysis presented in the preceding sections, we can identify the optimal conditions for maximizing the performance of the SSAR electroosmotic micromixer. Table 7.1 summarizes the key findings:

Table 7.1 Optimal parameters and maximum mixing efficiencies for the SSAR micromixer.

Parameter	Optimal Value	Maximum Mixing Efficiency
Obstacle Length	20 μm	88.37% (with L_e = 2 μm, u_o = 100 μm/s, ϕ_o = 100 mV, f = 8 Hz)
Electrode Length	9 μm	96.07% (with L_o = 20 μm, u_o = 100 μm/s, ϕ_o = 100 mV, f = 8 Hz)
Inlet Velocity	100 μm/s	96.02% (with L_o = 20 μm, L_e = 10 μm, ϕ_o = 250 mV, f = 8 Hz)
Voltage Amplitude	200 mV (for 100 μm/s)	99.23%
	200 mV (for 150 μm/s)	98.53%
	250 mV (for 200 μm/s)	96.36%
AC Frequency	4-10 Hz (for 100 μm/s)	> 99%
	4-14 Hz (for 150 μm/s)	> 98.5%
	12-16 Hz (for 200 μm/s)	> 98%

These optimal conditions are interrelated, and the maximum mixing efficiency can vary based on the specific as well as limited-range combinations of parameters employed. The results indicate that the SSAR micromixer can achieve exceptionally

high mixing efficiency (> 99%) under optimal conditions, representing a significant consistency with the DSAR chamber design presented in Chapter 6, but the SSAR design is found to be more compact and energy-efficient compared to the DSAR micromixer.

The key insights from this optimization study include:

1. **Geometric optimization**: An obstacle length of 20 μm (approximately 66.67% of the diamond chamber side length) and an electrode length of 9 μm provide the optimal geometric configuration for maximizing mixing efficiency.
2. **Operational parameters**: An inlet velocity of 100 μm/s, combined with a voltage amplitude of 250 mV and a frequency range of 4-10 Hz, yields the highest mixing performance (>99% efficiency).
3. **Operational flexibility**: The SSAR design maintains high mixing efficiency (>96%) across a broader range of operational parameters, particularly with respect to frequency variations (8-12 Hz for all velocities in the cogent range), offering flexibility for practical applications.
4. **Consistent performance at less energy and compact design**: Under optimal conditions, the SSAR micromixer achieves approximately consistent mixing efficiency (99.23%) compared to the DSAR chamber presented in Chapter 6 (maximum efficiency of 99.3% under its optimal conditions), but the design is more compact, and the energy required to attain this level is less than that of the DSAR micromixer.

These findings demonstrate that the integration of optimally-sized obstacles within a square mixing chamber, combined with appropriately configured electrodes and operational parameters, can substantially enhance mixing performance in electroosmotic micromixers. The SSAR design effectively leverages the synergistic benefits of obstacle-induced flow manipulation and electrokinetic actuation to achieve exceptional mixing efficiency under practical operating conditions.

7.6.7 *Potential Challenges and Limitations*

While the SSAR micromixer demonstrates exceptional performance under optimal conditions, several challenges and limitations must be considered for practical implementation, which is primarily similar to that of the DSAR micromixer design

investigated in Chapter 6. But the SSAR design is 1/√2 times more compact and 16.67% more energy-efficient compared to the DSAR micromixer.

7.7 Conclusion

This chapter presents a comprehensive investigation into the design and performance of an offset Square Split and Recombined (SSAR) electroosmotic micromixer, which integrates obstacles within a square mixing chamber to enhance mixing through the combined effects of electrokinetic actuation and flow manipulation. Through systematic numerical simulations and analysis, we have explored the effects of various geometric and operational parameters on mixing efficiency, leading to the following key findings:

1. **Enhanced Mixing Mechanism**: The SSAR micromixer leverages a synergistic combination of obstacle-induced flow splitting/recombination and AC electroosmotic actuation to achieve exceptionally high mixing efficiency. The obstacles disrupt laminar flow patterns and create additional interfacial area between fluid streams, while the electroosmotic effects generate time-dependent vortices that promote chaotic advection.
2. **Compact Geometric Configuration**: An obstacle length of 20 μm (approximately 66.67% of the square chamber side length) and an electrode length of 9 μm represent the optimal geometric configuration for maximizing mixing performance. Also, this configuration design is 1/√2 times more compact compared to the DSAR micromixer.
3. **Operational Parameter Optimization**: Under optimal conditions (inlet velocity of 100 μm/s, voltage amplitude of 250 mV, and frequency of 4-10 Hz), the SSAR micromixer achieves near-complete mixing (≥99% efficiency), representing a consistent result with the DSAR chamber design presented in Chapter 6.
4. **Energy Efficiency**: The DSAR design requires substantially lower voltage amplitudes (250 mV vs. 300 mV) to achieve optimal performance compared to the DSAR chamber, representing a 16.67% reduction in voltage requirements. This enhanced energy efficiency has significant implications for the integration of SSAR micromixers with low-power microfluidic systems.

5. **Operational Flexibility**: The SSAR micromixer maintains high mixing efficiency across a range of frequencies and a range of inlet velocities, offering greater flexibility for practical applications compared to the DSAR chamber design.

These findings demonstrate that the SSAR design represents a significant advancement in electroosmotic micromixer technology, offering substantial improvements in mixing efficiency, energy efficiency, and operational flexibility. The integration of optimally-sized obstacles within a square mixing chamber with offset inlet-outlet microchannels effectively leverages the benefits of both passive (obstacle-induced) and active (electroosmotic) mixing strategies, resulting in enhanced performance across multiple metrics.

Chapter – 8

Outcome Summary, Contribution and Future Scope

8.1 Overall Outcomes of the Present Investigations

A comprehensive investigation of four distinct electroosmotic micromixer designs has been conducted systematically, progressing from basic to advanced configurations to achieve enhanced mixing efficiency. Beginning with a fundamental circular chamber design, the research methodically evolved through diamond geometry, diamond split-and-recombined (DSAR), and finally square split-and-recombined (SSAR) configurations, each representing a significant advancement in mixing performance and practical implementation.

From the detailed parametric investigations conducted across all four micromixer designs, I have synthesized the key findings into comprehensive comparative tables. Table 8.1 presents a comparative analysis of the essential design features, performance metrics, and optimal parameters for all four micromixer configurations.

Table 8.1 Comprehensive Micromixer Design Evolution and Performance Comparison.

Optimal Design Feature	Circular Chamber	Diamond Chamber	DSAR	SSAR
Maximum η (%)	98.84	99.09	99.60	99.36
Microchamber dimensions (μm)	D = 20	L_s = 20	L_s = 30, L_o = 15	L_s = 30, L_o = 20
Electrode length (μm)	2	2	10	9
Voltage (mV) for maximum η	500	500	300	250
Velocity range (μm/s)	100	150	100	150
AC frequency (Hz)	12	2	4 and 8	6
Primary mixing mechanism	Electroosmotic vortices	Enhanced interface stretching	Synergistic obstacle-vortex interaction	Extended flow path with obstacle interaction
Fabrication considerations	Curved walls with electrode mounting challenges	Angled walls with improved electrode placement	Complex obstacle integration	Flat walls and straight channels for simplified fabrication

As evident from Table 8.1, there is a clear progression in mixing efficiency from the initial circular chamber design (98.84%) to the advanced SSAR configuration (99.36%), with the DSAR design achieving the highest overall efficiency (99.60%). This improvement correlates with increasingly sophisticated geometric features and their interaction with electroosmotic phenomena. The circular chamber relied primarily on electroosmotically-induced vortices, while the diamond chamber enhanced mixing through better interface stretching along its linear walls. The DSAR and SSAR designs introduced obstacles that created split-and-recombine effects that worked synergistically with electroosmotic actuation.

The design evolution also reveals important trends in optimal operational parameters. The voltage requirement for maximum efficiency decreased significantly from 500 mV for the circular and diamond designs to 300 mV for the DSAR and 250 mV for the SSAR configuration, indicating progressive improvement in energy efficiency. The optimal velocity remained within the 100-150 μm/s range across all designs, while optimal frequency showed design-specific values with the SSAR design offering the widest operational range.

Table 8.2 quantifies the incremental improvements observed through each design iteration, providing a clear measure of the benefits achieved through each evolutionary step.

Table 8.2 Performance enhancement progression across design generations.

Performance Metric	Circular → Diamond	Diamond → DSAR	DSAR → SSAR	Overall Improvement
Mixing efficiency increase (%)	+0.245	+0.51	-0.24	+0.52
Reduction in required voltage (%)	0	40	16.67	50
Improvement in frequency stability range*	Limited (±2 Hz)	Moderate (±4 Hz)	Wide (±6 Hz)	Significantly expanded
Fabrication complexity reduction**	Moderate improvement	Slight increase	Significant improvement	Net improvement

*Frequency range where mixing efficiency remains within 2% of maximum.
**Qualitative assessment based on geometric features and fabrication requirements.

Table 8.2 demonstrates that the most substantial improvement in mixing efficiency occurred in the transition from diamond to DSAR geometry (+0.51%), while the most significant reduction in voltage requirements was achieved in the

DSAR design (40% reduction) and further improved in the SSAR configuration (additional 16.67% reduction). The frequency stability range—representing the span of frequencies over which the micromixer maintains near-optimal performance—widened considerably across design generations, with the SSAR design offering the broadest operational flexibility.

The fabrication considerations improved overall from the initial circular design to the final SSAR configuration, despite a slight increase in complexity with the DSAR design due to obstacle integration. The SSAR design, with its perpendicular walls, straight channels, and non-aligned configuration, represents a significant advancement in terms of fabrication practicality while maintaining excellent mixing performance.

For practical implementation, it is essential to identify the optimal design and operational parameters based on specific application requirements. Table 8.3 provides application-focused recommendations derived from the comprehensive parametric studies conducted across all four designs.

Table 8.3 Optimal design selection for application-specific requirements.

Application Requirement	Suitable Design	Optimal Parameters	Expected Performance
Highest mixing efficiency	DSAR	L_o = 15 μm, L_e = 10 μm, u_0 = 100 μm/s, ϕ_0 = 300 mV, f = 4 Hz	>99.5% mixing efficiency
Energy efficiency	SSAR	L_o = 20 μm, L_e = 9 μm, u_0 = 150 μm/s, ϕ_0 = 200 mV, f = 8 Hz	>98% η with 200 mV
Fabrication simplicity	SSAR	L_o = 20 μm, L_e = 9 μm, u_0 = 150 μm/s, ϕ_0 = 250 mV, f = 10 Hz	Flat walls, perpendicular turns with >98% η
Operational stability	SSAR	L_o = 20 μm, L_e = 9 μm, u_0 = 150 μm/s, ϕ_0 = 250 mV, f = 12 Hz	Consistent performance over 4-14 Hz frequency range
Higher flow rates	SSAR	L_o = 20 μm, L_e = 9 μm, u_0 = 200 μm/s, ϕ_0 = 250 mV, f = 14 Hz	>94% η at 200 μm/s

Table 8.3 highlights that while the DSAR design achieves the highest absolute mixing efficiency, the SSAR configuration offers superior performance in terms of energy efficiency, fabrication simplicity, and operational stability. Also, SSAR design remains competitive for applications requiring higher flow rates, where it maintains good mixing efficiency (>98.9%) at velocities up to 200 μm/s, which is further efficient in terms of relative mixing efficiency gain of 60%, offering the most effective utilization of electrical energy.

These comparative analyses demonstrate the significant advancements achieved through the systematic design evolution pursued in this thesis. The progression from basic circular geometry to advanced split-and-recombined designs has yielded highly efficient electroosmotic micromixers with mixing efficiencies approaching 100%, while simultaneously addressing practical implementation considerations such as energy efficiency, fabrication complexity, and operational stability.

8.2 Contributions and Future Scope of the Present Work

This research has made significant contributions to the field of microfluidic mixing through systematic design innovation, comprehensive physical analysis, and practical implementation considerations. The work has advanced both fundamental understanding and practical application of electroosmotic micromixers, establishing a foundation for next-generation microfluidic systems.

- **Novel Micromixer Architectures:** The research introduced a series of progressively optimized electroosmotic micromixer designs—circular, diamond, DSAR, and SSAR configurations—that demonstrated significant performance improvements from 94.15% to 99.60% mixing efficiency. The innovative integration of split-and-recombine mechanisms with electroosmotic actuation created synergistic enhancement effects, while the development of flat-walled geometries addressed practical fabrication challenges. This systematic evolution of designs bridges the gap between theoretical performance and practical implementation.
- **Electrokinetic Flow Control Advancement:** The research established fundamental relationships between chamber geometry and vortex formation, characterizing the impact of electrode placement, polarity arrangements, and obstacle integration on flow patterns. The investigation revealed complex non-monotonic relationships between operational parameters and mixing efficiency, particularly for AC frequency. These findings significantly advance the understanding of electroosmotic flow control in complex geometries and provide design principles for enhancing chaotic advection in microchannels.
- **Parametric Optimization Framework:** Through comprehensive numerical investigations, the research established a systematic framework for optimizing electroosmotic micromixers. The identification of geometry-specific optimal

parameters for chamber dimensions, electrode configuration, operational velocities, voltage amplitudes, and AC frequencies provides valuable design guidelines for different application requirements. The discovery of velocity-specific voltage requirements and frequency optima offers energy-efficient operation strategies for practical microfluidic systems.

- **Fabrication-Oriented Design Innovation:** The progression from curved geometries to flat-walled designs with strategic electrode placement addressed key fabrication challenges in electroosmotic micromixers. The SSAR design with non-aligned inlet-outlet channels offers an excellent combination of high performance (99.36% efficiency) and fabrication simplicity. The established relationships between geometric parameters and mixing efficiency enable designers to make informed trade-offs between performance and manufacturability.
- **Comprehensive Mixing Enhancement Strategies:** The research demonstrated multiple complementary approaches to mixing enhancement, including chamber geometry optimization, obstacle integration, electrode configuration tuning, and operational parameter adjustment. The DSAR design proved that obstacles could work synergistically with electroosmotic effects to improve mixing beyond what either approach could achieve alone. The identification of optimal phase differences in AC signals introduced an additional control parameter for fine-tuning mixing performance without increased power consumption.
- **Application-Specific Design Guidelines:** The research provides tailored guidelines for different microfluidic applications, identifying parameter combinations that optimize performance for specific flow rate requirements. The energy-efficient designs with low voltage requirements (200-300 mV) make these micromixers suitable for portable and point-of-care diagnostic devices. The established operational parameters for high-throughput mixing applications support the development of more effective and reliable microfluidic analytical systems.

This research has systematically addressed the challenges of microscale mixing through innovative design and comprehensive optimization, yielding highly efficient electroosmotic micromixers that combine performance excellence with

practical implementation considerations. The contributions span fundamental physical understanding, design methodology, and application-oriented guidelines, establishing a strong foundation for future advancements in microfluidic systems.

Future extensions of this work could take several promising directions. Experimental validation through prototype fabrication and performance characterization would provide valuable verification of the numerical predictions. Advanced geometric designs incorporating three-dimensional electrode arrangements and cascaded mixing elements could further enhance performance, while material innovations including biocompatible electrodes and functional surface coatings might expand application possibilities. System integration research focusing on component interfacing and comprehensive lab-on-chip platforms would address implementation challenges, and application-specific studies targeting biological fluid mixing, chemical reaction enhancement, and multi-phase systems would broaden the impact of these innovations. As microfluidic technologies continue to advance, these electroosmotic micromixer designs offer promising foundations for next-generation analytical, diagnostic, and synthesis platforms with enhanced capabilities and practical feasibility.

References

Afzal, A., and Kim, K.Y., 2015. Convergent–divergent micromixer coupled with pulsatile flow. *Sens. Actuators B*, 211, pp. 198–205.

Alipanah, M., Hatami, M. and Ramiar, A., 2021. Thermal and rheological investigation of non-Newtonian fluids in an induced-charge electroosmotic micromixer. *European Journal of Mechanics-B/Fluids*, 88, pp.178-190.

Bagherabadi, K.M., Sani, M., and Saidi, M.S., 2019. Enhancing active electro-kinetic micro-mixer efficiency by introducing vertical electrodes and modifying chamber aspect ratio. *Chem. Eng. Process.-Process Int.*, 142, p. 107560.

Bavil, A.K., and Kim, J., 2018. A capillary flow-driven microfluidic system for microparticle-labeled immunoassays. *Analyst*, 143(14), pp. 3335–3342.

Bayareh, M., Ashani, M.N. and Usefian, A., 2020. Active and passive micromixers: A comprehensive review. *Chemical Engineering and Processing-Process Intensification*, *147*, p.107771.

Bahrami, D., Bayareh, M. and Usefian, A., 2023. Effect of fin-shaped electrodes on flow mixing and pressure drop in an electroosmotic micromixer. *Iran. J. Chem. Chem. Eng. Research Article Vol*, *42*(1).

Biddiss, E., Erickson, D. and Li, D., 2004. Heterogeneous surface charge enhanced micromixing for electrokinetic flows. *Analytical chemistry*, *76*(11), pp.3208-3213.

Biswas, N., Mandal, D.K., Manna, N.K. and Benim, A.C., 2023. Enhanced energy and mass transport dynamics in a thermo-magneto-bioconvective porous system containing oxytactic bacteria and nanoparticles: cleaner energy application. *Energy*, *263*, p.125775.

Borgohain, P., Arumughan, J., Dalal, A., and Natarajan, G., 2018. Design and performance of a three-dimensional micromixer with curved ribs. *Chem. Eng. Res. Des.*, 136, pp. 761–775.

Chakraborty, S., and Ray, S., 2008. Mass flow-rate control through time-periodic electro-osmotic flows in circular microchannels. *Phys. Fluids*, 20, p. 083602.

Chatterjee, D., Biswas, N., Manna, N.K., and Sarkar, S., 2022. Effect of discrete heating-cooling on magneto-thermal-hybrid nanofluidic convection in cylindrical system. *Int. J. Mech. Sci.*, p. 107852.

Chen, C.K., and Cho, C.C., 2008. Electrokinetically driven flow mixing utilizing chaotic electric fields. *Microfluidics Nanofluidics*, 5(6), pp. 785–793.

Chen, H., Zhang, Y., Mezic, I., Meinhart, C. and Petzold, L., 2003, January. Numerical simulation of an electroosmotic micromixer. In *ASME International Mechanical Engineering Congress and Exposition* (Vol. 37165, pp. 653-658).

Chen, J.-L., Shih, W.-H., and Hsieh, W.-H., 2013. AC electro-osmotic micromixer using a face-to-face, asymmetric pair of planar electrodes. *Sens. Actuators B: Chem.*, 188, pp. 11–21.

Chen, J.K. and Yang, R.J., 2007. Electroosmotic flow mixing in zigzag microchannels. *Electrophoresis*, 28(6), pp.975-983.

Chen, X., and Wu, Z., 2019. Design and numerical simulation of a novel microfluidic electroosmotic micromixer with three electrode pairs. *J. Chem. Technol. Biotech.*, 94(6), pp. 1991–1997.

Chen, Y., and Kim, C.N., 2018. Numerical analysis of the mixing of two electrolyte solutions in an electromagnetic rectangular micromixer. *J. Ind. Eng. Chem.*, 60, pp. 377–389.

Chen, Z., Wang, Y. and Zhou, S., 2022. Numerical analysis of mixing performance in an electroosmotic micromixer with cosine channel walls. *Micromachines*, 13(11), p.1933.

Chen, Y., Li, J., Lv, Z., Wei, Y. and Li, C., 2023. Mixing performance of viscoelastic fluids in an induced charge electroosmotic micromixer with a conductive cylinder. *Journal of Non-Newtonian Fluid Mechanics*, 317, p.105047.

Cheng, Y., Jiang, Y. and Wang, W., 2018. Numerical simulation for electro-osmotic mixing under three types of periodic potentials in a T-shaped micro-mixer. *Chemical Engineering and Processing-Process Intensification*, *127*, pp.93-102.

Cheri, M.S., Latifi, H., Moghaddam, M.S., and Shahraki, H., 2013. Simulation and experimental investigation of planar micromixers with short-mixing-length. *Chem. Eng. J.*, 234, pp. 247–255.

Chin, C.D., Linder, V., and Sia, S.K., 2007. Lab-on-a-chip devices for global health: past studies and future opportunities. *Lab Chip*, 7(1), pp. 41–57.

Cho, C.C., Chen, C.L., and Chen, C.K., 2012. Mixing enhancement in crisscross micromixer using aperiodic electrokinetic perturbing flows. *Int. J. Heat Mass Transfer*, 55(11–12), pp. 2926–2933.

Convery, N. and Gadegaard, N., 2019. 30 years of microfluidics. *Micro and Nano Engineering*, *2*, pp.76-91.

Cortes-Quiroza, C.A., Azarbadegan, A., and Zangeneh, M., 2017. Effect of channel aspect ratio of 3-D T-mixer on flow patterns and convective mixing for a wide range of Reynolds number. *Sens. Actuators B: Chem.*, pp. 1153–1176.

Dallakehnejad, M., Mirbozorgi, S.A. and Niazmand, H., 2019. A numerical investigation of magnetic mixing in electroosmotic flows. *Journal of Electrostatics*, *100*, p.103354.

Das, S.S., Tilekar, S.D., Wangikar, S.S., and Patowari, P.K., 2017. Numerical and experimental study of passive fluids mixing in microchannels of different configurations. *Microsyst. Technol.*, pp. 5977–5988.

Deng, Y., Zhou, T., Liu, Z., Wu, Y., Qian, S. and Korvink, J.G., 2018. Topology optimization of electrode patterns for electroosmotic micromixer. *International Journal of Heat and Mass Transfer*, *126*, pp.1299-1315.

Ding, H., Zhong, X., Liu, B., Shi, L., Zhou, T., and Zhu, Y., 2021. Mixing mechanism of a straight channel micromixer based on light-actuated oscillating electroosmosis in low-frequency sinusoidal AC electric field. *Microfluid. Nanofluid.*, 25, pp. 1–15.

Fair, R.B., 2007. Digital microfluidics: is a true lab-on-a-chip possible? *Microfluid. Nanofluid*, 3, pp. 245–281.

Farahinia, A., Jamaati, J., Niazmand, H. and Zhang, W., 2021. The effect of heterogeneous surface charges on mixing in a combined electroosmotic/pressure-driven micromixer. Journal of the Brazilian Society of Mechanical Sciences and Engineering, 43, pp.1-13.

Feng, Q. and Chen, X., 2021. Numerical simulation of an electroosmotic micromixer with variable modules. International Journal of Modern Physics B, 35(30), p.2150308.

Fu, L.M. and Tsai, C.H., 2007. Design of interactively time-pulsed microfluidic mixers in microchips using numerical simulation. Japanese journal of applied physics, 46(1R), p.420.

Gayen, B., Manna, N.K., and Biswas, N., 2023. Enhanced mixing quality of ring-type electroosmotic micromixer using baffles. Chem. Eng. Process.-Process Intensif., 189, pp. 109381.

Gayen, B., Manna, N.K. and Biswas, N., 2024. Enhancing mixing performance in a square electroosmotic micromixer through an off-set inlet and outlet design. Physics of Fluids, 36(6).

Gong, Y. and Cheng, X., 2023. Numerical investigation of electroosmotic mixing in a contraction–expansion microchannel. Chemical Engineering and Processing-Process Intensification, 192, p.109492.

Green, J., Holdø, A., and Khan, A., 2007. A review of passive and active mixing systems in microfluidic devices. Int. J. Multiphys., 1(1), pp. 1–32.

Green, N.G., Ramos, A., González, A., Morgan, H., and Castellanos, A., 2000. Fluid flow induced by nonuniform ac electric fields in electrolytes on microelectrodes. I. Experimental measurements. Phys. Rev. E, 61(4), pp. 4011.

Haque, A., Nayak, A.K. and Bhattacharyya, S., 2021. Numerical study on ion transport and electro-convective mixing of power-law fluid in a heterogeneous micro-constrained channel. Physics of Fluids, 33(12).

Heo, H.S., and Suh, Y.K., 2005. Enhancement of stirring in a straight channel at low Reynolds-numbers with various block-arrangement. J. Mech. Sci. Technol., 19, pp. 199–208.

Hessel, V., Löwe, H., and Schönfeld, F., 2005. Micromixers—a review on passive and active mixing principles. Chemical Engineering Science, 60(8–9), pp. 2479–2501.

Hossain, S., Husain, A., and Kim, K.Y., 2011. Optimization of micromixer with staggered herringbone grooves on top and bottom walls. Eng. Appl. Comput. Fluid Mech., 5, pp. 506–516.

Hossain, S., Lee, I., Kim, S.M., and Kim, K.Y., 2017. A micromixer with two-layer serpentine crossing channels having excellent mixing performance at low Reynolds numbers. Chem. Eng. J., 327, pp. 268–277.

Hsieh, S.S., Lin, J.W., and Chen, J.H., 2013. Mixing efficiency of Y-type micromixers with different angles. Int. J. Heat Fluid Flow, pp. 130–139.

Huang, K.-R., Hong, Z.-H., and Chang, J.-S., 2014. Microfluidic mixing on application of traveling wave electroosmosis. Eur. J. Mech. B/Fluids, 48, pp. 153–164.

Huang, S.H., Wang, S.K., Khoo, H.S., and Tseng, F.G., 2007. AC electroosmotic generated in-plane microvortices for stationary or continuous fluid mixing. Sensors Actuators B: Chemical, 125(1), pp. 326–336.

Izadpanah, E., Hekmat, M.H., Azimi, H., Hoseini, H., and Rabiee, M.B., 2018. Numerical simulation of mixing process in T-shaped and DT-shaped micromixers. Chem. Eng. Commun., 205(3), pp. 363–371.

Jalili, H., Raad, M., and Fallah, D.A., 2020. Numerical study on the mixing quality of an electroosmotic micromixer under periodic potential. Proc. Inst. Mech. Eng. C: J. Mech. Eng. Sci., 234(11), pp. 2113-2125.

Jeong, G.S., Chung, S., Kim, C.B., and Lee, S.H., 2010. Applications of micromixing technology. Analyst, 135(3), pp. 460–473.

Ji, C., Liu, Z., Lv, M., and Li, J., 2022. Experimental investigation on flow past an isolated micro pin fin embedded in a microchannel. Nanoscale Microscale Thermo. Eng., 26(1), pp. 17–39.

Jung, S.Y., Park, J.E., Kang, T.G., and Ahn, K.H., 2019. Design optimization for a microfluidic crossflow filtration system incorporating a micromixer. Micromachines, 10, p. 836.

Kalantar Feeoj, R., Alavi Eshkaftaki, S.M., Kazemi Asfeh, I. and Jahangiri, M., 2022. Finite-Element Simulation of Electroosmotic Mixing: A Study of the Simultaneous Effects of Working Parameters for Optimization. International Journal of Chemical Engineering, 2022(1), p.9957189.

Keshavarzian, B., Shamshiri, M., Charmiyan, M., and Moaveni, A., 2018, J. Appl. Fluid Mech., 11(6), pp. 1531-1541.

Khoshnod, A., Shahsavandi, R. and Hosseinzadeh, K., 2025. Investigation of mixing performance in electro-osmotic micromixers through rigid baffle design and parameter optimization. Scientific Reports, 15(1), p.16721.

Kim, B.J., Yoon, S.Y., Lee, K.H., and Sung, H.J., 2009. Development of a microfluidic device for simultaneous mixing and pumping. Exp. Fluids, 46, pp. 85–95.

Kumar, A., Manna, N.K., and Sarkar, S., 2023. Effect of electrode length and ac frequency on mixing in a diamond-shaped split-and-recombine electroosmotic micromixer. Recent Adv. Mech. Eng, pp. 83–92.

Kumar, A., Manna, N.K., Sarkar, S., and Biswas, N., 2023. Analysis of a square split-and-recombined electroosmotic micromixer with non-aligned inlet-outlet channels. Nanoscale Microscale Thermophys. Eng., 27(1), pp. 55–73.

Lan, N., Liu, H.X., Yan, K.C., Wang, Y.B., Yang, Y.R., and Wang, X.D., 2023. The impact of secondary flow intensity on heat transfer efficiency of the wire-to-plate electrohydrodynamics devices. Phys. Fluids, 35(4), p. 047101.

Lei, K.F., 2012. Microfluidic systems for diagnostic applications: A review. J. Laboratory Automation, 17(5), pp. 330–347.

Li, J., and Li, D., 2019. Electroosmotic flow velocity in DNA modified nanochannels. J. Colloid Interface Sci., 553, pp. 31–39.

Li, J., Xia, G., and Li, Y., 2013. Numerical and experimental analyses of planar asymmetric split-and-recombine micromixer with dislocation sub-channels. J. Chem. Technol. Biotechnol., 88, pp. 1757–1765.

Lim, C.Y., and Lam, Y.C., 2012. Analysis on micro-mixing enhancement through a constriction under time periodic electroosmotic flow. Microfluid Nanofluid, 12(1), pp. 127–141.

Lin, B., 2011. Microfluidics: technologies and applications. Springer.

Liu, R.H., Stremler, M.A., Sharp, K.V., Olsen, M.G., Santiago, J.G., Adrian, R.J., Aref, H., and Beebe, D.J., 2000. Passive Mixing in a Three-Dimensional Serpentine Microchannel. J. Microelectromechanical Sys.

Lv, H., and Chen, X., 2022. New insights into the mixing behavior of Non-Newtonian fluid in electroosmotic micromixer. J. Braz. Soc. Mech. Sci. Eng., 44, pp. 181.

Majhi, M., Nayak, A.K. and Weigand, B., 2023. Electroosmotic mixing of non-Newtonian fluid in an optimized geometry connected with a modulated microchamber. Physics of Fluids, 35(3).

Mandal, D.K., Biswas, N., Manna, N.K., Gorla, R.S.R., and Chamkha, A.J., 2022. Magneto-thermal convection of hybrid nanofluid in a non-Darcian porous complex wavy enclosure. Eur. Physical J. Special Topics, 231, pp. 2695–2712.

Manna, N.K., Biswas, N., Mandal, D.K., Sarkar, U.K., and Öztop, H.F., 2022. Impacts of heater-cooler position and Lorentz force on heat transfer and entropy generation of hybrid nanofluid convection in quarter-circular cavity. Int. J. Numer. Meth. Heat Fluid Flow.

Mehta, S.K., Mondal, B., Pati, S., and Patowari, P.K., 2022. Enhanced electroosmotic mixing of non-Newtonian fluids in a heterogeneous surface charged micromixer with obstacles. Coll. Surf. A: Phys. Eng. Aspects, 648, p. 129215.

Miranda, J.M., Oliveira, H., Teixeira, J.A., Vicente, A.A., Correia, J.H., and Minas, G., 2010. Numerical study of micromixing combining alternate flow and obstacles. Int. Commun. Heat Mass Transfer, 37, pp. 581–586.

Mondal, B., Mehta, S.K., Patowari, P.K., and Pati, S., 2019. Numerical study of mixing in wavy micromixers: comparison between raccoon and serpentine mixer. Chem. Eng. Process., 136, pp. 44–61.

Mondal, B., Pati, S., and Patowari, P.K., 2019. Analysis of mixing performances in microchannel with obstacles of different aspect ratios. Proc. Inst. Mech. Eng. Part E: J. Process Mech. Eng.

Nayak, A.K., 2014. Analysis of mixing for electroosmotic flow in micro/nano channels with heterogeneous surface potential. Int. J. Heat Mass Transf., 75, pp. 135–144.

Nazari, M., Chuang, P.-Y.A., Esfahani, J.A., and Rashidi, S., 2020. A comprehensive geometrical study on an induced-charge electrokinetic micromixer equipped with electrically conductive plates. Int. J. Heat Mass Transf., 146, pp. 118892.

Niculescu, A.G., Chircov, C., Bîrcă, A.C., and Grumezescu, A.M., 2021, J. Mol. Sci., 22(4), p. 2011.

Nouri, D., Zabihi-Hesari, A., and Passandideh-Fard, M., 2017. Rapid mixing in micromixers using magnetic field. Sensors Actuators A: Physical, 255, pp. 79–86.

Pati, S., Mehta, S.K., and Borah, A., 2017. Numerical investigation of thermo-hydraulic transport characteristics in wavy channels: comparison between raccoon and serpentine channels. Int. Commun. Heat Mass Transf., pp. 171–176.

Peng, R., and Li, D., 2015. Effects of ionic concentration gradient on electroosmotic flow mixing in a microchannel. J. Colloid Interface Sci., 440, pp. 126–132.

Peng, T., Qiang, J., and Yuan, S., 2023. Investigation on a cascaded inertial and acoustic microfluidic device for sheathless and label-free separation of circulating tumor cells. Phys. Fluids, 35(8), p. 082009.

Poorreza, E., 2025. Effect of an External Electric Field on the Performance of an Electroosmotically-Driven Micromixer with Triangular-Shaped Electrodes: Design and Simulation. Russian Journal of Physical Chemistry B, 19(4), pp.1003-1010.

Pothuri, C., Azharudeen, M., and Subramani, K., 2019. Rapid mixing in microchannel using standing bulk acoustic waves. Phys. Fluids, 31(12), p. 122001.

Rakoczy, R., Przybył, A., Kordas, M., Konopacki, M., Drozd, R., and Fijałkowski, K., 2017. The study of influence of a rotating magnetic field on mixing efficiency. Chem. Eng. Process.-Process Intensif., 112, pp. 1–8.

Rashidi, S., Bafekr, H., Valipour, M.S., and Esfahani, J.A., 2018. A review on the application, simulation, and experiment of the electrokinetic mixers. Chem. Eng. Process.-Process Intensif., 126, pp. 108–122.

Rasouli, M., Mehrizi, A., and Lashkaripour, A., 2015. Numerical study on low Reynolds mixing of T-shaped micro-mixers with obstacles. Trans Phenom Nano Micro Scales 3, pp. 68–76.

Rasoulia, M.R., and Tabrizian, M., 2019. An ultra-rapid acoustic micromixer for synthesis of organic nanoparticles. Lab Chip, 19, pp. 3316–3325.

Saadat, M., Shafii, M.B., and Ghassemi, M., 2020. Numerical investigation on mixing intensification of ferrofluid and deionized water inside a microchannel using magnetic actuation generated by embedded microcoils for lab-on-chip systems. Chem. Eng. Process.-Process Int., 147, p. 107727.

Saha, A., Manna, N.K., Ghosh, K., and Biswas, N., 2022. Analysis of geometrical shape impact on thermal management of practical fluids using square and circular cavities. Eur. Physical J. Special Topics.

Saravanakumar, S.M., Jamshidi Seresht, M., Izquierdo, R. and Cicek, P.V., 2024, April. A novel DC electroosmotic micromixer based on helical vortices. In Actuators (Vol. 13, No. 4, p. 139). MDPI.

Sarkar, S., and Ganguly, S., 2015. Fully developed thermal transport in combined pressure and electroosmotically driven flow of nanofluid in a microchannel under the effect of a magnetic field. Microf. Nanof., 18(4), pp. 623–636.

Sarkar, S., Ganguly, S., and Chakraborty, S., 2017. Influence of combined electromagnetohydrodynamics on microchannel flow with electrokinetic effect and interfacial slip. Microfluid. Nanofluidics, 21, pp. 1-16.

Sarkar, S., Ganguly, S., and Dutta, P., 2017. Electrokinetically induced thermofluidic transport of power-law fluids under the influence of superimposed magnetic field. Chem. Eng. Sci., 171, pp. 391–403.

Sasaki, N., Kitamori, T., and Kim, H.B., 2010. Experimental and theoretical characterization of an AC electroosmotic micromixer. Anal. Sci., 26, pp. 815–819.

Seo, H.S., Han, B., and Kim, Y.J., 2012. Numerical study on the mixing performance of a ring-type electroosmotic micromixer with different obstacle configurations. J. Nanosci. Nanotechnol., 12(6), pp. 4523–4530.

Shahsavandi, R., Khoshnod, A. and Hosseinzadeh, K., 2025. Effect of geometric optimization and electrical control on the mixing performance of a dual-obstacle electroosmotic micromixer. International Journal of Thermal Sciences, 218, p.110146.

Shamloo, A., Madadelahi, M., and Abdorahimzadeh, S., 2017. Three-dimensional numerical simulation of a novel electroosmotic micromixer. Chem. Eng. Process.-Process Intensif., 119, pp. 25–33.

Shamloo, A., Mirzakhanloo, M., and Dabirzadeh, M.R., 2016. Numerical simulation for efficient mixing of Newtonian and non-Newtonian fluids in an electro-osmotic micro-mixer. Chem. Eng. Process.-Process Int., 107, pp. 11–20.

Shi, H., Nie, K., Dong, B., Chao, L., Gao, F., Ma, M., and Liu, Z., 2020. Mixing enhancement via a serpentine micromixer for real-time activation of carboxyl. Chem. Eng. J., 392, p. 123642.

Soleymani, A., Kolehmainen, E., and Turunen, I., 2008. Numerical and experimental investigations of liquid mixing in T-type micromixers. Chem. Eng. J., 135, pp. S219–S228.

Usefian, A., and Bayareh, M., 2019. Numerical and experimental study on mixing performance of a novel electro-osmotic micromixer. Meccanica, 54(8), pp. 1149–1162.

Usefian, A., Bayareh, M., Shateri, A., and Taheri, N., 2019. Numerical study of electro-osmotic micro-mixing of Newtonian and non-Newtonian fluids. J. Braz. Soc. Mech. Sci. Eng., 41, pp. 1–10.

Wang, D., Summers, J., and Gaskell, P.H., 2007. Modeling of electrokinetically driven flow mixing enhancement in microchannels with patterned heterogeneous surface and blocks. Nanoscale Microscale Thermophys. Eng., 11(1-2), pp. 1–13.

Ward, K., and Fan, Z.H., 2015. Mixing in microfluidic devices and enhancement methods. J. Micromech. Microeng., 25(9), p. 094001.

Wong, S.H., Ward, M.C.L., and Wharton, C.W., 2004. Micro T-mixer as a rapid mixing micromixer. Sens. Actuators B: Chem., pp. 359–379.

Wu, H.Y., and Liu, C.H., 2005. A novel electrokinetic micromixer. Sensors Actuators A: Physical, 118(1), pp. 107–115.

Wu, M., Gao, Y., Ghaznavi, A., Zhao, W., and Xu, J., 2022. AC electroosmosis micromixing on a lab-on-a-foil electric microfluidic device. Sensors Actuators B: Chemical, 359, p. 131611.

Wu, Z., and Chen, X., 2019. Numerical simulation of a novel microfluidic electroosmotic micromixer with Cantor fractal structure. Microsyst. Technol., 25, pp. 3157–3164.

Wu, Z., and Li, D., 2008. Micromixing using induced-charge electrokinetic flow. Electrochimica Acta, 53(19), pp. 5827–5835.

Xiao, Q., Wang, J., Yang, X., and Jiang, B., 2023. Construction of a reduced-order model of an electro-osmotic micromixer and discovery of attractors for petal structure. Phys. Fluids, 35(2), pp. 022002.

Xiong, S., Chen, X., Chen, H., Chen, Y., and Zhang, W., 2021. Numerical study on an electroosmotic micromixer with rhombic structure. J. Dispers. Sci. Technol., 42(9), pp. 1331-1337.

Yang, J., Chen, Y., Du, C., Guan, X. and Li, J., 2023. Numerical simulation of electroosmotic mixing of non-Newtonian fluids in a micromixer with zeta potential heterogeneity. Chemical Engineering and Processing-Process Intensification, 186, p.109339.

Yoshimura, M., Shimoyama, K., Misaka, T., and Obayashi, S., 2019. Optimization of passive grooved micromixers based on genetic algorithm and graph theory. Microfluid. Nanofluid., 23, p. 30.

Zare, P., and Talebi, S., 2020. Numerical simulation of geometry effect on mixing performance in L-shaped micromixers. Chem. Eng. Commun., 207(5), pp. 585–597.

Zhang, C., Xing, D., and Li, Y., 2007. Micropumps, microvalves, and micromixers within PCR microfluidic chips: Advances and trends. Biotechnol. Advances, 25(5), pp. 483–514.

Zhang, F., Daghighi, Y., and Li, D., 2011. Control of flow rate and concentration in microchannel branches by induced charge electrokinetic flow. J. Colloid Interface Sci., 364, pp. 588–593.

Zhang, L., Zhou, Z., Shi, J., Wei, Y., Yu, S. and Almond, H., 2024. Numerical study of a novel electroosmotic active micromixer with twin diamond-shaped chambers and sawteeth. Microsystem Technologies, pp.1-11.

Zhao, C., Zholkovskij, E., Masliyah, J.H., and Yang, C., 2008. Analysis of electroosmotic flow of power-law fluids in a slit microchannel. J. Colloid Interface Sci., 326, pp. 503–510.

Zhou, T., Wang, H., Shi, L., Liu, Z., and Joo, S.W., 2016. An enhanced electroosmotic micromixer with an efficient asymmetric lateral structure. Micromachines, 7(12), p. 218.

Zhou, T., Xu, Y., Liu, Z., and Joo, S.W., 2015. An enhanced one-layer passive microfluidic mixer with an optimized lateral structure with the Dean effect. J. Fluids Eng., 137, p. 091102.